GDAŃSK UNIVERSITY OF TECHNOLOGY

The author of the doctoral dissertation: Szymon Potrykus
Scientific discipline: automation, electronics, electrical engineering and space technologies

DOCTORAL DISSERTATION

Title of doctoral dissertation: Study of the microbial fuel cell and its circuit modeling to improve its performance as a source of electric energy combined with wastewater treatment.

Title of doctoral dissertation (in Polish): Badania mikrobiologicznego ogniwa paliwowego oraz jego modelowanie obwodowe w celu poprawy jego wydajności jako źródła energii elektrycznej skojarzonej z oczyszczaniem ścieków.

Title of doctoral dissertation (in Spanish): Estudio de la celda de combustible microbiana y su modelado de circuito para mejorar su rendimiento como fuente de energía eléctrica combinada con el tratamiento de aguas residuales.

Supervisor *signature*	Second supervisor *signature*
Dr hab. inż. Piotr Musznicki	Dr Francisco Jesús Fernández Morales

Gdańsk, year 2024

GDAŃSK UNIVERSITY OF TECHNOLOGY

STATEMENT

The author of the doctoral dissertation: Szymon Potrykus

I, the undersigned, declare that I am aware that in accordance with the provisions of Art. 27 (1) and (2) of the Act of 4th February 1994 on Copyright and Related Rights (Journal of Laws of 2021, item 1062), the university may use my doctoral dissertation entitled: "*Study of the microbial fuel cell and its circuit modeling to improve its performance as a source of electric energy combined with wastewater treatment."*
for scientific or didactic purposes.[1]

Gdańsk,..... .....
signature of the PhD student

Aware of criminal liability for violations of the Act of 4th February 1994 on Copyright and Related Rights and disciplinary actions set out in the Law on Higher Education and Science(Journal of Laws 2021, item 478), as well as civil liability, I declare, that the submitted doctoral dissertation is my own work.

I declare, that the submitted doctoral dissertation is my own work performed under and in cooperation with the supervision of Piotr Musznicki, the second supervision of Francisco Jesús Fernández Morales *.

This submitted doctoral dissertation has never before been the basis of an official procedure associated with the awarding of a PhD degree.

All the information contained in the above thesis which is derived from written and electronic sources is documented in a list of relevant literature in accordance with Art. 34 of the Copyright and Related Rights Act.

I confirm that this doctoral dissertation is identical to the attached electronic version.

Gdańsk,..... .....
signature of the PhD student

I, the undersigned, agree/~~do not agree~~* to include an electronic version of the above doctoral dissertation in the open, institutional, digital repository of Gdańsk University of Technology.

Gdańsk,..... .....
signature of the PhD student

**delete where appropriate*

[1] Art 27. 1. Educational institutions and entities referred to in art. 7 sec. 1 points 1, 2 and 4–8 of the Act of 20 July 2018 – Law on Higher Education and Science, may use the disseminated works in the original and in translation for the purposes of illustrating the content provided for didactic purposes or in order to conduct research activities, and to reproduce for this purpose disseminated minor works or fragments of larger works.

2. If the works are made available to the public in such a way that everyone can have access to them at the place and time selected by them, as referred to in para. 1, is allowed only for a limited group of people learning, teaching or conducting research, identified by the entities listed in paragraph 1.

ABSTRACT

This dissertation studies the influence of selected electric and non-electric parameters on microbial fuel cell (MFC) performance. It explores the relationship between voltage, current, pH, and chemical oxygen demand parameters on energy efficiency and wastewater treatment. The new mathematical model is proposed to estimate MFC performance under different load conditions and environmental scenarios. The study also presents a mathematical model for predicting MFC performance and investigates the effects of different electric operating conditions on power generation and wastewater treatment.

STRESZCZENIE

W niniejszej rozprawie doktorskiej zbadano wpływ wybranych parametrów elektrycznych i nieelektrycznych na działanie mikrobiologicznych ogniw paliwowych (MFC). Został zbadany związek między parametrami, takimi jak napięcie, natężenie, pH i chemiczne zapotrzebowanie tlenu, na efektywność energetyczną i oczyszczanie ścieków. Zaproponowano nowy model matematyczny do szacowania wydajności MFC w różnych warunkach obciążenia i scenariuszach środowiskowych. W badaniach laboratoryjnych zbadano także wpływ obciążeń zewnętrznych na generowanie energii elektrycznej i oczyszczanie ścieków przez MFC.

RESUMEN

Esta disertación examina la influencia de parámetros eléctricos y no eléctricos seleccionados en el rendimiento de la celda de combustible microbiana (MFC). Explora la relación entre parámetros como voltaje, corriente, pH y demanda química de oxígeno en la eficiencia energética y el tratamiento de aguas residuales. Se propone un nuevo modelo matemático para estimar el rendimiento de la MFC bajo diferentes condiciones de carga y escenarios ambientales. El estudio también presenta un modelo matemático para predecir el rendimiento de la MFC e investiga los efectos de diferentes condiciones operativas eléctricas en la generación de energía y el tratamiento de aguas residuales.

Table of Contents

LIST OF IMPORTANT SYMBOLS AND ABBREVIATIONS

A		parameter of the exponential zone voltage (V)
b	-	The time constant of COD evolution
b_{ref}	-	The time constant of COD evolution for reference test
B		parameter of the exponential zone voltage (A^{-1})
C_d	-	Diffusion capacitance
C_{dl}	-	Double-layer capacitance
CE	-	Coulombic efficiency
CE_a	-	Coulombic efficiency value
COD	-	Chemical oxygen demand
COD_0	-	Initial COD concentration
COD_f	-	Final COD concentration
COD_{rem}	-	COD removal efficiency
ΔCOD	-	COD changes
E	-	Difference between cathode potential from anode potential
E_{OCV}	-	Potential at OCV
E_0	-	Theoretical thermodynamic equilibrium potential (1.23 V)
e	-	Charge of 1 electron ($1.602\ 176\ 634 \times 10^{-19}$ C)
E_{MFC}	-	MFC output voltage
EE	-	Energy efficiency
ε_E	-	Energy efficiency value
EH	-	Energy harvesting
EIS	-	Electrochemical impedance spectroscopy
F	-	Faraday constant (9.6485 104 C mol^{-1}).
FC	-	Fuel cell
G	-	Gibbs free energy
ΔG	-	Change in the free enthalpy
$\overline{g}$	-	Free enthalpy function at a given temperature for one mole of the substance
Gdańsk Tech	-	Gdańsk University of Technology
H	-	Enthalpy
ΔHac	-	The heat of combustion of sodium acetate (709.32 kJ/mol)
HPLC	-	High-performance liquid chromatography
HRT	-	Hydraulic retention time
I	-	Electric current
i_{MFCav}	-	Terminal current of MFC average value
$i_{MFCav_{ref}}$	-	Terminal current of MFC average value for reference test
I_{max}	-	The maximum electric current of the cell / short-circuit current

I_{MFC}	-	MFC current
i_o	-	Terminal voltage of MFC
i_{MFC}	-	Terminal current of MFC
$i_{\mathrm{MFC_{ref}}}$	-	Terminal current of MFC for reference test
ITQUIMA	-	Instituto de Tecnología Química y Medioambiental
j	-	Electric current density
J		The MFC current at the maximum power point (A)
k		The polarization consta ($\mathrm{A^{-1}}$)
l	-	Activation losses model constant (V^{-1}/A)
M	-	Molecular weight
$\mathrm{M_{NaOAc}}$	-	The molecular weight of sodium acetate (82.034 g/mol)
m	-	mass transfer limitations model constant (V)
m_i	-	molar variation of reactant
MEA	-	Membrane-electrode assembly
MEP	-	Maximum energy point
MPP	-	Maximum power point
MFC	-	Microbial fuel cell
N_A	-	Avogadro's constant (6.022141023 mol^{-})[1]
n	-	Mass transfer limitations model constant ($\mathrm{A^{-1}}$)
n_m	-	Number of measurements
n_b	-	The number of electrons transferred per mole of COD removed
η_0	-	Activation losses
η_c	-	Concentration losses
η_{Jac}	-	Maximum power transfer efficiency
η_{MFC}	-	Maximum power transfer efficiency of MFC
$\eta_{\mathrm{MFC_{ref}}}$	-	Maximum power transfer efficiency of MFC for reference test
η_t	-	Total losses
η_Ω	-	Ohmic losses
OCV	-	Open circuit voltage
OLR	-	Organic loading rates
PEM	-	Proton exchange membrane
P_{max}	-	Maximum power
R	-	Gas constant
R_1	-	Resistance used in Larminie-Dicks model of MFC
R_2	-	Resistance used in Larminie-Dicks model of MFC
R_{ct}	-	Charge transfer resistance
R_d	-	Diffusion resistance

R_{el}	-	Electron resistance of the electrodes
R_{ext}	-	External load resistance
R_i	-	Ohmic losses resistance
R_{int}	-	The internal resistance of MFC
R_{ions}	-	Ionic resistance of the PEM
Rs	-	Resistors representing ohmic loses in Randles model of MFC
r	-	COD removal rate (g/L d)
r_{COD}	-	COD removal rate (mg COD/h)
RMSE	-	Root mean square error
$RSME_V$	-	Root mean square error for voltage
$RSME_I$	-	Root mean square error for current
S	-	Entropy
S_{COD}	-	COD concentration (mg/L)
S_e	-	COD concentration effluent (mg/L)
S_i	-	COD concentration influent (mg/L)
T	-	Temperature expressed in Kelvin
t	-	Time
t_0	-	Initial time
t_{ref}	-	Duration of reference test
τ	-	Time constant
UCLM	-	University of Castilla-La-Macha
V_{OCV}	-	OCV
V	-	The volume of the chamber
V_0	-	Terminal voltage of MFC
$\dot{V}$	-	Flow rate
V_d	-	Diffusion voltage
V_i	-	Ohmic voltage
V_{int}	-	Fixed internal DC source
VFA	-	Volatile fatty acids
VRM	-	Voltage-relaxation method
VSS	-	Volatile suspended solids
W_{el}	-	Electrical work
$W_{external}$	-	MFC external electric work
$W_{internal}$	-	MFC internal losses
W_{total}	-	Total electric work of MFC
WWTP	-	Wastewater treatment plant
Z_w	-	Warburg impedance

1. SUMMARY

Fuel Cells (FCs) are power source technology with associated energy harvesting for the hydrogen economy. There are many types of FCs, and all have a similar feature: a gaseous form of hydrogen as fuel. Most conventional FCs require a high concentration of hydrogen as fuel, which is rare in nature, particularly on Earth. Preparing hydrogen with the proper parameters is an energy-demanding process, which may be challenging to obtain in some geopolitical regions. The solution may be Microbial Fuel Cells (MFCs), which couple sustainable energy generation and wastewater treatment. As FCs, MFCs contain an anode, usually called a bioanode, and a cathode. The MFCs harvest energy from wastewater by electroactive bacteria with biocatalytic redox reactions. Depending on the microorganisms used to construct one reactor/cell, it is possible to obtain energy from different types of wastewater. MFCs are an up-and-coming technology for wastewater treatment. However, it is still at an early stage of development and requires further research.

The Microbial Fuel Cell (MFC) is described by nonlinear parameters such as substrate concentration, pH and flow rate of medium, and hydraulic retention time (HRT), which could be defined as the ratio between the reactor/cell volume and the flow rate and represents the average time of substrates stay inside the reactor/cell, temperature, and varying load parameters (incl. voltage, current, power, and more) that affect the performance. This dissertation aims to evaluate various electrical parameters, such as voltage and current, under different load conditions, as well as non-electrical parameters, including COD and pH, in MFCs. Additionally, it explores the relationship between these electrical and non-electrical parameters and their impact on energy efficiency (EE) and the wastewater treatment process. This thesis presents the influence of the most critical parameters on anodic performances, such as hydraulic retention time and varying load parameters. The presented work also includes the new quasi-empirical mathematical scalable MFC models and the description.

Chapter 2 includes the objectives and scopes of the work being carried out, and the dissertation's structure is described.

Chapter 3 introduces the principles of FC technologies, including MFC technology, briefly describing phenomena inside the cell. Both technologies were compared, emphasizing the difference between MFC and other FCs. This Chapter defines the typical parameters that characterize cells and their impact on performance. The review presents the current state of the art in terms of MFC technology and examples of their applications.

Chapter 4 describes studies on one of the operational parameters, i.e., the varying flow rate influence on MFC performance. The conditions and results of laboratory experiments of MFC operated under a continuous flow of media are presented in this Chapter. The investigation was focused especially on high flow rate fluctuations and their short-term effects. The design of the test stand, the MFC laboratory model of MFC and the measurement methodology are presented. During this study, the flow rate of the media was changed in order to verify the possible occurrence

of hysteresis of the processes. In order to assess the performance of the MFC and its susceptibility to change in flow, the focus was aimed at the following indicators: COD removal rates, which could be defined as delta of measures of the oxygen equivalent of organic matter in a water sample that a strong chemical oxidant can oxidize in the beginning and in the end of presses, electric power generation capability and coulombic efficiencies (CEs) which is a ratio between changes of electrical and chemical energy.

Chapter 5 describes studies on the influence of varying external loads on the performance of MFCs. The study focused on the MFC's short-term performance changes under varying external passive loads in the form of power resistors. The construction of the test stand, the design of the MFC laboratory model, and the measurement methodology are presented. The load changes were based on a stepwise modification of the external resistance value to record the hysteresis of the processes. This Chapter presents the results of the effect of the external load on the output current, power generation capabilities, fuel consumption, and pollutant removal by MFCs.

Chapter 6 presents the mathematical description of MFC performance to estimate and extrapolate the experiments for other possible load types and environmental parameters scenarios. This Chapter includes proposed mathematical models. It was decided to develop a model incorporating such physical phenomena as voltage dependencies on the COD of wastewater and internal resistance. The critical aspect of accurate system modeling is model parameter estimation. For this estimation, the terminal behavior of the MFC was studied, and it was used to estimate the MFC parameters as functions of its physical properties. The MFC model has been implemented in the MATLAB Simulink simulation environment. Laboratory measurements on the early-stage device of MFC have been performed to validate.

Chapter 7 includes investigating other varying loads on the performance of MFCs. The MFC external load has been forced by constant-current type, constant-voltage, and constant-power active loads, unlike the used passive loads presented in Chapter 5. The studies have shown the influence of different load parameters on MFC performances. In the first part, the effect of the external load on energy generation and pollutant removal by an MFC was studied by stepwise modifying the external load, and the results were compared with the resistive load.

Chapter 8 aims to analyze how modifying the external load, using maximization methods presented in Chapter 7, affects the electric power generation and synthetic wastewater treatment (COD removal) of the MFC. The specific goals include evaluating MFC performance under different electric operating conditions, selecting electrical load values, and comparing the effects of various electric operational parameters on MFC performance.

Chapter 9 concludes the work.

The bibliography provides an extensive list of literature concerning mainly the issues of MFC operating parameters, with particular emphasis on the bond between electrical and non-electrical parameters and their impact on the performance of the MFCs, as well as selected items on the subject of MFC applications.

2. OBJECTIVES AND SCOPES

This doctoral dissertation has been prepared based on an international collaboration between the Faculty of Electrical and Control Engineering, Gdańsk University of Technology (Gdańsk Tech), and the Instituto de Tecnología Química y Medioambiental (ITQUIMA) research group of the Chemical Engineering Department, University of Castilla-La-Macha (UCLM). It is included in the Cotutelle agreement between Gdańsk Tech and UCLM. The research group ITQUIMA has been working on the development of wastewater treatment technologies through electrochemical processes. The Faculty of Electrical and Control Engineering research group has been working on modeling, control development, and power system integration of new power sources. The presented studies required a multidisciplinary approach to the problem related to MFC operations and their modeling. Through the collaboration of two research groups, it was possible to perform an analysis of MFCs that fell within two disciplines: Chemical and Electrical Engineering.

The MFCs study includes an analysis of the conversion process of ambient energy, presented in the environment, into electrical energy. This energy conversion process, called energy harvesting (EH) is characterized by low-power output because EH devices could be used as a part of self-sustaining systems. The study of EH from wastewater was considered broadly, including different MFCs operational configurations and parameters, to accomplish a better EE wastewater treatment system. Recognition and evaluation of varying critical parameters and their influence on the performance indicators of MFCs was the main component of the study. Recognition of critical parameters describing MFCs was required to achieve a fully scalable mathematical model.

This doctoral dissertation is the continuation of research and development of the MFC technology for different applications, including different types of wastewater treatment. This work identifies the critical parameters influencing MFC performance and mathematically describes the relationship between parameters and performance. Proposed models use the empirical and physical approach to identify the phenomena occurring in MFCs. Based on the literature review, the scientific gaps in MFC technology, such as the study of the effect of specific flow rates and varying load parameters on MFC performance, have been identified and analyzed. Hence, this work allowed to define the general, unsolved issues that were developed through laboratory experiments and computer simulations. All these factors enable to formulate a research hypothesis:

Accurate modeling of energy conversion in a microbial fuel cell allows for identifying the mutual influence between non-electrical and electrical parameters and predicts maximum performance in the operational context.

This doctoral dissertation attempts to answer the following questions related to MFC technology:

- How can changing the flow parameters of the fuel media affect the efficiency of electrochemical processes in the flow-type MFCs?

- Can varying electric load parameters change the physicochemical properties of the medium in flow MFCs in the long term?
- How can varying electrical load parameters (voltage and current) affect the performance of electrochemical processes in MFCs?
- Can the reduced-order circuit lumped model of an MFC be sufficiently accurate to represent the dynamics of the system?

The MFC power output is mainly affected by operational parameters, i.e., pH, temperature, solids retention time, HRT, and external load. The individual parameters, as mentioned above, interact non-linearly. Due to the nature of MFCs, it is challenging to isolate the appropriate operational parameters that were the research subject. Because of that, all experiments were carefully prepared and carried out. In the prepared and conducted laboratory experiments, efforts were made to isolate the studied phenomena (e.g., external load and HRT influence on the MFC performance) from the side effects of uncontrolled factors (e.g., fluid flow or medium pH fluctuations, which may affect: the output voltage and current, power generation capabilities, fuel consumption). Because of that, two different types of MFCs were used to conduct the experiments. The MFCs were working under continuous and semi-continuous batch modes, that is, 80% of the anolyte volume, and all catholytes were replaced by fresh synthetic wastewater every cycle. In addition, MFCs measurements are affected by a long time of acclimatization of microorganisms inside the chambers. Because of that, it was necessary to develop appropriate mathematical models through which one could estimate and extrapolate the MFC parameters and phenomena occurring in different modes of operation, environmental parameters, etc. Acquired data from laboratory experiments have been used to develop and evaluate simulation models of MFCs.

The research carried out as a part of the presented doctoral dissertation can be divided into three main parts representing different issues. The influence of non-electrical parameters on the electrical parameters and the EE and wastewater treatment process efficiency of MFC has been analyzed. Different models have described the main and specific phenomena occurring in MFC. The division into parts and the publications correspond to the individual issues studied by the laboratory experiment.

The first part of the research includes:

- Critical review of the operational conditions regarding the electrochemical performance of MFC;
- The short-term impact evaluation of the medium flow rate changes on the electrochemical performance of an MFC;
- MFC mathematical model development and model parametrization.

The second part includes:

- A critical literature review of the varying electric parameters impact on MFC performance;

- The evaluation of the influence of external active load variations on the electrochemical performance of an MFC operating in a continuous load mode;
- The evaluation of the influence of external load parameters variations on the electrochemical performance of an MFC working under continuous load mode;
- Analysis of the influence of varying external load parameters on energy generation and fuel consumption.

The third part includes:

- A critical review of the selected MFC models dedicated to power analyses presented in this work;
- Based on the laboratory tests, modeling approach validation, and advanced, general, case-independent, and time-varying MFC terminal model verification.
- Model implementation and analysis of different load values for maximalizing electric energy generation and intensive wastewater treatment.

3. INTRODUCTION

3.1. Energy and environmental objectives

Nowadays, development efforts are focused on increasing the EE of sources and energy saving. Additionally, modern power systems are designed with a focus on environmental concerns. There is a global agreement to reduce and eliminate environmental pollution caused by human activity. The carbon-neutral strategy of the European Commission assumes that in the year 2050, the European Union will be able to reach carbon neutrality [1]. The proposed solution to this problem was to use renewable energy sources for power generation combined with energy storage systems [2], [3]. Due to the low energy density in batteries, compared to natural gas or hydrogen, and relatively short lifetime (depending on fully the charge and discharge cycles), battery energy storage systems can be treated as a part or intermediate stage in specific systems [4]. The tendency towards more energy-efficient components and new conceptions based on EH has set new standards for system designers and manufacturers. EH as the means for diversifying energy production from renewable sources.

In this context, the MFC is a promising device that could generate energy by using waste, mainly wastewater, as fuel [5]. In this application, the MFC couples sustainable energy generation with wastewater treatment, which could reduce the environmental impact of the conventional energy generation process. Comparing the energy demand of conventional wastewater treatment with MFC wastewater treatment shows the possibility of reducing the energy demanded for the treatment of one unit of sewage by up to 80% [6]. Unlike traditional renewable sources where energy production is tied to environmental conditions such as solar or wind, the proposed energy source is tied to human activity.

3.2. Fuel cells historical view

A FC is a low-voltage source continuously generating direct current through a redox reaction. The Welshman William Robert Grove is considered a pioneer in FC technology. In 1839, he developed a new form of the galvanic cell, which consisted of two electrodes: a positive electrode containing platinum and a negative electrode containing zinc. The positive electrode was immersed in nitric acid and placed in a porous ceramic cup surrounded by a larger jar containing sulfuric acid and the negative electrode. Grove noticed a change in electrode potentials during this experiment. This was the basis for his development in 1842 of the first FC, a gas galvanic battery. It generates electric energy by combining hydrogen and oxygen [7], [8].

This discovery waited for practical application until 1965, when the National Aeronautics and Space Administration used it as a power source for spacecraft in the Gemini and Apollo programs. In the nineties of the twentieth century, FCs experienced their renaissance and were widely used for testing and commercial purposes. The research led to the development of this type of energy generation technology. Several different types of FCs have been developed based on the oxidation reaction of not only pure hydrogen itself but also of a fuel-rich in this element, such as

methanol and natural gas. The oxidant remained unchanged in these reactions and is oxygen, either pure or directly from the air [9], [10].

3.3. Construction of a fuel cell

An FC has a straightforward structure. It consists of only a few parts, the most important of which is: the electrolyte (membrane), electrodes, and plates that distribute the reagents evenly over the entire cell surface. – Figure 3.1.

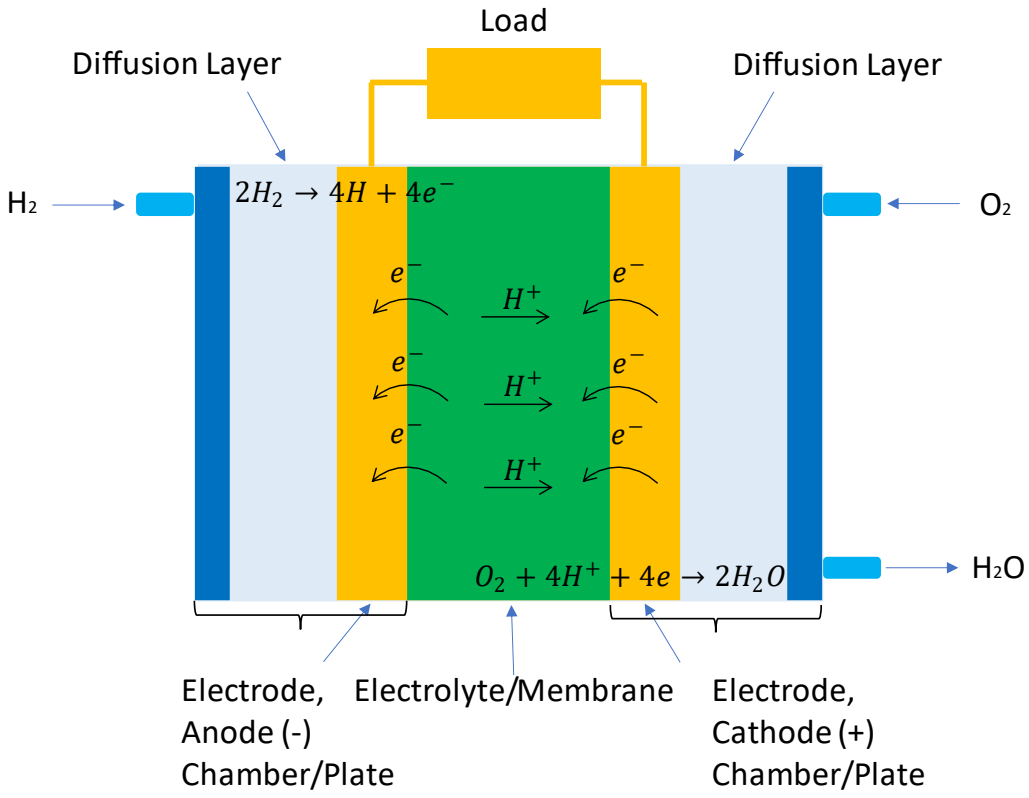

Figure 3.1 Fuel cell general concept

A single cell in an FC consists of four basic elements: electrolyte, membrane, electrodes, diffusion layers, and chambers or plates. Each of the basic elements of the cell will be presented and characterized in the following sections.

3.3.1. Chambers

Depending on the form of fuel, FC can be divided into those powered by gaseous hydrogen and fueled by a liquid mixture of hydrogen-containing substances. In the case of fuels with a low concentration of hydrogen, FC requires a longer reaction time due to the presence of other substances. Unlike the plates, the chambers have a simple construction and are not structurally prepared for the flow of the medium, and there may be differences in solution densities. Because of that, the chambers are responsible for distributing the fuel in the low-power FC.

3.3.2. Plates

Their main function is to distribute fuel and oxygen over the active surface of components (membrane and/or electrodes) depending on the construction, and they must also act as current collectors. They have the shape of small channels with different patterns so that the reactants can flow through them. In the case of an FC consisting of many cells, the plates have channels on both sides. This structure is called bipolar. The material used depends on the cell's operating temperature, so the plates can be made of graphite for high-temperature cells or stainless steel for low-temperature cells.

3.3.3. Electrolyte

The electrolytic diaphragm has three main functions in an FC. It conducts ions while isolating electrons and separating anode and cathode reagents. The ions must pass through the membrane to maintain the electrochemical balance between the anode and cathode. The direction of the reaction depends on the type of the cell - Chapter 3.5. Therefore, the reaction must occur without disturbance in the direction of the electric current flow or the reactants. For some types of FC, the electrolyte function is performed by an anolyte in the anode chamber and a catholyte in the cathode chamber, respectively.

3.3.4. Diffusion layers

This type of layer occurs only in low-temperature FCs and is responsible for the distribution of reagents and removal of post-reaction products from the electrode surfaces. It is this layer that is responsible for the drainage of water from the cathode. Therefore, it must be highly hydrophobic and, at the same time, must have good conductivity.

3.3.5. Electrodes

Electrochemical reactions take place on the surface of the electrodes and drive the generation of a potential difference and current flow. The fuel oxidation process happens at the anode, while the oxygen reduction reaction takes place at the cathode. In acidic cells, platinum or its alloys are required to construct electrodes, whereas in other types of cells, it's possible to use various precious and non-precious metal alloys.

3.4. Fuel cell thermodynamics and theoretical potential

3.4.1. Fuel cell thermodynamics

Like any device that generates electric energy, an FC has principles describing how it works. The chemical energy of the reactants (hydrogen and oxygen) and reaction products (water) is converted into electric and thermal energy. Inside the cell, the following reactions take place:

Hydrogen oxidation at the anode:

$$\mathrm{H_2} \rightarrow 2\mathrm{H^+} + 2\mathrm{e^-} \tag{3.1}$$

Oxygen reduction at the cathode:

$$\tfrac{1}{2}\mathrm{O_2} + 2\mathrm{H^+} + 2\mathrm{e^-} \rightarrow \mathrm{H_2O} \tag{3.2}$$

Total proton exchange membrane fuel cell reaction:

$$\mathrm{H_2} + \tfrac{1}{2}\mathrm{O_2} \rightarrow \mathrm{H_2O} \tag{3.3}$$

The emission of energy released by the FC during the redox reaction is associated with the change in the value of the free enthalpy in the system:

$$\Delta G = \Delta H - T\Delta S \tag{3.4}$$

where:

G - free enthalpy (Gibbs free energy);

H - enthalpy, S – entropy;

T - temperature expressed in Kelvin.

The change in the free enthalpy is caused by the difference in the free enthalpy between the products and the reactants:

$$\Delta G = \Delta G_{(products)} - \Delta G_{(substrates)} \tag{3.5}$$

If we assume that inside the FC, the reaction, according to equation (3.6), the reactants are a mole of hydrogen and half a mole of oxygen, and the post-reaction product is one mole of water. We can write it as a formula:

$$\Delta\overline{g} = (\overline{g})_{H_2O} - (\overline{g})_{H_2} - \frac{1}{2}(\overline{g})_{O_2} \tag{3.6}$$

where:

$\overline{g}$- is the value of the free enthalpy function at a given temperature for one mole of the substance.

As the temperature changes, the value of the free enthalpy of substrates and products changes. Therefore, to correctly calculate the efficiency of the cell, it is necessary to constantly monitor the operating temperature of the FC.

The negative value of the free enthalpy indicates that the FC gives up energy to the environment. If we know the values of the temperature and pressure of the substrates, we can determine the total value of energy. The emission of this energy is related to the production of one mole of water, and this energy is related to the orderly movement of electrons through the external electrical circuit. Each mole of produced water is accompanied by a simultaneous flow of electrons with a specific charge. The equation can determine the value of the charge flowing through the external circuit:

$$-2N_A e = -2F \tag{3.7}$$

where:

N_A- Avogadro's constant expressed for one mole (6.022141023 mol^{-1});

e - charge of 1 electron;

F - Faraday constant expressed for 1 mole (9.6485 104 C mol^{-1}).

The number 2 in equation 3.8 represents the number of electrons occurring in a single reaction of the reactants described by equation 3.9.

Electric work is described by equation 3.8:

$$W_{el} = -2FE \tag{3.8}$$

where:

W_{el} - electrical work;

E - a difference between cathode potential and anode potential.

Assuming that the processes taking place in the FC are lossless, a link can be derived that connects the change of the free enthalpy with the difference of potential between the cathode and the anode:

$$\Delta\overline{g} = -2FE \tag{3.9}$$

After transforming equation 3.10, we can express the potential for one proton exchange membrane fuel cell:

$$E = \frac{-\Delta\overline{g}}{2F} \tag{3.10}$$

3.4.2. Fuel cell potential

The maximum value of $E = E_0$ is a theoretical value assuming that the electrochemical process in the cell is reversible and the cell is no-load. The actual processes taking place in nature are irreversible, and the connection of the cell with the load system is the source of losses. There are three primary losses: η_0 - activation, η_Ω - ohmic, and η_c - concentration. The partial losses are easiest to present using the voltage-current characteristic called the polarization curve. Figure 3.2 shows the theoretical FC polarization curve with the contribution of partial losses. The total losses η_c are described by the equation (3.11):

$$\eta_t = \eta_0 + \eta_\Omega + \eta_c \tag{3.11}$$

When the potential difference between the cathode and anode is large enough that a current begins to flow in the system, the value of which will exceed the value of the exchange current, a nonlinear voltage drop will occur. This decrease is due to the limited reaction speed related to the

charge transport through the electrode-electrolyte junction. That may cause impurities in the fuel and the possibility of the reaction going in the opposite direction. The loss η_0 is given by the equation 3.12:

$$\eta_0 = E_0 - \Delta U_0, \tag{3.12}$$

Another source of loss is the resistance losses in the electrodes and electrolytes, as the value of the current flowing through the electrolyte and electrodes increases, the values of their resistance increase. They are linear. The loss η_Ω is given by equation 3.13:

$$\eta_\Omega = (R_{el} + R_{ions}) \cdot I, \tag{3.13}$$

where:

R_{el}- electron resistance of the electrodes;

R_{ions}- ionic resistance of the PEM;

I - current cell value.

The third main source of losses is limited diffusion in the gas diffusion layers of substrates and products of the processes taking place. They occur for high current values. Then, the voltage-current characteristic becomes nonlinear, and there is a rapid increase in the share of concentration losses in the balance sheet. The loss ηc is given by equation 3.14:

$$\eta_c = -\frac{RT}{2F}\ln\left(1 - \frac{I}{I_{max}}\right), \tag{3.14}$$

where:

R - gas constant;

I_{max} - the maximum current value can be obtained at the maximum speed at which the gas can be supplied to the cell.

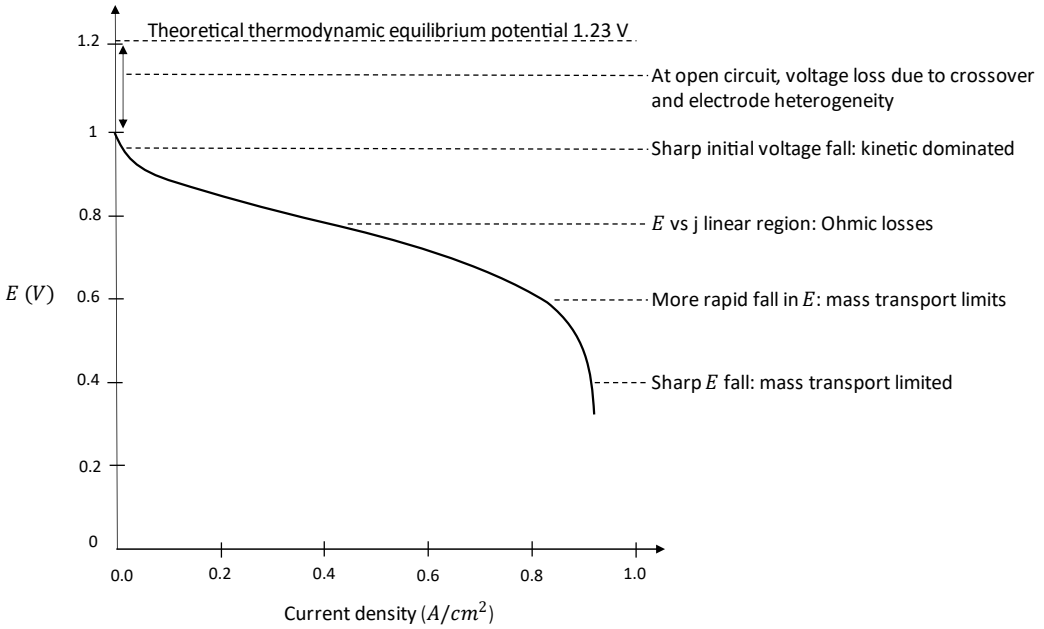

Figure 3.2 Theoretical polarization curve of FC

3.5. Classification of fuel cells

The most popular method of dividing FCs is based on the material used to build the membrane, and the type of electrolyte used implies the operating temperature of the entire cell. In order to construct the table below, it was necessary to download news from various sources and even from producer catalogs. Table 3.1 lists the types of FCs depending on the type of membrane.

Table 3.1 Fuel cells classification

Cell type	Type of membrane	Standard operating temperature	Energy efficiency	Fuel	Source
Proton Exchange Membrane Fuel Cell	Solid state polymer	Low operating temperature (60 ÷ 100)°C high operating temperature (100÷ 200)°C	(60% ÷ 80%)	Hydrogen	[10], [11]
Direct Methanol Fuel Cell	Solid state polymer	(25 ÷ 90)ºC	About 40%	Methanol-water solution	[12], [13]

Cell type	Type of membrane	Standard operating temperature	Energy efficiency	Fuel	Source
Microbial Fuel Cell	Solid state polymer	Low operating temperature (15 ÷ 35)°C high operating temperature (50 ÷ 60)°C	up to 50%	Glucose, Wastewater	[14], [15]
Alkaline Fuel Cell	The potassium base	(65 ÷ 220)ºC	up to 70%	Hydrogen	[16], [17]
Phosphoric Acid Fuel Cells	Orthophosphoric acid	Low operating temperature (130 ÷ 180)ºC high operating temperature (180 ÷ 220)ºC	(35 ÷ 45)%, in cogeneration up to 80%	Hydrogen, natural gas	[16], [18]
Molten Carbonate Fuel Cell	Potassium carbonate	(600 ÷ 700)ºC	up to 60%, in cogeneration , up to 80%	Hydrogen, methanol,	[19], [20], [21]
Solid Oxide Fuel Cells	Oxygen ceramics, stabilized zirconium, or yttrium	Medium operating temperature (550 ÷ 800)ºC high operating temperature (700 ÷ 1000)ºC	in cogeneration up to 80%	natural gas, digester gas, synthetic gas	[22], [23], [24]

Continued

3.6. Microbial fuel cells

3.6.1. Historical view

The phenomenon of the release of electrical energy by bacteria and fungi was studied and described by M. Potter in 1911 [25]. The same phenomenon of the release of electrons by microbes was confirmed by Cohen only 20 years later. The inventor called this a half-cell electric device [26]. Due to the characteristic feature of energy recovery devices, the low energy density obtained, this technology was not developed so intensively. In 1962, Davis defined the Half-Cell of Cohen as MFC [27]. A breakthrough period for the MFCs was the National Aeronautics and Space Administration space programs in which it was planned to potentially use this technology to convert biowaste into energy in spacecraft [28]. Since the late 1990s, research into MFC

technology and its potential applications have become particularly important in the fight against environmental issues [15], [29].

3.6.2. Principles

MFCs work much like FCs powered by gaseous hydrogen. Still, MFC fuel delivered to the anode could be any organic matter containing hydrogen. MFCs convert the energy of substances containing hydrogen, such as acids or hydrocarbons, into electric energy through microbial consortia (also named microbial culture) metabolic processes. In the basic MFC, the anode and cathode are placed in separate chambers filled with aqueous solutions separated by a membrane. MFC has attracted great interest in the scientific community since the beginning of this century, which has resulted in a significant amount of research focused on developing MFC technology. The general concept of MFC is presented in Figure. 3.3 [14], [30].

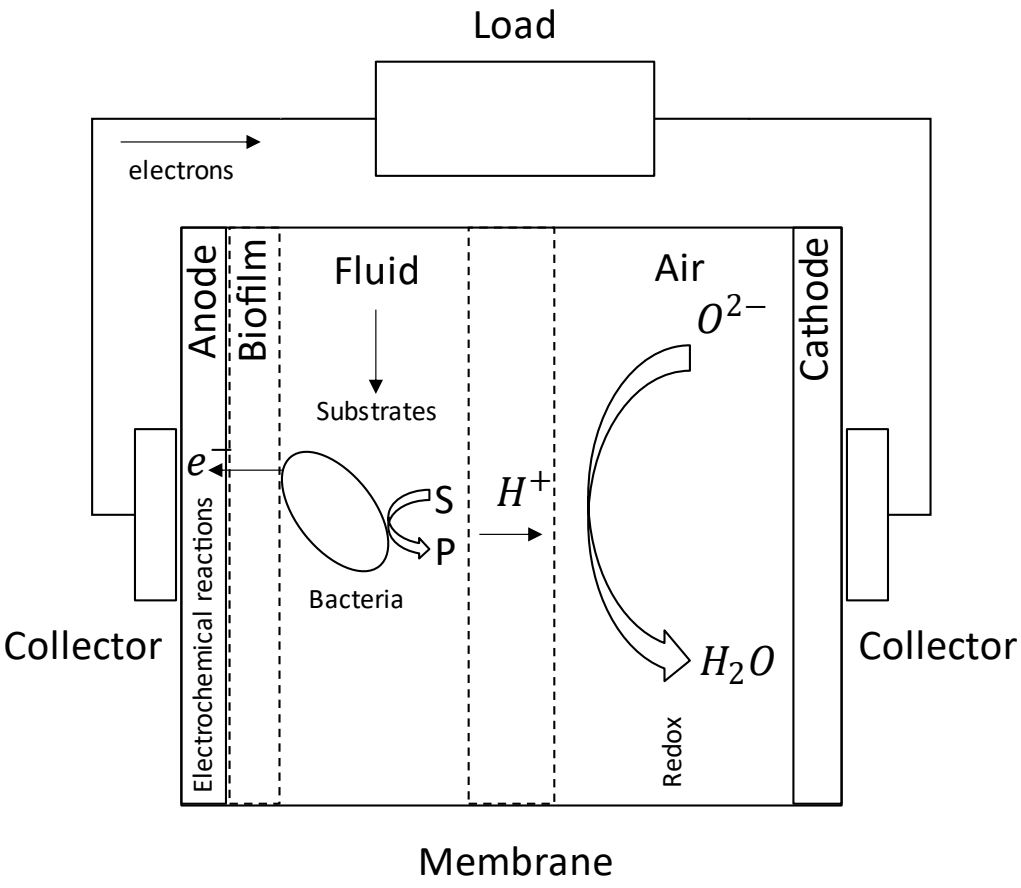

Figure 3.3 General concept of MFC

However, the MFC's energy-generating ability has not increased significantly. In recent years, the power generated by MFCs has remained relatively low due to the difficulties in scaling the technology. The use of MFC as a power systems is limited. Attempts to scale up by increasing the size of the electrodes have failed because of the mistaken assumption that the relationship between the amount of power generated by the MFC and its size is linear. The researchers note that MFCs are more energy-efficient when used with miniaturized cells. Parallel to the cell size reduction, the gross EE of the system increases. This led to a new approach to scaling based on

miniaturization and replication. The resulting MFC microcells can be electrically connected in series to increase the total potential and, in parallel, to increase the total current. However, for this approach to succeed, the cell voltage reversal and ion short-circuit issues must be addressed. Figure 3.4 shows the typical polarization curves of the MFC with the contribution of partial losses.

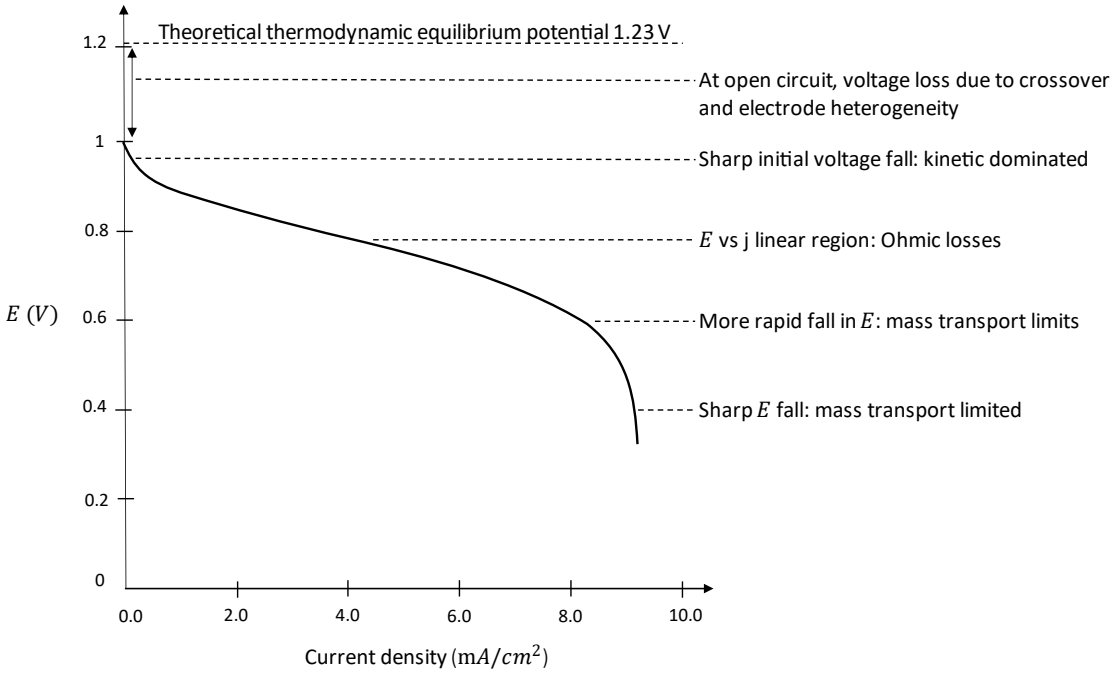

Figure 3.4 Typical polarization curve of MFC

3.6.3. Applications

Nowadays, using MFC technology in commercial solutions requires additional efforts from scientists. However, MFCs can be used for combined wastewater treatment, power generation, and other technologies such as biosensors and bio-inspired robots.

The global efforts focus on reducing greenhouse gas emissions and increasing the EE of the waste treatment processes [31], [32]. In this sector, the MFC is a promising device that could generate energy by using wastes, mainly wastewater, as fuel [5]. In this application, the MFC couples sustainable energy generation with wastewater treatment, which could reduce the environmental impact of the conventional energy generation process. Comparing the energy demand of conventional wastewater treatment with MFC wastewater treatment shows the possibility of reducing the energy demanded by treating one unit of sewage by up to 80% [6].

Additionally, to maximize the EE of the MFC wastewater treatment technology, it could be coupled with the extraction of metals from mineralized wastewater [33]. The proposed solution is relatively new and requires further electrochemical research and the development of energy harvesting methods.

The proposed project investigates the correlation between MFC operating parameters and treated wastewater or sewage quality. The experimental study focuses on treating the aqueous liquid current from a mining site. Raw acid mine drainage effluent from the mine is processed

simultaneously with general wastewater from urbanized areas. MFC will be used to perform the cathodic electrodeposition of the metals in acid mine drainage. The anode fuel is a readily biodegradable carbon source from easily accessible waste streams (domestic wastewater or agro-food effluents).

A conventional wastewater treatment process consists of three stages: mechanical, chemical, and biological. This treatment may be considered the final third stage in the wastewater treatment process. Initial characterization of the chemical composition of the acid mine drainage is necessary to design the synthetic acid waters used in the proposed solution.

3.7. Conclusions

In this chapter, fundamental information about FC technology is presented. Various types of FCs are discussed, highlighting their basic characteristics. A more detailed examination is provided for MFC technology, including its origin, construction, and potential applications. The chapter delves into the development history of MFCs, explaining the principles behind their operation, the materials and methods used in their construction, and the diverse range of applications where this technology could be effectively utilized.

4. INFLUENCE OF THE FLOW RATE ON THE PARAMETERS OF MICROBIAL FUEL CELL

4.1. Introduction

MFCs are bio-electrochemical devices wherein the reduction and oxidation reactions, typically carried out by microorganisms, occur in separate compartments. In MFCs, we can distinguish four main areas of variables controlling the performance: fluidic, thermal, bio-chemical, and electrochemical. One of the variables controlling the performance of the MFC is the change in the flow rate profile. Variations in the fuel flow rate in conventional hydrogen FCs cause changes in the partial pressure exerted on the PEM, thereby changing power output [34]. In the case of the MFC, the analysis of the changing flow rate should also consider the biological factor. The microbial consortia of MFC have been described based on a pure or mixed culture [35], [36], [37], [38], [39], [40]. The MFCs with pure cultures are operationally stable and yield very high CE values [41]. However, pure cultures are distinguished by several inherent limitations, including a heightened susceptibility to microbial contamination and a high degree of sensitivity to low substrate doses. The MFC operated with mixed cultures, and this type of limitation was significantly reduced [42], [43], compared to MFCs where consortia of microorganisms compete for the same substrates [44], [45]. The competition that ensues is indicative of the survival of the fittest microorganisms [46]. Because of that, the MFCs operated using mixed cultures achieve substantially greater output power densities than those operated with pure cultures. The activity of the microorganism consortium depends on the operational conditions within the MFC.

Considering the electrochemical performance, it is imperative to acknowledge that the operational conditions maintained throughout the process significantly influence the steady-state output power density of the MFC [47], [48]. In the literature, it has been observed that the output power is mainly affected by Organic Loading Rates (OLR) [49], pH [50], [51], temperature [52], [53], solids retention time [47], [54], hydraulic configuration [55], [56], [57], [58], HRT [56], external load [59], [60], the type of the membranes used [61], [62], reactor configuration [63], type of wastewater [64], [65], anode potential, etc. Unfortunately, the impact of fluctuations in the flow rate of domestic wastewater on the efficacy of MFCs has not been adequately documented in the literature. A comprehensive understanding of this influence is required to successfully implement MFC technology as a low-energy cost for a domestic wastewater treatment system.

This part of the Chapter presents research on the dependence of the short-term effects of varying influent flow rate profiles on electric energy output and the quality of effluent purification of wastewater treatment processes. During laboratory tests, efforts were made to isolate the flow profile from other operating conditions, i.e. pH, substrate concentration, and external load. The research was focused on the influence of the flow rate on the output current density and the COD removal effect.

4.2. Objectives

The main goal of the research presented in this Chapter is to analyze the short-term effect of the influent flow rate on the output of electric power generation and (synthetic) domestic wastewater purification level of the MFC system. Specific objectives are as follows:

- To study the effect of the base load profiles with polarization and power curves on the cell performance;
- Analysis of the MFC performance related to electric power generation output parameters, CE, pollutants removal rates at the selected operating conditions;
- Quantitive analysis of the quality of the treated wastewater by measurements of Volatile Suspended Solids (VSS) and COD;
- Analysis of the flow-type MFC mathematical model performance and model parametrization estimation.

4.3. Materials and methods

4.3.1. Experimental research assumptions

In the experimental study of the effect of the change of the flow rate profile on MFC performances, attempts were made to perform the experiments taking into account the constancy of the laboratory experiment conditions. For this purpose, the influence of individual phenomena accompanying the normal operation of MFCs would be eliminated or negligibly small. The proposed cells had a minimal volume to eliminate turbulent flow during the experiment. Care was taken to keep the COD value constant to avoid the effect of the COD changes on the Open Circuit Voltage (OCV) of MFC during the laboratory experiment. It was decided to use an air-breathing cathode to minimize the energy demand needed to sustain the electrochemical reaction inside the MFC. The laboratory experiment results of this study were used to parameterize the MFC mathematical model. This study does not address the carbon footprint issues associated with using MFC.

4.3.2. Experimental setup

Prepare the experimental conditions to be as close as possible to the natural conditions of the wastewater treatment plant (WWTP). For this purpose, the synthetic wastewater was prepared on the basis of the compositions presented in [66]. This study analyzes the effect of the influent flow rate on the output of electric power generation, COD removal rate, COD removal efficiency, and CE. Experiments were conducted at varying flow rates while maintaining a constant substrate concentration at an approximate level of 322 mgCOD/L (chemical oxygen demand per liter), which aligns with typical values observed in domestic wastewater [54]. Laboratory experiments investigated the effect of a short-term change in the flow rate profile. Because of that, it was assumed that the medium inside the cell should be exchanged in the range descending from 120 s to 12 s, which means HRT was changed from 120 s to 12 s. A shorter HRT was impossible to

achieve due to the risk of washing out the bacteria from the MFC chamber. Initially, the influent flow rate increased stepwise, from 0.72 to 7.20 L/d (liter per day), and afterward, the influent flow rate decreased stepwise. The proposal experiment work was planned to evaluate the possible hysteresis of the flow rate effect. Each level of the influent flow rate was maintained for 24 hours to ensure a steady state and evaluate the short-term effects occurring in MFC [54]. The results of the experimental investigation were used as the basis for parameterizing the mathematical model of the MFC proposed in [67]. That model is further developed considering the influence of flow rate on MFC performance determined in this Chapter

The experimental work was conducted in a two-chambered early-stage device of MFC. The anodic and cathodic chambers had a volume of 0.93 cm^3 and 0.53 cm^3, respectively. Both chambers were constructed using graphite plates. The electrodes of the anode and cathode had active areas of 2.65 cm^2 and contained carbon papers of Toray TGPH-120 (E-Tek, USA). A layer of 0.5 mg Pt/cm^2 was deposited on the surface of the cathodic electrode to take advantage of the catalytic properties offered by the Pt presence [61]. Due to the elevated flow rates of the medium, it was necessary to improve the mechanical properties of the electrodes. Because of that, the anodic and cathodic electrodes were doped with 20% and 10% Teflon, respectively. The anode and cathode were connected by wires and an external resistance of 120 Ω to close the electrical circuit externally.

The anodic chamber was supplied with synthetic wastewater, although the cathodic chamber was opened to the atmosphere to take oxygen from the air. A Proton Exchange Membrane (PEM) was used for the anodic and cathodic chamber separation. The task of the membrane was to block the flow of electrons while opening channels for the flow of hydrogen protons. Because of that, the Sterion® membrane with high ionic conductivity (0.9-0.02 meq/g) and low electronic conductivity ($8 \cdot 10^{-2}$ S/cm) was used. The MFC was configured as an MEA to reduce the internal resistance to a minimum. The preparation of MEA involved using a hot-pressing method between two stainless steel blocks with heating surfaces and a system for controlling temperature. The hot-pressing process took place at 130 °C with a load of 1 Ton applied for 15 minutes. A schematic view of the MFC is presented in Figure 4.1.

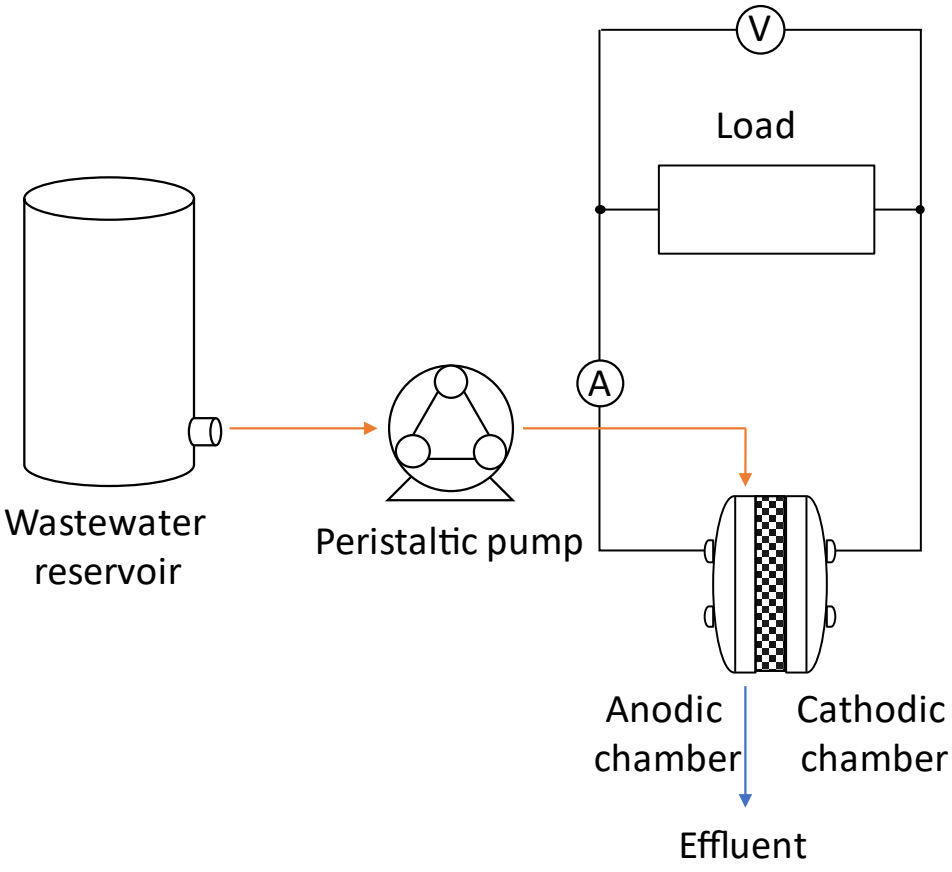

Figure 4.1 MFC schematic view of experiment setup

4.3.3. Anolyte composition

To facilitate the setup for experiments, such as in the case of the WWTP, the anodic compartment of the MFC received activated sludge from the Ciudad Real WWTP. Afterward, the mixed microbial culture underwent a four-month acclimatization process to adapt to the MFC operational conditions. The anodic chamber was linked to a 0.25 L auxiliary tank during this process. On the first day, this tank was filled with 0.2 L of activated sludge inoculum and 0.05 L of wastewater, which was then recirculated at a flow rate of 0.75 L/d. Subsequently, a daily purge of 0.05 L of the tank's liquid bulk took place, and it was replaced with fresh synthetic wastewater. The synthetic water used in this study has biochemical properties that make it suitable for assuming neutrality for microbes within the MFC. Following acclimatization, the MFC operated continuously, and the wastewater was supplied at a flow rate of 0.75 L/d. The medium supplied to the MFC was sterilized synthetic wastewater from a wastewater reservoir of 5 L. The components and concentrations of the synthetic wastewater can be found in Table 4.1.

Table 4.1 Synthetic wastewater composition

Component	Concentration (mg/L)
Fructose	161.0
Glucose	161.0

NaHCO3	111.0
(NH4)2SO4	74.2
KH2PO4	44.5
MgCl2	37.1
CaCl2	30.7
(NH4)2 Fe(SO4)2	3.1

Continued

4.3.4. Sampling and analytical methods

To evaluate MFC performance in terms of electric power generation parameters under specific operating conditions, the MFC voltage (v_{MFC}) between the terminals was continuously observed with a digital multimeter (Keithley 2000). The MFC voltage is directly proportional to the electric current (i_{MFC}) flowing between the electrodes through the Ohm Law. The power density was determined by dividing the obtained power by the anode surface area. Polarization curves were performed using potentiostat/galvanostat Autolab PGSTAT30 (Ecochemie, The Netherlands), with a scan rate of 1 mV/s and a step potential of 1 mV. These curves allow for the discerning of three critical parameters of MFC performance: the OCV (V_{OCV}), the short-circuit current (I_{max}), and the maximum achievable power (P_{max}). The internal resistance (R_{int}) is calculated from the power P_{max} and the current density at P_{max} (I_{Pmax}) using the formula as follows:

$$R_{int} = \frac{P_{max}}{(I_{max})^2} \tag{4.1}$$

The Volatile Suspended Solids (VSS) were performed to assess the water quality. The standard methods presented in [68] were used to determine VSS concentrations. The concentration of COD was determined using a spectrophotometer (Pharo 100 Merck). The pH was measured using pH meter PCE-228 (PCE Holding GmbH, Hamburg, Germany). The COD removal rate was calculated through equation 4.2, and COD removal efficiency (COD_{rem}) was obtained with equation 4.3:

$$r = \frac{(COD_0 - COD_f) \cdot \dot{V}}{V} \tag{4.2}$$

$$COD_{rem} = \frac{COD_0 - COD_f}{COD_0} . 100\ \% \tag{4.3}$$

where: COD_0 represents the influent COD concentration, grams per liter (g COD/L), COD_f corresponds to the effluent COD concentration, grams per liter (g COD/L), $\dot{V}$ is the flow rate, liters per day (L/d), and V is the volume of the anodic chamber in liters (L)

The CE was calculated as follows:

$$CE = \frac{M \int_0^t \mathrm{i}_{\mathrm{MFC}} dt}{F\, n_b\, V\, \Delta COD} \tag{4.4}$$

where M is the molecular weight of oxygen (32), I corresponds to the current intensity generated by MFC, F is Faraday's constant, n_b the number of electrons transferred per mole of COD removed (for glucose and fructose, 4 moles of electrons/mol of COD), V is the volume of liquid in the anode compartment, and ΔCOD idicates the variation in COD concentration over the time period.

The value of the number of moles of electrons produced per mole of substrate measured as COD is 4 as can be observed in the reactions occurring in the anodic chamber of the MFC [68]. The presented reaction in equations 4.5 and 4.6 requires additional comments regarding CO_2 emissions. In this case, CO_2 emission is a metabolic product of bacteria and one of the side effects of MFC electric energy generation. It is also observed with conventional WWTPs [32], and it is worth mentioning that in this case, it is no energy gain such as in MFCs. There are concepts for minimizing the carbon footprint of MFCs [14], [15], however, they go outside of the goals of this study:

Global reaction:

$$\mathrm{C_6H_{12}O_6} + 6\mathrm{O_2} \rightarrow 6\mathrm{CO_2} + \mathrm{H_2O} \tag{4.5}$$

Anodic oxidation:

$$\mathrm{C_6H_{12}O_6} + 6\mathrm{H_2O} \rightarrow 6\mathrm{CO_2} + 24\mathrm{H^+} + 24\mathrm{e^-} \tag{4.6}$$

Cathodic reduction:

$$\mathrm{O_2} + 4\mathrm{H^+} + 4\mathrm{e^-} \rightarrow 2\mathrm{H_2O} \tag{4.7}$$

Biomass characterization was conducted using a MALDI-TOF AXIMA (Shimadzu). The matrix solution for the analysis was prepared by saturating α-cyano-4-hydroxycinnamic acid in acetonitrile:water acid (1:48:2) solution. The microorganisms were dehydrated with 75% ethanol and then centrifuged at 1000 rpm for ten minutes. Following centrifugation, the supernatant was discarded. The biomass was then recovered from the precipitate using 20 µL of an acetonitrile/formic acid/water (50:35:15) solution, according to established procedures in the literature [69].

4.4. Results and discussion

4.4.1. Influence of the flow rate on output current density and chemical oxygen demand removal

As previously stated, the medium flow was modified in a stepwise manner. In order to test for the existence of hysteresis of electric MFC output, forward and reverse scans were carried out. Figure 4.2 presents the voltage output for the different influent flow rates studied [D1].

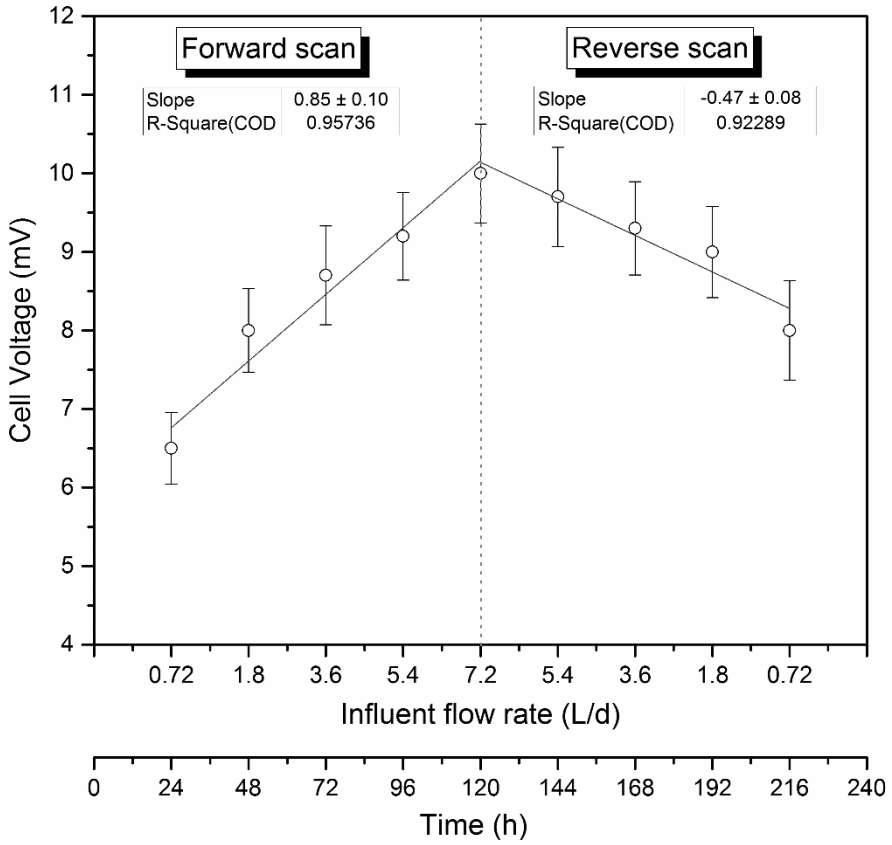

Figure 4.2 Effect of the influent flow rate on the steady-state voltage output

The voltage output showed a significant increase, rising from 6.5 mV to 10.0 mV, as the influent flow rate surged from 0.72 to 7.20 L/d. This can be attributed to the fact that higher flow rates provide more organic load for microbial oxidation. Gude [70], also demonstrated this phenomenon, noting that higher OLR led to higher electrical energy outputs. Furthermore, increased flow rates result in turbulence, which promotes more efficient mass transfer within the biofilm along with the higher OLR. This, in turn, enhances diffusion and proton-motive potentials, ultimately leading to improved electrochemical performance of the MFC in terms of electric power generation [71]. In Figure 4.2, it can be observed that there was a linear trend with a slope of 0.85 mV per L/d during the forward scan, showing a regression coefficient of 0.957. Following the completion of the forward scan, a reverse scan was conducted, revealing a decrease in the voltage output from 10.0 mV to 8.0 mV. A linear trend was also detected during the reverse scan. However, the decrease in the output current density was not as large as expected, at 0.47 mV for each L/d decrease in the flow rate. The regression coefficient was 0.923, resulting in higher voltages than those obtained in all cases in the forward scan at the same influent flow rate. The behaviors observed in the forward and reverse scans made a hysteresis loop. This behavior may be explained by the proliferation of electrogenic microorganisms or by the enhanced development of electrogenic metabolisms during the experiments conducted at high flow rates.

The mineralization of the effluent was assessed to determine if the rise in electric power generation was associated with increased COD removal. To accomplish this, the influent and effluent COD was analyzed, and the COD removal efficiency and rate were determined. The COD

removal efficiency and the COD removal rate as functions of the influent flow rate are presented in Figure 4.3 [D1].

In Figure 4.3, it is evident that the flow rate surged from 0.72 to 7.20 L/d, increasing the COD removal rate by 235% and reaching the value of 331.6 g/(L d). This upward trend continued even during the reverse scan. As the flow rate decreased from 7.2 to 5.4 and then to 3.6 L/d, the COD removal rate further increased to 396.4 g/(L d). The inertia of the MFC may explain this behavior. According to the literature, exposure to high OLR could lead to biomass growth and/or an increase in microbial enzymatic production for maximum COD degradation [47, 70]. In this case, this effect was sustained for about 60 hours, indicating enhanced enzymatic activity as a possible explanation. Finally, when the flow rate decreased to 0.72 L/d (value of initial flow rate), the COD removal rate decreased to 187.5 g/(L d). Notably, in all cases, the rates of removal of chemical oxygen demand (COD) were higher in the reverse scan than in the forward scan. The removal rates reached a peak of 396.4 g/(L d) in the reverse scan at an influent flow rate of 3.6 L/d.

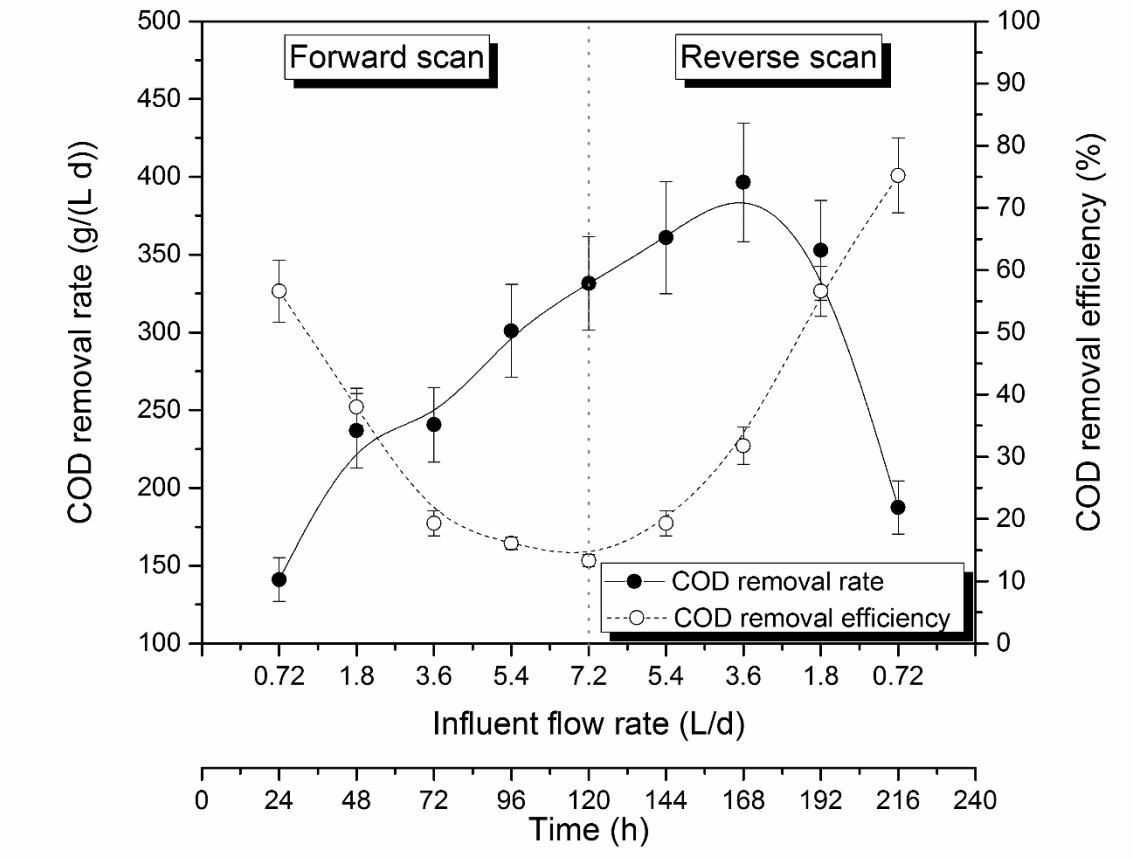

Figure 4.3 Effect of the influent flow rate on the COD removal efficiency and rate

Conversely, the efficiency of substrate removal dropped from 57% to 13% as the inflow rate increased during the forward scan. The lowest COD removal efficiency was achieved when operating at the highest inflow rate, specifically 7.20 L/d. Subsequently, the efficiency of substrate removal increased from 13% to 75% as the inflow rate decreased in the reverse scan. Once again, it appears that the MFC exhibits better electrochemical performance in the reverse scan than in the forward scan, with an increase of approximately 25%. However, to finally verify the

hypothesis, additional tests should be carried out in the opposite order of increases and decreases in flow.

The relationship between influent flow rate, OLR, turbulence, and HRT in the anodic chamber can explain the observed behaviors. With higher influent flow rates, there is an increase in OLR and turbulence, and a decrease in HRT. This leads to enhanced mass transfer, making more substrate available for oxidation by the mixed microbial culture. As a result, the amount of COD removed increases, even though the percentage of COD removed decreases at higher OLR. Also, the reduced HRT due to higher influent flow rates results in less time for microorganisms to degrade the incoming substrate [14], [72], [73]. It can be seen in Figure 4.4, it is evident that the behavior of MFC differed during the forward (decreasing flow rate) and reverse (increasing flow rate) scans, in terms of both COD removal efficiency and COD removal rate. The presence of hysteresis also indicates that behavior of the microbial culture shifted after the influent flow rate tests [52]. As in the output voltage case, the hysteresis curve can be attributed to the expansion of electrogenic microorganisms or the heightened synthesis of enzymes during periods of high load. In these conditions, the increase of COD removal was maintained for about 48 h. Hence, in such scenarios, the microbial culture in the MFC was capable of breaking down COD at increased rates.

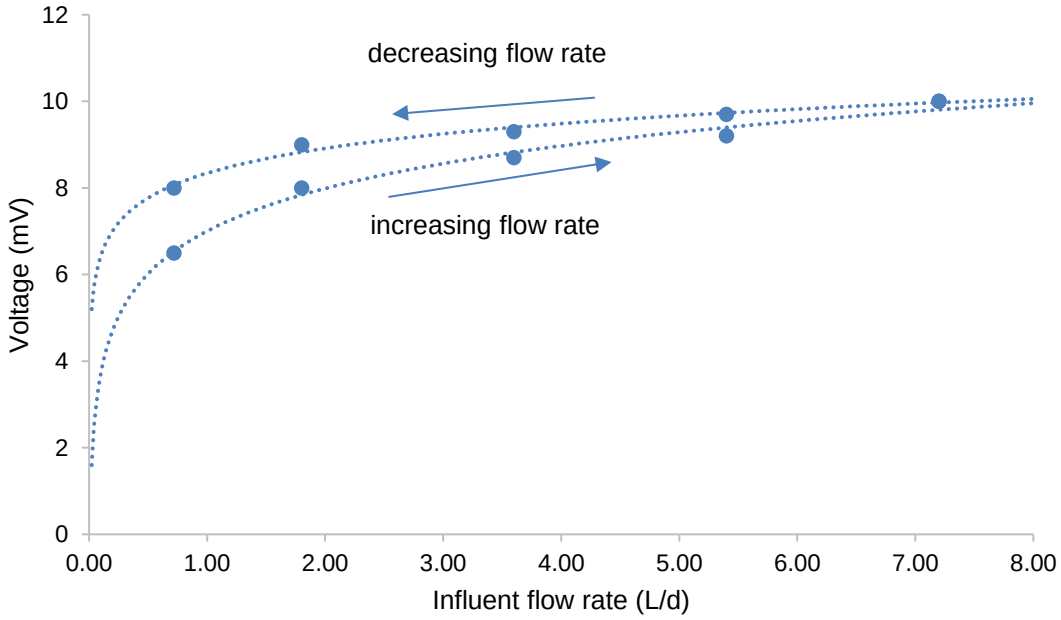

Figure 4.4 Dependence of output voltage in the function of influent flow rate for forward and reverse scan

Once the current density output and the COD removal rate had been evaluated, similar trends were observed for both parameters. In addition, it is important to analyze both cases and check whether or not the incise was CE proportional. A parameter involving both variables, the CE, was examined to do that.

4.4.2. Influence of the flow rate on the coulombic efficiency

The CE in both forward and reverse scans was determined to assess the change in the efficiency of converting chemical energy into electrical energy. Figure 4.5 [D1] shows how the influent flow rate affected the CE in both scans. The CE experienced a decline from 0.27% to 0.20% with an increase in flow rate from 0.72 to 1.8 liters per day (L/d). As the flow rate continued to increase from 1.8 to 7.2 L/d, the CE remained relatively constant. In the reverse scan, decreasing the flow rate led to a decrease in CE from 0.22% to 0.14%. Surprisingly, by reducing the flow rate to 0.72 L/d, the CE experienced a significant increase, reaching 0.25%. Figure 4.5 also showed that the CE for the same flow rate was lower in the reverse scan than in the forward scan, demonstrating a shift in the behavior of the microbial culture. This trend can be attributed to the fact that while microorganisms degraded more COD in the reverse scan, they utilized less substrate for electric power generation, resulting in a lower CE value. The results are in line with the data shown in Figures 4.2 and 4.3, indicating that the COD removal increased at a higher rate compared to the electrical energy output.

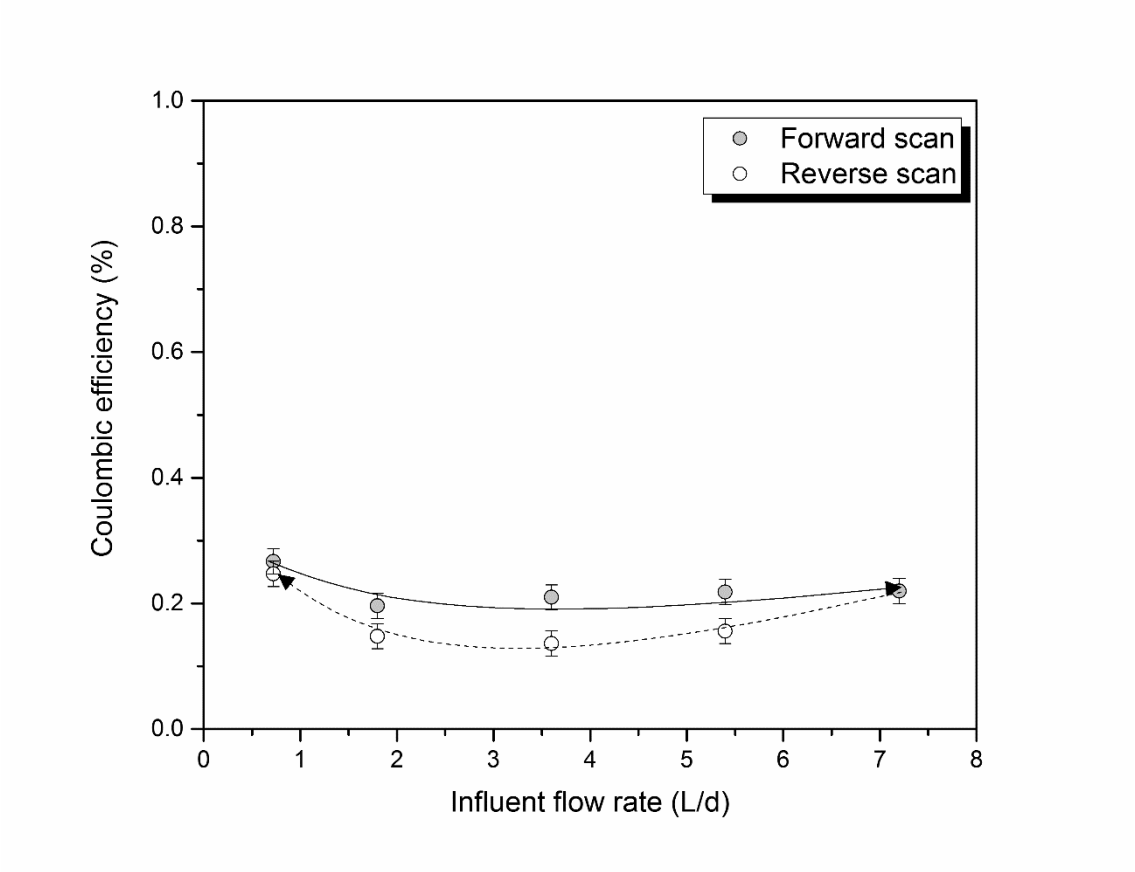

Figure 4.5 Dependence of CE on the influent flow rate

At higher flow rates and OLR, non-electrogenic microorganisms consumed more COD without generating electric power. In Figure 4.5, it was observed that the COD removal efficiency was lower at high OLR. This could be due to increased substrate consumption by non-electrogenic microorganisms, including sulfate-reducing bacteria or methanogenic archaea [74] and also due to the intrusion of oxygen through the PEM [75], whose dissolution is favored at high flow rates

[76]. Based on previous research findings, it has been suggested that the increased OLR encountered by the microorganisms capable of generating electricity may lead to a reduction in CE. [77]. To verify the statements, the microbial population was characterized using MALDI-TOF analysis. After the flow rate tests, it was noted that the distribution of microbial populations was similar, with an increase in the presence of microorganisms from the *Clostridium genus*, a main fermenter strain with limited electrogenic abilities. Additionally, a gravimetric analysis indicated an increase in the concentration of microorganisms in the MFC. These results indicate that the increased electric power generation was associated with higher concentrations of microorganisms.

The most efficient CE and COD removal occurred at the lowest flow rate, based on the results. However, higher influent flow rates led to improved COD removal and electric power generation rates. Because of that, for practical applications in industrial-scale plants, the system design should aim to meet discharge limits set for receiving water bodies by balancing the high percentages of COD removal and CE achieved at low influent flow rates with the improved COD removal rates and electricity generation observed at higher influent flow rates.

4.4.3. Performance modeling of the microbial fuel cell

To evaluate the short-term impact of influent flow rate changes on MFC performance, polarization curves were modeled both before and after conducting stepwise flow rate tests. Both tests (before and after) were performed at the initial flow rate value of 0.72 L/d. The polarization and power density curves shown in Figure 4.6 [D1] have slight differences, suggesting that the changes in influent flow rate during the test affected the behavior of the MFC. The maximum power density, OCV, and internal resistance were determined from these polarization curves.

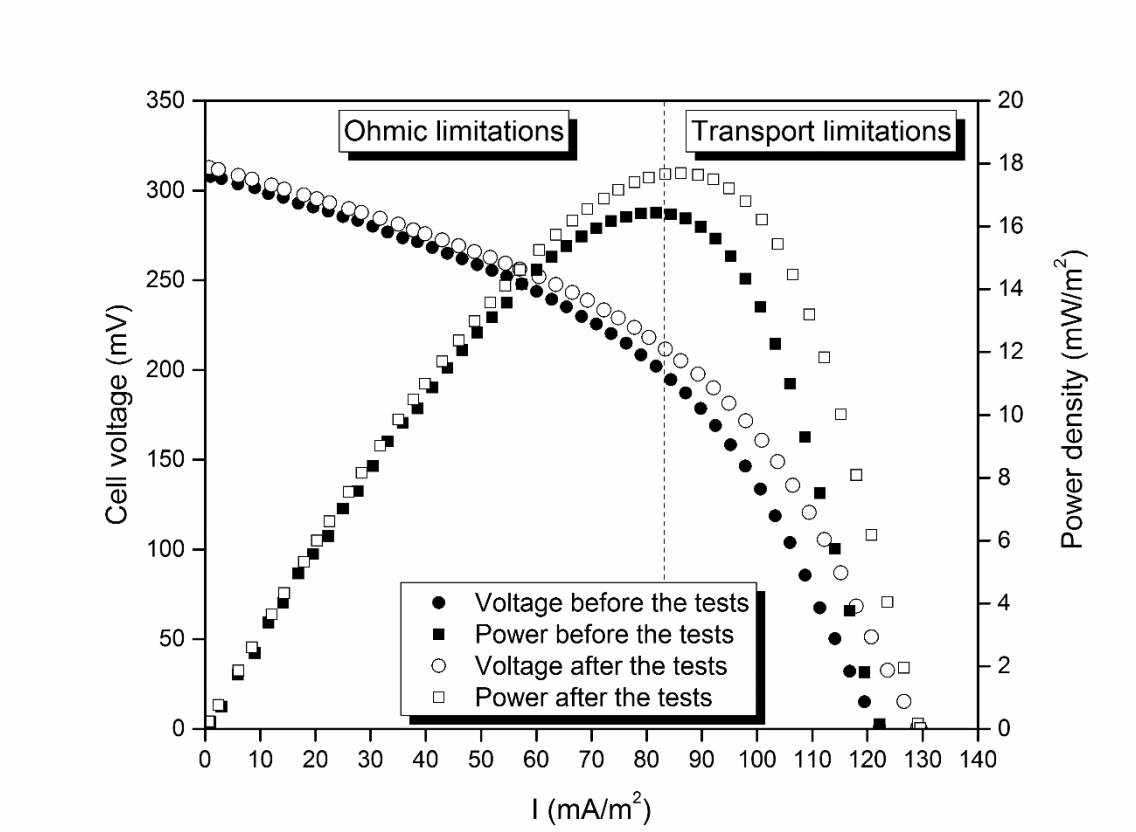

Figure 4.6 Polarization and power curves of the MFC before and after the experiments

The polarization curves for theoretical FC have three distinct regions where various types of losses contribute to reducing the output current. First, the kinetic limitation dominates at low current densities. Second, the intermediate region is governed by ohmic limitation. Finally, the transport limitation is found at high current densities [30]. Only the ohmic and transport limitation regions were observed in the polarization curve obtained in this study (refer to Figure 4.6). This indicates that the primary limitations were ohmic losses and mass transfer losses. Ohmic losses in the MFC arise from resistance linked to ion conduction in the solution, membrane, and electron flow through the electrode.

Conversely, mass transfer losses occur when the reactant flux to the electrode or the product flux from the electrode is insufficient, thereby limiting the reaction rate. It was observed that the reduction in ohmic losses became less pronounced after the flow rate tests, and a similar trend was seen with mass transfer losses. This suggests that the limitations were partially mitigated after conducting experiments with higher influent flow rates. To assess these effects, Table 4.2 presents the maximum power and current density outputs of the MFC before and after the flow rate tests.

Table 4.2 Polarization and power curves parameters

When	P_{max} (mW/m^2)	j_{max} (mA/m^2)
Before the tests	16.5	122
After the tests	17.7	130

In Table 4.2, it was observed that the maximum power density achievable with the MFC increased from 16.5 to 17.7 mW/m^2, and the maximum current density increased from 122 to 130 mA/m^2. These results are consistent with the behavior of electric power generation described in Section 4.4.1, where the current density output under short circuit conditions at the end of the experiment exceeded the initial value. This indicates that the electrogenic activity of the MFC was enhanced following exposure to high influent flow rates.

After conducting influent flow rate tests on the MFC to improve its performance, the results of the polarization curves were analyzed using a mathematical model suggested in existing literature [67]. In Equation 4.8, the MFC output voltage is determined by subtracting several voltage losses from the maximum achievable potential, i.e., the OCV (E_{OCV}). These losses include activation losses, represented by the term $l \cdot \log(i_{MFC})$, ohmic losses, represented by $R_i \cdot i_{MFC}$, and mass transfer limitations, represented by the empirical term $-m \cdot \exp(n \cdot i_{MFC})$

$$E_{MFC} = E_{\mathrm{OCV}} - l \cdot \log(i_{MFC}) - R_i \cdot i_{MFC} - m \cdot \exp\,(n \cdot i_{MFC}) \tag{4.8}$$

The results indicated that the E_{OCV} values remained unchanged at approximately 0.3 V before and after the flow rate tests. This consistency suggests that variations in flow rate had no impact on the output standard voltage. The reason for this is that the flow rate tests do not impact the reactions occurring in both the anode and the cathode. When it comes to the activation losses, all the experimental data sets were adjusted using the same *b* value of 0.005 V/decade, indicating minimal short-term effects of the influent flow rate changes on the bioelectrocatalytic activity of the MFC. This *b* value aligns with the standard value found in the literature when fitting polarization curves [67] of MFC operating with bioanodes. After the flow rate tests, a different internal resistance (R_{int}) value was observed, with the value before the tests being about 20% higher than after the tests. This indicates that the flow rate modifications influenced the MFC's internal resistance. Given that neither the wastewater composition nor the MFC configuration was altered, the most likely explanation is an increase in the concentration of electrogenic microorganisms performing the electrogenic reactions. As previously mentioned, microbial composition was analyzed using MALDI-TOF, revealing a slight increase in Clostridium presence and overall biomass concentration after the flow rate tests. Thus, the observed changes in the MFC can be attributed to the growth of electrogenic microorganisms. Finally, mass transfer limitations were also studied.

The fitting values for the parameter mmm remained consistent in both scenarios; however, the parameter nnn decreased by approximately 5% following the flow rate tests. The nnn parameter

is associated with the threshold value that induces deviations in the voltage linearity due to mass transfer limitations. Because of that, the alteration in the n parameter value indicated that different mass transfer limitations occurred before and after the flow rate tests. Table 4.2 shows that the n parameter decreased after the flow rate tests, suggesting that the threshold current density for the limitations decreased after the tests. This outcome suggests a direct correlation between the flow rate changes and the limitations experienced during mass transfer. Considering that similar microbial populations (*Geobacter* and *Clostridium*) were observed in both tests, and the same flow rate and substrate concentrations were used, these limitations could only be attributed to the increase in electrogenic microorganism concentration in the MFC. In the case of MFC technology, both direct and indirect electron transfers are influenced by the biomass concentration in the system [78]. Therefore, higher biomass concentration in the examined range results in enhanced electrogenic performance of the MFC.

The results of model parameter estimation are summarized in Table 4.3, and modeling results are shown in Figure 4.7 [D1]

Table 4.3 Parameters values obtained in modeling the polarization curves

Polarization curve	Parameter					
	E_{OCV} (V)	I (V^{-1}/A)	R_i (Ω)	m (V)	n (A^{-1})	Correlation coefficient R^2
Before the tests	0.3	0.005	1.86	0.005	121.2	0.999
After the tests	0.3	0.005	1.52	0.005	115.4	0.999

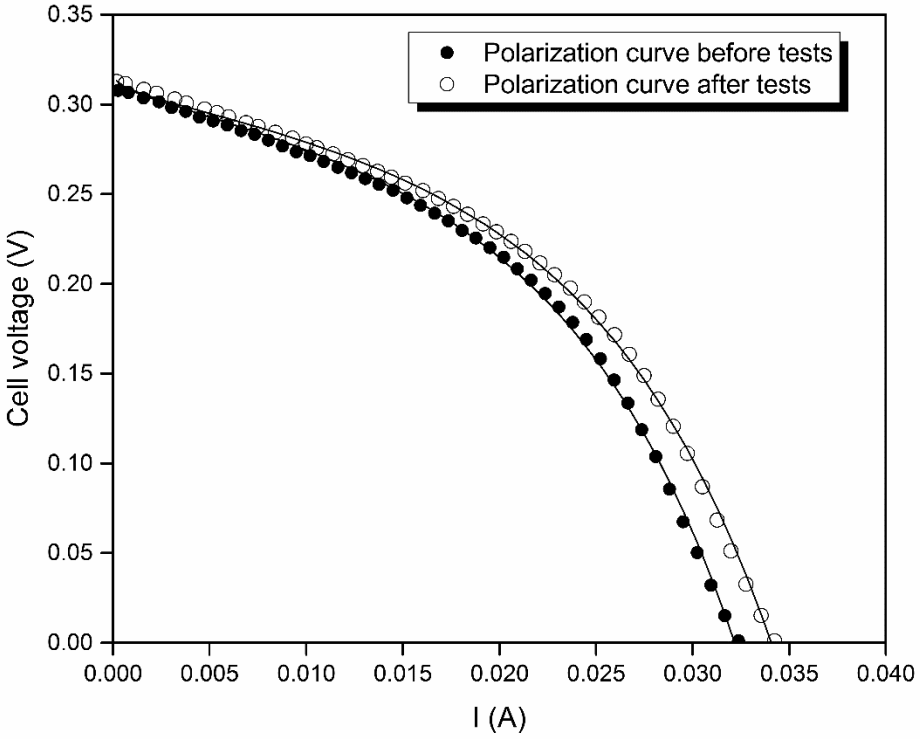

Figure 4.7 Simulation of the polarization curves that were acquired by the flow rate test at 0.72 L/d.

4.5. Conclusions

This Chapter addresses one of the most significant challenges related to the real-world implementation of MFCs, namely handling changes in flow rate. For this reason, the short-term effects of flow rate variations were investigated.

The results show that surge of the flow rate from 0.72 to 7.2 L/d enhanced both electricity generation and COD removal rate while reducing COD removal efficiency and CE efficiency. The increase in flow rate leads to higher organic loading rates, intensified mixing, and reduced mass transfer limitations.

During the return to the initial conditions of flow rate was observed a hysteresis loop which was caused by the growth of the microbial culture when exposed to high OLR. The CE efficiency values reflect a decrease in electrogenic activity at high flow rates.

5. THE EFFECT OF EXTERNAL LOAD ON THE PERFORMANCE OF MICROBIAL FUEL CELLS

5.1. Introduction

In the MFC, microbial cultures can be involved in oxidation and reduction processes. An active microbial culture at the anode typically oxidizes organic substrates, releasing electrons to the anode and protons into the liquid bulk. At the cathode, the electrons and the protons are used to reduce an oxidant, usually oxygen [4]. The movement of electrons through an external electrical circuit generates an electric current, while the protons are conveyed to the cathode by passing through the membrane. The major limitation of MFC technology is its low power generation density [7]. However, MFC power density may increased by enhancing favorable operating conditions such as COD, pH, flow rate, temperature, or configuration options such as electrode area, external load, etc. [8-17]. One of the most relevant variables is the external load. The external load controls the current and cell voltage output [18]. The external load can be classified as either high or low resistance, with this classification referring to the internal resistance of the MFC. A high external resistance leads to a high cell voltage and low current, while a low external resistance results in a low cell voltage and high current. High and low loads can be subcategorized as passive ones, i.e., simple resistors, and active ones, i.e., DC-DC converters with pulse-width modulation of internal transistor bridge. According to Jacobi's law, the maximum power transferred from a source to a load occurs when the values of load resistance and the internal resistance of the source are the same [19]. One of the key aspects of energy generation in MFC technology is maximizing power or efficiency based on modifying external load [20-22].

The effect of the external load over batch-operated MFC was described in [23]. However, for full-scale implementation and process automatization, studying the influence of external load on MFC performance during continuous mode operation is required. Because of that, this Chapter focused on studying the effect of passive external load value on the performance of MFCs. Attention was paid to the electric energy generation, fuel consumption, and microorganism consortia of the anodic compartment.

5.2. Objectives

The main goal of this Chapter is to analyze the effect of the varying external load on the output parameters of electric power generation and (synthetic) domestic wastewater purification level of the MFC. The partial objectives were the following:

- Analysis of the performance of MFC related to an output voltage level for the selected operating conditions, CE, and pollutants removal rates;
- Evaluate the quality of the treated wastewater by studying the effect of the varying external load on the anode pH, VSS, and Volatile Fatty Acids (VFA);

- Determination of the correlation of changes in the bacterial population under the influence of changes in the external load of the MFC.

5.3. Materials and methods

5.3.1. Experimental research assumptions

In the experimental study of the effect of the passive external load level, attempts were made to perform the experiments considering the constancy of the laboratory experiment conditions. For this purpose, the influence of individual phenomena accompanying the normal operation of MFCs would be eliminated or negligibly small. The proposed cells had a minimal volume to eliminate turbulent flow during the experiment. Care was taken to keep the COD value constant to eliminate the influence of the COD changes on the OCV of MFC during the laboratory experiment. The experimental laboratory results of this study were used to develop the MFC mathematical model.

5.3.2. Experimental setup

Based on the experience from previous laboratory experiments, the same MFC is used to study the effect of the passive external load on the performance of the MFC. The MFC operated continuously, with various passive external loads connected to the load circuit. These experiments maintained a constant influent flow rate of 7.2 L/d. The experiment lasted for 92 days and involved using a two-chambered MFC. The cathode and anode were connected using an external resistance (R_{ext}), which was altered in various experiments. To observe the effect of the external load, direct and reverse scans are used to test the performance of MFC under varying external resistances. In a direct scan, the external resistance is increased stepwise, while in a reverse scan, it is decreased stepwise. The range of loads selected for the study was designed to encompass the internal resistance value of 2210 Ω, as well as values both above and below this threshold. Consequently, the range from 120 Ω to 3300 Ω was chosen based on the information in [25]. Starting with an initial external resistance of 120 Ω, the resistance was gradually increased to 560, 1000, 1500, 2200, 2700, and 3300 Ω. After reaching 3300 Ω, the external resistance was stepwise decreased back to the initial 120 Ω. Figure 5.1 presents the setup used in this work.

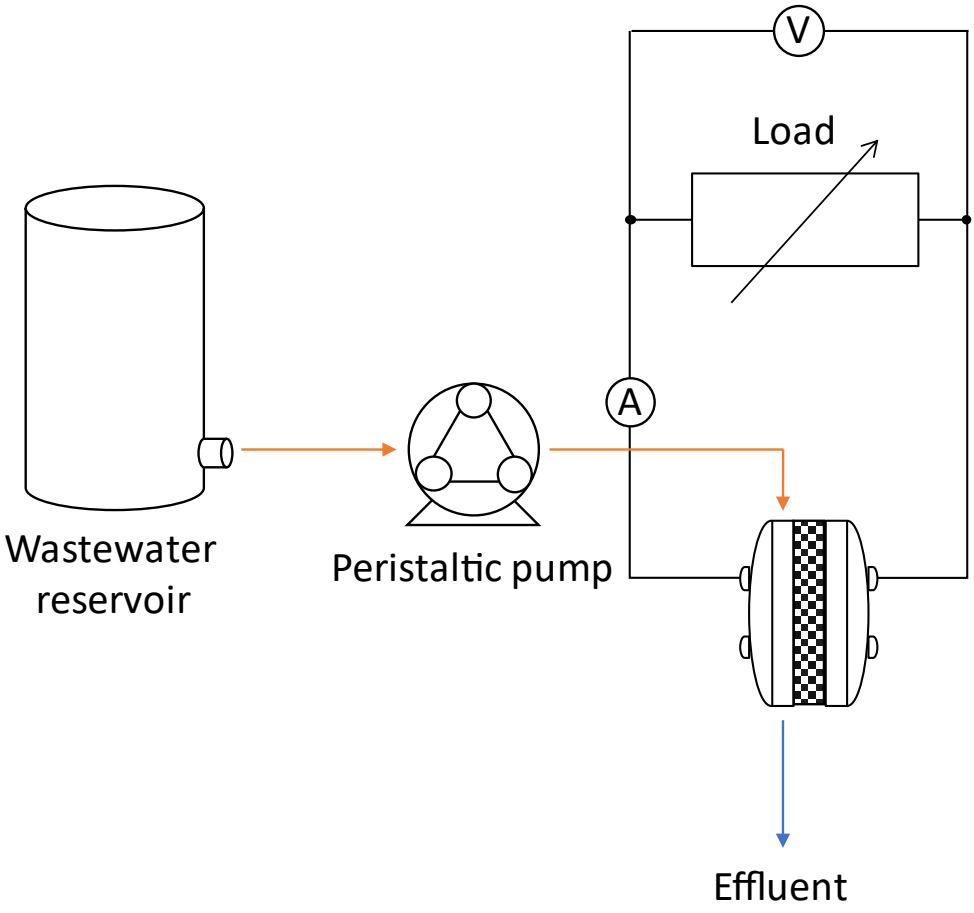

Figure 5.1 Setup configuration

The electrogenic culture described in the literature [26] was used to inoculate the anodic compartment. The MFC used in this study was operated continuously by feeding the anodic chamber with synthetic wastewater at a flow rate of 7.2 L/d. The synthetic wastewater composition is presented in Table 4.1. The synthetic wastewater underwent a sterilization process at 105°C for 30 minutes to guarantee consistent and reproducible conditions [27]. According to the literature, an air-breathing cathode was used because of its high performance [28].

5.3.3. Characterization techniques and analytical methods

The MFC operation was continuously monitored using a digital multimeter connected to the R_{ext}. The potential (V_{MFC}) was directly related to the electrical current (I_{MFC}) between the external load terminals by Ohm's law. Power was calculated using the relationship between *I* and *V*. In this setup, the electric current was generated due to the anodic oxidation process of the organic compounds in the synthetic wastewater supplied to the MFC. The oxidation process was observed by determining the COD removal rate (r_{COD}), measured as mg COD/h, and the COD removal percentage ($CODrem$) [29]. These parameters are calculated according to equations 5.1 and 5.2, respectively,

$$r_{COD} = \dot{V} \cdot \Delta COD \tag{5.1}$$

$$\mathrm{CODrem} = \frac{\Delta COD}{COD_o} \cdot 100\% \quad (5.2)$$

where $\dot{V}$ is the influent flow rate ΔCOD is the COD removed from the wastewater and COD_o is the initial COD concentration of the wastewater. The initial concentration was about 343 mg/L.

According to the literature, spectrophotometric and gravimetric methods measured the COD and VSS concentrations in the anodic effluent, respectively [30]. The pH measurement was performed on the influent and effluent medium. The pH value was determined by using pH meter PCE-228. The biomass populations were characterized by using MALDI-TOF Axima Assurance (Shimadzu Corporation). The matrix solutions were prepared according to the procedure outlined in the literature [8]. The effluent concentration of acetic, propionic, and butyric acids was determined using gas chromatography (Perkin Elmer) with flame ionization detection, following the procedure described in the literature. [31].

5.4. Results and discussion

5.4.1. External load effect on electric parameters

The influence of the external load on electric energy generation was studied taking into account the current and power output. The electrical current output by the cell at various external loads is presented in Figure 5.2 [D2]. The results were recorded at the steady-state response to ensure reproducibility. Figure 5.2 shows a decrease in current as the external load increases. This observation can be attributed to the external load's influence on the relationship between current generation and cell voltage [12]. The literature has described that high external resistance leads to high cell voltages and low currents. [21]. The most significant changes occurred when the external load resistance increased from 560 to 1500 ohms, reaching a minimum current of 0.02 mA when the external resistance of 3300 ohms was applied. After completing the direct scan, the performance of a reverse scan was carried out to compered the intensity obtained when the external resistance was stepwise increased and then stepwise decreased. Contrary to the expectations, the intensity output by the MFC did not increase during the reverse scan. The current was kept almost constant around 0.02 mA independently of the external resistance applied. Because of that, the current generated by the MFC for each external resistance was higher in the direct than in the reverse scan. In other words, after the operation with high external loads, the intensity output decreased. This behavior indicates that the system has permanently changed due to exposure to high external resistances. This change can only be explained by a shift in the population distribution. Previous research suggests that changes in external loads can affect the growth and population distribution in the biotic compartments of the MFC. [32]. In order to ratify that, the microbial population was analyzed employing MALDI-TOF, observing the apparition of *Clostridium* when the external resistance increased. Other recent research works have also identified this behavior [33]. The microorganisms in the fermenter have a higher growth rate of approximately 0.1 h^{-1} [34] compared to the electrogenic microorganisms, which have a

growth rate of about 0.05 h^{-1} [35]. This could be the reason why the population did not revert to its initial conditions when the external resistance was decreased.

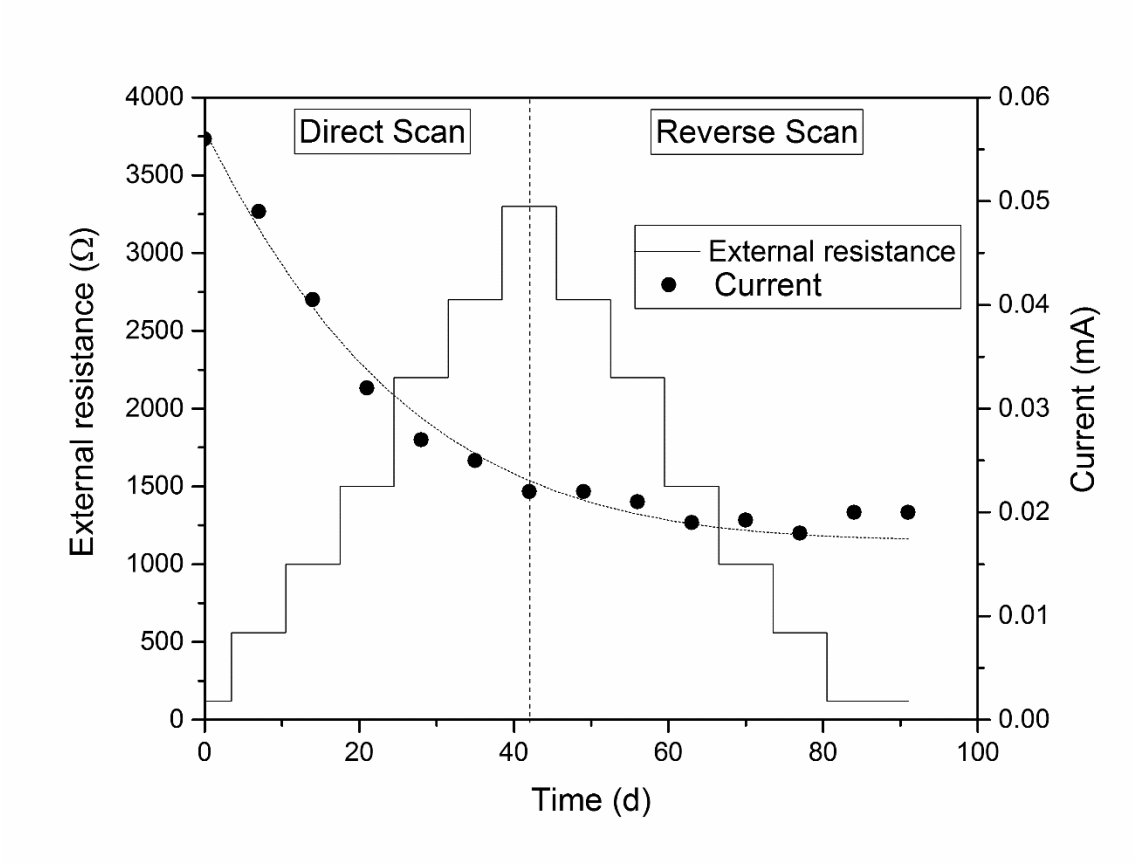

Figure 5.2 Current output by the MFC at every external resistance

The Jacobi theorem explains that the highest amount of power can be achieved when the external resistance matches the internal resistance. Jacobi introduced the maximum power transfer theorem in 1840, demonstrating that the effectiveness of power transfer can be described as shown in equation 5.3. When maximum power transfer occurs, the efficiency is only 50%, but it nears 100% as the external resistance increases towards infinity.

$$\eta_{Jac} = \frac{R_{ext}}{R_{ext} + R_{int}}, \tag{5.3}$$

Because of that, to determine the internal resistance of the MFC was carried out a polarization curve was done using equation 4.1. The analysis revealed that the internal resistance has a value of 2210 ohms. Figure 5.3 [D2] shows the power generated at various external resistances to verify Jacobi's theorem.

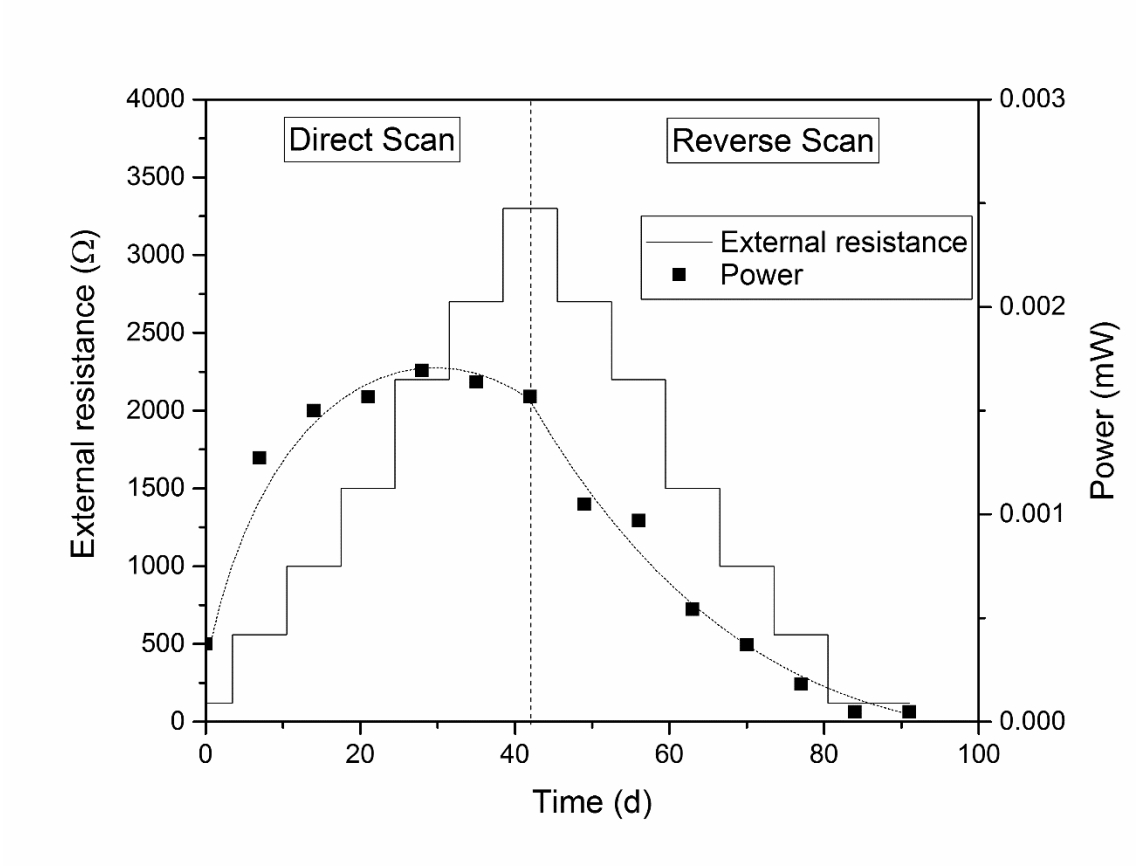

Figure 5.3 The power output by the MFC at every external resistance

As shown in Figure 5.3, the power output increment was observed when the external resistance increased from 120 to 560 Ω. The power output increased from 0.4 to 1.4·µW. Then, the subsequent stepwise increments in the external resistance slightly increased the power output, reaching a maximum at about 2200 Ω, exerting 1.6 µW. This power output value represents the maximum value obtained with the MFC utilized in this study, thereby validating the Jacobi theorem. When the external resistance was stepwise decreased, a significant reduction in the power output was observed from 1.6 to 0.05 µW. It must be remarked that this behavior generates a hysteresis loop. Because of that, the power output for each external resistance was consistently higher in the direct scan when the external resistance was stepwise increased, compared to operating in the reverse scan when the external resistance was stepwise decreased. The literature reports that these changes may be due to changes in the distribution of the microbial population within the culture in reaction to modifications in the external load [20]. This change in the microbial population could be the reason for the reduction in the power output after the operation under high value of external resistance. In the literature, variations in anodic potentials during the operation of the MFC under different external loads serve as a determining factor in the selection of distinct electrogenic microorganisms [36]. The literature reports that these changes in the distribution of microorganisms could alter the activation losses and internal resistance of the anode, which depend on the electrochemical activity of the anodic electrogenic microorganisms [37]. In this study, as mentioned earlier, there was a notable shift in the

distribution of microbial populations following the experiments, with a significant increase in fermenter microorganisms, particularly those belonging to the *Clostridium genus*.

5.4.2. External load effect on fuel consumption

The performance of the microbial culture in the MFC is affected by changes in external resistance, which makes it interesting to see how it affects fuel consumption. In this case, the fuel refers to the biodegradable substances in synthetic wastewater. To measure fuel consumption, we determined the COD of the synthetic wastewater before and after it was processed in the MFC. Figure 5.4 [D2] shows the COD removal based on the applied external resistance. It is evident that fuel consumption slightly increased when the external resistance was raised up to the internal resistance of the MFC value of 2200 Ω. When the external resistance exceeded this threshold, fuel consumption began to decline. This decrease persisted even as the external resistance values were reduced during the reverse scan. Considering that electric energy generation also decreases, it was considered attractive to determine CE. The CE is a measurement that indicates the percentage of electron equivalents converted into electric energy generation when oxidizing fuel in the MFC. The observed CE values decreased as the experiments progressed. This decrease may attributed to changes in the population distribution of the previously described microbial culture. In this scenario, the reduced CE can be explained by the outcompeting growth of non-electrogenic microorganisms over the growth of the electrogenic ones.

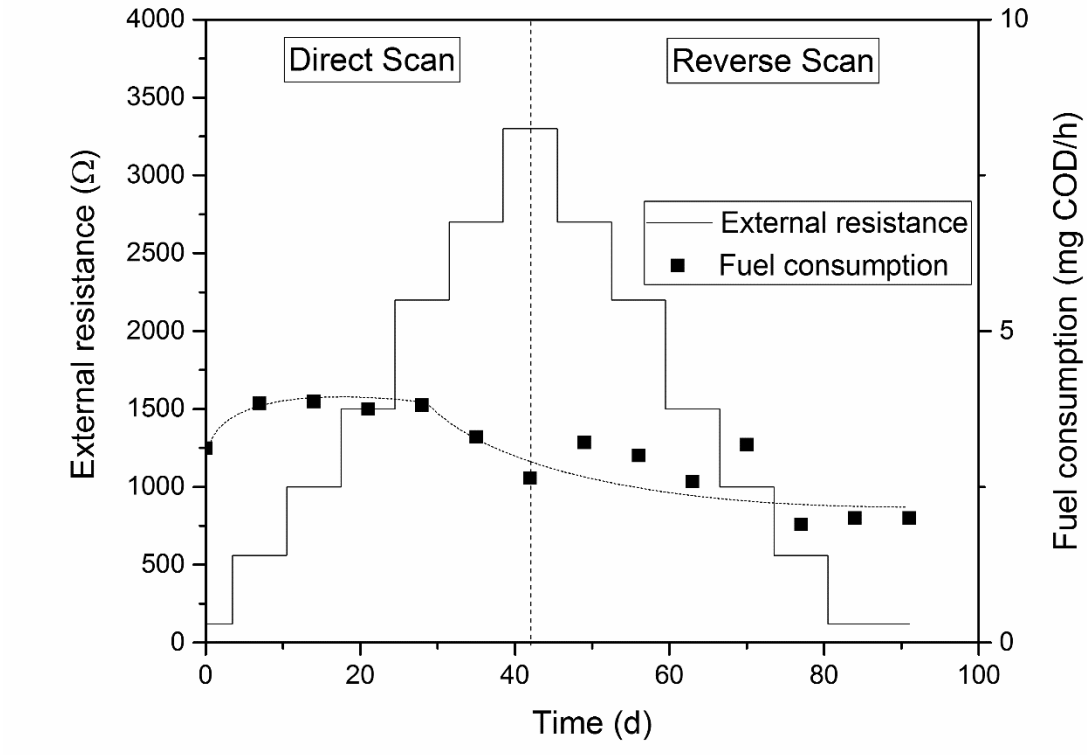

Figure 5.4 Fuel consumption in a steady state at every external resistance

To investigate changes in the fuel, experiments measured the pH, production of fermentation products, and biomass concentration in the effluent marked as VSS. Figure 5.5 [D2] shows the VSS and pH based on the external resistance.

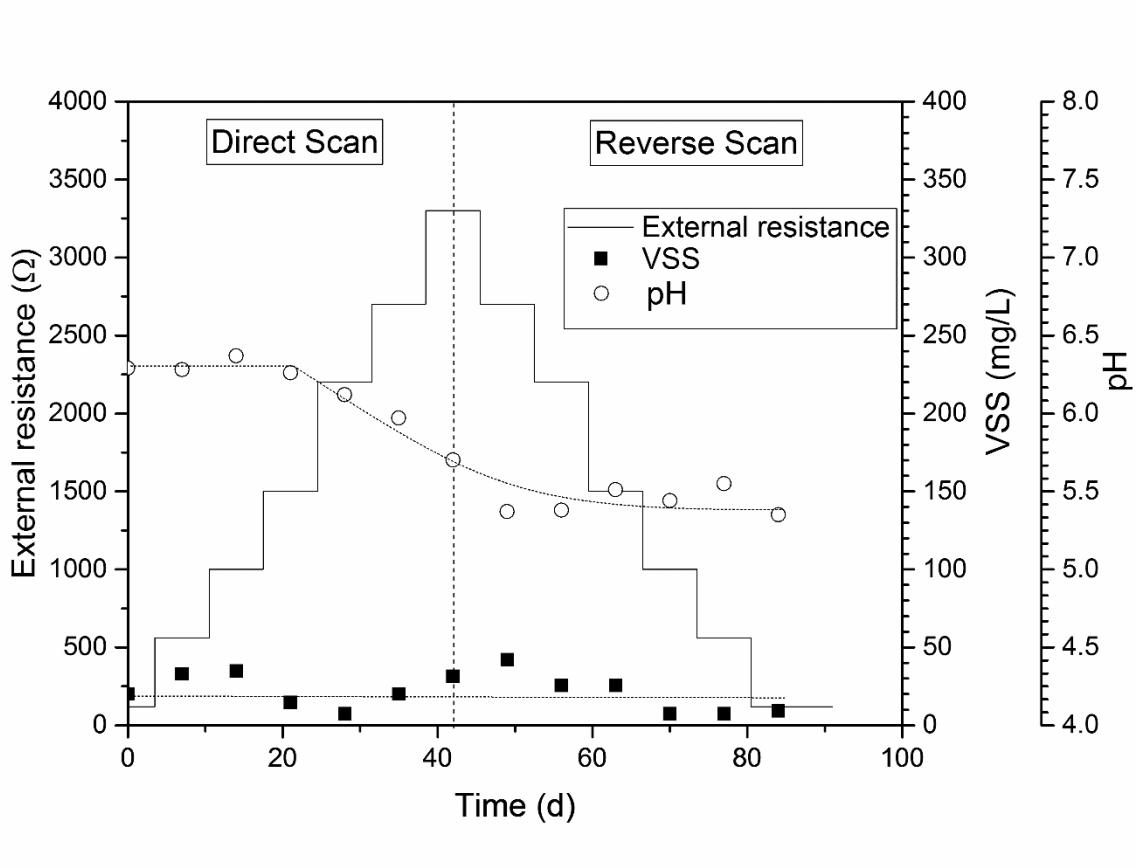

Figure 5.5 Volatile suspended solids concentration and pH of effluent at every external resistance

Figure 5.5 reports that the concentration of microorganisms in the outflow remained constant despite changes in external resistance. However, given that the current produced at higher external resistances was lower, it can be inferred that the community shifted towards a less electrically active culture. The pH is a significant factor in the performance of the MFC. This is because pH impacts microbial metabolic reactions and could potentially halt vital microbial functions if the microorganisms are exposed to pH levels outside of their optimal range. [38]. Because of that, most MFCs operated at neutral pH to maximize microbial growth [39]. The pH can influence oxidative metabolisms and affect the proton generation mechanisms and, consequently, the electron transference to the electrode [40]. In Figure 5.5, it can be seen that pH was maintained constant, around 6.3, when external resistance was lower than 2200 Ω (the initial resistance value of MFC). This pH is close to the optimal pH for the growth of the electrogenic microorganisms [79], [80]. When external resistance was increased over 2200 Ω, the pH decreased to 5.8. These results indicate that the acidogenic processes are improved when the external resistance surpasses the internal resistance2200 Ω. Subsequently, in the reverse scan, as the external resistance decreased from 3300 Ω to 120 Ω, the pH remained in the acidic range, which is not within the optimal range for electrogenic microorganisms. This behavior may

be attributed to the proliferation of acidogenic microorganisms, which produce VFA through the acidogenic fermentation of the substrate, especially under conditions of higher external resistance compared to internal resistance. These results indicate an irreversible change in the population distribution during the direct scan, which was maintained even during the reverse scan. This hypothesis was ratified by the MALDI-TOF analysis previously performed, which identified the appearance of *Clostridium* microorganisms when the value of the external resistance overcame the value of the internal one. In the literature, Pinto et al. report that the development of an electroactive microbial culture may be achieved by external resistance. In this case, the value of external resistance needs to be under the value of the internal one. Because of that, the lower values of external resistance facilitate the electron transfer process, facilitating the development of the electrogenic culture [41]. In contrast, values of external resistance that are higher than internal ones facilitate the development of non-electrogenic cultures. The VFA released to the liquid bulk was analyzed to verify this hypothesis. Finally, in order to determine if the VFA generation caused the drop in pH, the effluent VFA concentration was determined. The analysis identified acetic and propionic acid as the main VFA in the anodic effluent. Figure 5.6 presents the VFA concentrations for each external load studied. The acetic acid concentration was very similar, about 0.8 mM, for all the external loads studied. The propionic acid concentration increased significantly from 0 to 0.6 mM as the external resistance was raised. A slight decrease in propionic acid concentration was noted when the external resistance was decreased. Consequently, there was an initial increase and subsequent slight decrease in VFA concentration, as depicted in Figure 5.6. The rise in VFA concentration and dissociation accounted for the observed pH drop [31].

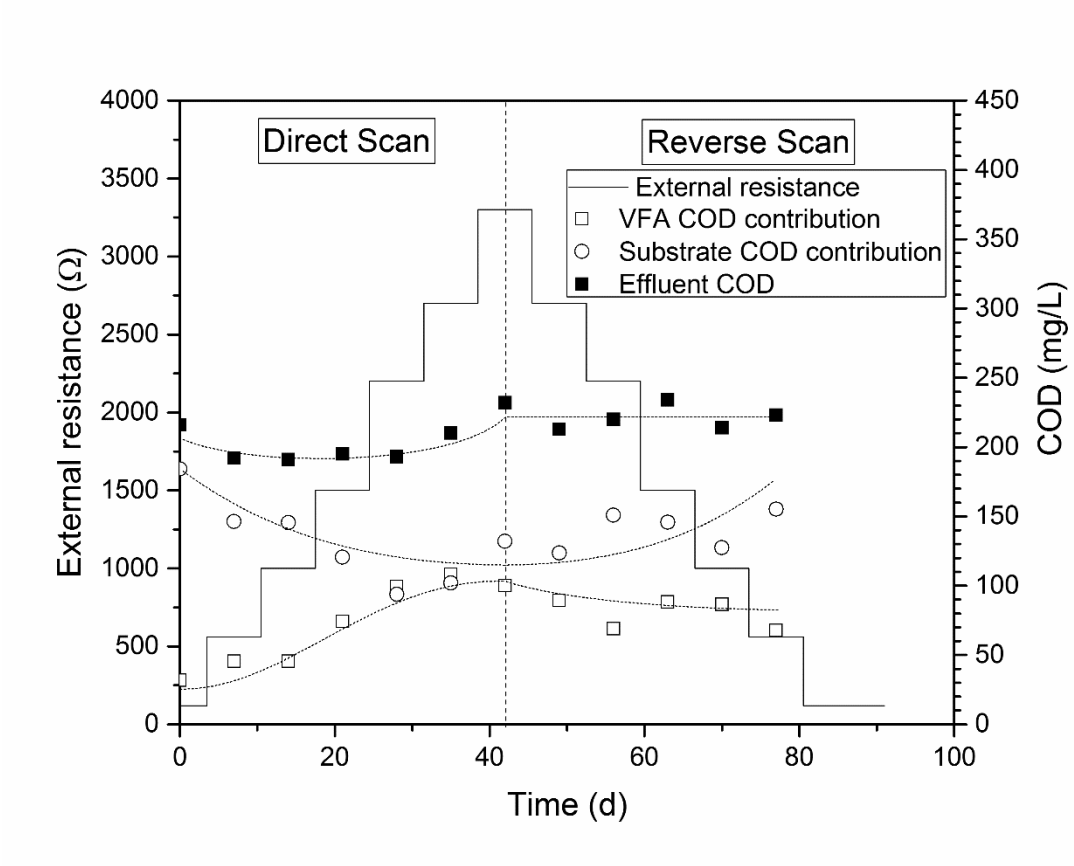

Figure 5.6 Acids COD, substrate COD, and total COD of effluent at every external resistance

Figures 5.5 and 5.6 show that increasing the external resistance promoted acidogenic metabolisms, leading to the growth of fermentative microorganisms without generating electric energy. According to Rismani-Yazdi et al., the total VFA concentration in the anolyte rose as the external resistance increased, reaching the highest concentrations when operating at maximum external resistance [37]. These observations were also previously reported by Picioreanu et al., which demonstrated that a higher external resistance, compared to internal resistance, encourages the proliferation of anaerobic microorganisms [42,43]. The shift from an electrogenic to a fermentative culture when the system operates under higher external resistances (higher than internal ones). This value electric parameter increased production of VFA indicates a. This shift can be explained by higher external resistance, making electron transfer to the anode more difficult, thereby reducing the electron transfer rate. This difficulty results in a lower growth rate of electrogenic microorganisms, which in turn leads to decreased current and electrical energy generation [21].

To determine the electrogenic and non-electrogenic contributions to fuel consumption in the MFC, we conducted a mass fuel balance based on COD measurements. We considered the influent COD, effluent COD, and the VFA COD contribution to the effluent to determine the net fuel consumption in the electrogenic and fermentative metabolisms. Figure 5.6 presents the different COD contributions as a function of external resistance.

Consequently, the effluent COD decreased as the external resistance increased (Figure 5.6). Specifically, when the external resistance was raised from 120 Ω to 3300 Ω, the COD of the effluent substrate dropped from 200 to 100 mg O_2/L due to the activity of fermentative non-electrogenic metabolisms. These metabolisms consumed a significant amount of COD while releasing VFAs, which contributed to the overall COD of the liquid bulk. Figure 5.6 also indicates that the VFA contribution to the effluent COD increases with the external load of the system. Therefore, it can be concluded that increasing external resistance results in higher VFA production and a lower effluent substrate concentration, attributed to the activity of non-electrogenic fermentative cultures.To assess net fuel consumption, the substrate removal rate was calculated, ranging from 3 to 4.5 mg/h, as the external resistance increased from 120 Ω to 3300 Ω. This rise is explained by the heightened non-electrogenic metabolic activity at higher external resistances. Consequently, the maximum pollutant removal from the MFC wastewater occurred at the highest external resistance. However, these conditions did not support the highest electric energy generation.

5.5. Conclusions

The results obtained from this Chapter allow us to draw the following conclusions. The external load significantly impacts the population distribution in the MFC. High external resistance causes the microbial population to evolve from a more electrogenic to a more fermentative culture. This shift in population distribution affects all operational variables and is primarily reflected in the current density, which decreased from 0.06 to 0.02 mA. Regarding power output, the system generally behaves as predicted by Jacobi's theorem, although the peak power production was achieved over a wide range of load resistances, from 1000 Ω to 3000 Ω, rather than being located at the point where external and internal resistances meet. Ultimately, in terms of fuel consumption, its value is practically independent of the external resistances, although a slight decrease was observed after operating with high external resistances.

6. TERMINAL VOLTAGE MODELING OF MICROBIAL FUEL CELLS

6.1. Introduction

MFCs enable the simultaneous energy extraction of the wastewater and the oxidation of the contaminants, which removes the pollutants. Recent publications demonstrate the strength and potential of this technology [81], demonstrating that the MFC technology could be used for commercial applications [6]. Moreover, a number of significant pilot MFC reactor treatment applications have been initiated in recent years. [82], [83], [84]. The MFC is at an early stage of development and requires special prototyping tools. The research results presented in this thesis aimed to investigate physical and electrochemical phenomena in MFC and their modeling. A future study proposed in this work is an original combined bioelectrochemical-electrical model of an MFC.

The MFC models can be classified into two main groups: mechanism-based models and application-based models [85]. Depending on the application area, the appropriate model is selected. Mechanism-based models are characterized by high accuracy, but multidimensional simulations of those models require high computing costs [86]. Application-based models aim to accurately predict the electrical response of the MFC through simplified representations of chemical and biological processes occurring within the MFC. Electrochemical models based on voltage-current characteristics (polarization curve) have been developed to simulate the continuous and batch modes of MFC operation [87]. These models include equivalent-circuit models, which represent the terminal behavior of the MFC and incorporate an ideal DC voltage source along with passive components [88].

The simple model consists of a fixed DC source (V_{int}) and a resistor (R_{int}). V_0 and i_0 represent the MFC terminal voltage and current values, respectively. The polarization test can be utilized to estimate the parameters of the model [89]. While this model effectively represents the steady state, it does not account for transient states induced by load changes [90], [91].

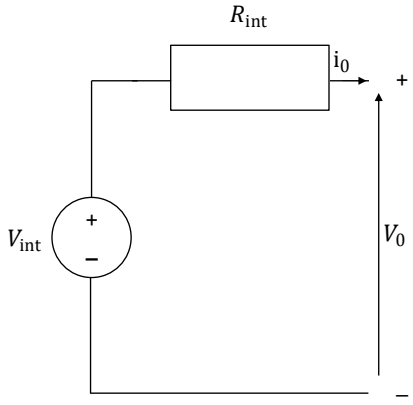

Figure 6.1 Simple equivalent circuit model of MFC

The Randles model comprises a fixed DC source (V_{int}), resistors representing ohmic loses (R_s) and charge transfer resistance (R_{ct}), a capacitor representing double-layer capacitance (C_{dl}), and

the Warburg impedance (Z_w), which represents the diffusion effect. Model parameters are typically estimated using impedance-frequency characteristics obtained through electrochemical impedance spectroscopy (EIS). However, for the EIS technique to yield accurate results, the modeled system should be steady [92], [93], which may not always apply to the MFC, especially in batch mode.

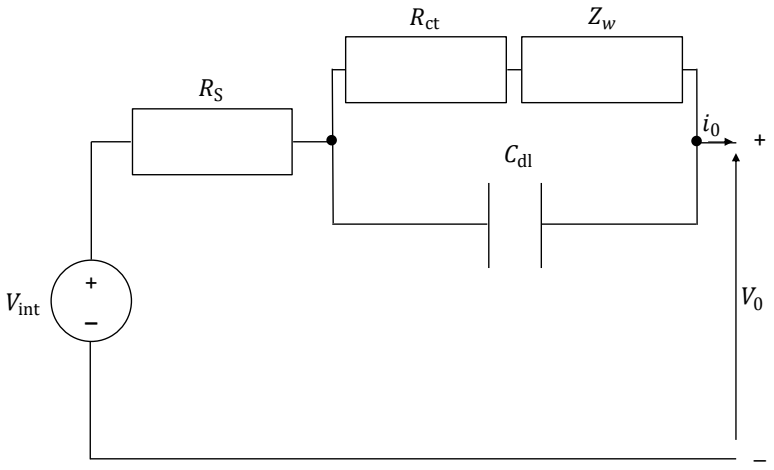

Figure 6.2 Equivalent circuit of Randles model of MFC

The Larminie-Dicks model, another equivalent circuit model used for modeling electrochemical devices [94], [95], [96], [97], is a simplified version of the Randles model. It consists of a fixed DC source (V_{int}), resistors (R_1), and a capacitor representing double-layer capacitance(C_{dl}) (omitting the Warburg impedance, with one of the resistors (R_2) assuming its role). A significant advantage of this model is that it enables parameter identification without relying on the EIS measurement technique [98]. This model is specifically designed to accurately describe the anodic electron flow and electric charge storage behavior of the MFC, particularly due to the MFC's capacitive energy storage nature. This behavior emerges from the biofilm on the working electrode, typically the anode. During MFC operation, the biofilm generates, accumulates, and releases electric charge, a process directly linked to the metabolic production of electrons by bacteria [99], [100], [101].

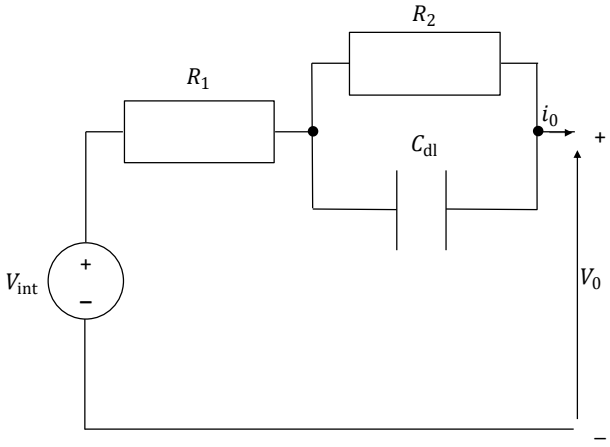

Figure 6.3 Equivalent circuit Larminie-Dicks model of MFC

The effectiveness of MFCs may be influenced by the bacterial community, as well as the specific parameters of the applied load and the medium used. To ensure an accurate representation of operational conditions, it is important to carefully consider the model's structure, appropriate parameterization, and laboratory verification methods. Environmental variables, such as the chemical oxygen demand (COD) concentration, have a significant impact on MFC performance across a wide range of operating conditions [67]. The discussed models often overlook the impact of environmental variables, such as changes in fuel concentration and their influence on MFC performance. Moreover, the performance of MFCs can also be significantly affected by load variables, which are frequently neglected by the discussed models. As a result, a comprehensive analysis of these factors and their interrelationships is crucial for assessing MFC performance.

Another important factor is the coupling of the model between changes in electrical parameters and their impact on the non-electrical parameters of the cell. As previously mentioned (Chapter 5), the electrical load of the MFC influences the energy conversion efficiency. For this purpose, in the presented model, the decline in the kinetics of fuel concentration is coupled with the electrical efficiency of the MFC.

The proposed solution could be the combined bioelectrochemical-electrical model. In the literature, some ready-made solutions for models have already been presented in [102], but due to the multi-level nature of the model, it is not dedicated for real-time simulation. The reduced-order combined model proposed in this work can solve the balance between the accuracy of phenomena rendering and the real-time simulation inside the cell.

6.2. Objectives

This chapter proposes a reduced-order application-based model of the single-cell and multiple cells (connected in series and/or in parallel) in high current generation operational mode to solve the balance between the accuracy of rendering phenomena and the capability of real-time simulation. From this modeling work, the main static and dynamic parameters of the system were determined by means of the stationary batch operation of the MFCs. Additionally, to perform an accurate and scalable study, the MFC was loaded with a programmable electric load (a power source used for controlling load current and/or voltage) and a passive load in the form of resistors.

To estimate the parameters of the proposed model, the Voltage-Relaxation Method (VRM) was used. The novelty of the approach is the repetition of the VRM with relatively short time intervals between each step. The parameters of the model have been divided into static parameters, such as the OCV, and dynamic parameters, like internal resistance (Ri) and diffusion resistance (Rd). The tests were carried out at different fuel concentrations and COD levels as well as under different electrical connections (series and parallel) between multiple cells.

6.3. Model development

6.3.1. Model assumption

In order to ease the model proposed in this work, the following assumptions have been made in accordance with previous literature studies [52], [67], [87], [103], [104], [105]:

- The influence of temperature on the OCV was considered negligible.
- The external load impact on the biofilm development and energy recovery were considered negligible.
- The effect of high COD concentration on MFC performance was neglected (at levels significantly lower than the toxic concentrations).
- High-frequency operational (more than 1 kHz) behavior is omitted.
- Internal ohmic resistance (Ri) and diffusion resistance (Rd) were assumed to be constant for the fuel concentrations studied.
- The anolyte and catholyte pH changes on MFC performance were considered negligible and, therefore, were not taken into account.

6.3.2. Equivalent circuit and model equations

As stated above, the balance between the accuracy and simplicity of the model is of crucial importance. Because of that, an example of such a compromise was proposed in this work. The equivalent circuit is presented in Figure 7.1.

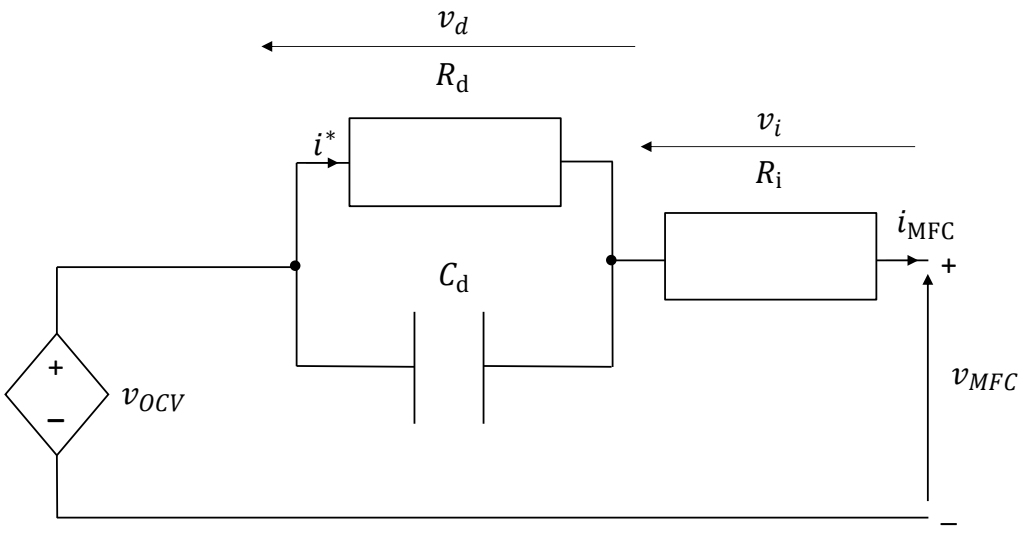

Figure 6.4 Equivalent circuit proposed for the MFC description

The following equation was proposed for the description of the voltage output by the MFC during the studies (equation 7.1).

$$v_{MFC} = v_{OCV} - v_d - v_i, \tag{6.1}$$

Where: v_{OCV} is the open circuit voltage (algebraic symbol for the OCV), v_d the diffusion voltage drop, and v_i is the ohmic voltage drop between electrodes.

The OCV represents non-loaded and electric stabilized MFC terminal voltage; this value is a time function that depends on the standard potential of the MFC and on the COD concentration. The dependence of OCV on the COD can be expressed by an appropriately adapted battery equation of [2], that is:

$$v_{OCV} = E_{0m} + A \cdot e^{-B \cdot S_{COD}(t)} - k \cdot J\left(\frac{1}{S_{COD}(t)} - 1\right), \tag{6.2}$$

Where: E_{0m} is the constant voltage in this study case is the value of v_{OCV} for fuel with COD concentration 1000 mg/L, pH 7 at standard ambient temperature and pressure, A and B are parameters of the exponential zone voltage, k is the polarization constant, J is the MFC current at the maximum power point, and $S_{COD}(t)$ is the estimated COD concentration value.

The diffusion voltage drops expressed the transition state of MFC. The impact of the MFC diffusion on the MFC voltage is represented by a voltage drop across the diffusion capacitance and diffusion resistance. This can be expressed as a product of the filtered component $i^*$of the load current and the diffusion resistance, that is:

$$v_d = R_d \cdot i^*, \tag{6.3}$$

with

$$i^* = i_{\mathrm{MFC}} - \tau \frac{\mathrm{d}i^*}{\mathrm{d}t} = i_{\mathrm{MFC}} - R_{\mathrm{d}} C_{\mathrm{d}} \frac{\mathrm{d}i^*}{\mathrm{d}t} \tag{6.4}$$

where i_{MFC} is the terminal MFC current, τ is the MFC diffusion time constant, R_{d} is the diffusion resistance, and C_{d} is the diffusion capacitance.

The ohmic voltage drop corresponds to the internal resistance R_{i} is:

$$v_i = R_i \cdot i, \tag{6.5}$$

Where: R_i is internal resistance in Ω and i is the MFC current.

In order to facilitate the modelling process, the evolution of COD over time is determined using combined COD evolution model. The model equation presented here is based on unstructured kinetic models presented in [106]. The COD evolution model incorporates the growth kinetics of microorganisms, the consumption of organic substrates, and the influence of external loads. The COD evolution model is as follows

$$S_{\mathrm{COD}}(t, \eta_{\mathrm{MFC}}, i_{\mathrm{MFC}}) = S_{\mathrm{COD}}(t_0) \cdot e^{(-b(\eta_{\mathrm{MFC}}, i_{\mathrm{MFC}}) \cdot t)} \tag{6.6}$$

where $S_{\mathrm{COD}}(t_0)$ is the initial COD concentration, S_{COD} is the COD concentration over time t, b is the COD removal rate for the given energy conversion efficiency η_{MFC} and MFC current i_{MFC}.

The η_{MFC} efficiency is defined as

$$\eta_{\mathrm{MFC}} = \frac{W_{\mathrm{external}}}{W_{\mathrm{internal}} + W_{\mathrm{external}}} = \frac{W_{\mathrm{external}}}{W_{\mathrm{total}}} \tag{6.7}$$

where W_{external} and W_{total} are the energy transferred to the load and the total energy supplied by the MFC (including the internal losses), respectively.

W_{external} and W_{internal} are defined as

$$W_{\mathrm{external}} = \int_{t_0}^{t} i_{\mathrm{MFC}} \cdot v_{\mathrm{MFC}}\, \mathrm{d}t \tag{6.8}$$

$$W_{\mathrm{total}} = \int_{t_0}^{t} i_{\mathrm{MFC}} \cdot v_{\mathrm{OCV}}\, \mathrm{d}t \tag{6.9}$$

The evaluation of b is outlined in the next section

6.3.3. Model parameters estimation techniques

To estimate the parameters of the proposed model, the Voltage-Relaxation Method (VRM) described in [107]. VRM is used to determine the relationship between the open-circuit voltage (OCV) of an unloaded and relaxed electrochemical battery and its state of charge (SoC). This method can also be applied to microbial fuel cells (MFCs) due to certain similarities between MFCs and electrochemical batteries, specifically in how ion concentration changes during redox reactions. These changes lead to corresponding variations in OCV in both types of systems. Hence, it is reasonable to adapt the VRM method for estimating the electrical parameters of MFCs. Additionally, VRM enables the approximation of the relationships between electrical and environmental parameters across a wide operating range of MFCs. To monitor voltage recovery and estimate MFC electrical parameters, the MFC load can be disconnected in a controlled manner, or its value can be reduced to a negligible level. Furthermore, when the MFC terminals are open, the bioanode can accumulate charge and exhibit its internal capacity [108], [109].

The novelty of this approach is the repetition of the VRM with relatively short time intervals between each step and the low-frequency resolution of measurements (0.01 Hz). The following test scenario was used during the VRM tests: the starting point was a change of medium in the anode and cathode after the MFCs had operated 5 min under external electrical load ($I_{MFC} = 2\,mA$). The next step was to open the circuit for 1 hour, record the OCV value, and calculate Ri, Rd, and Cd. After the records of OCV, the MFCs were operated 4 hours under external electrical load ($I_{MFC} = 2\,mA$), and again the circuit was open 1 hour to record of OCV value and calculate Ri, Rd, and Cd. The used scenario is presented in Figure 6.5.

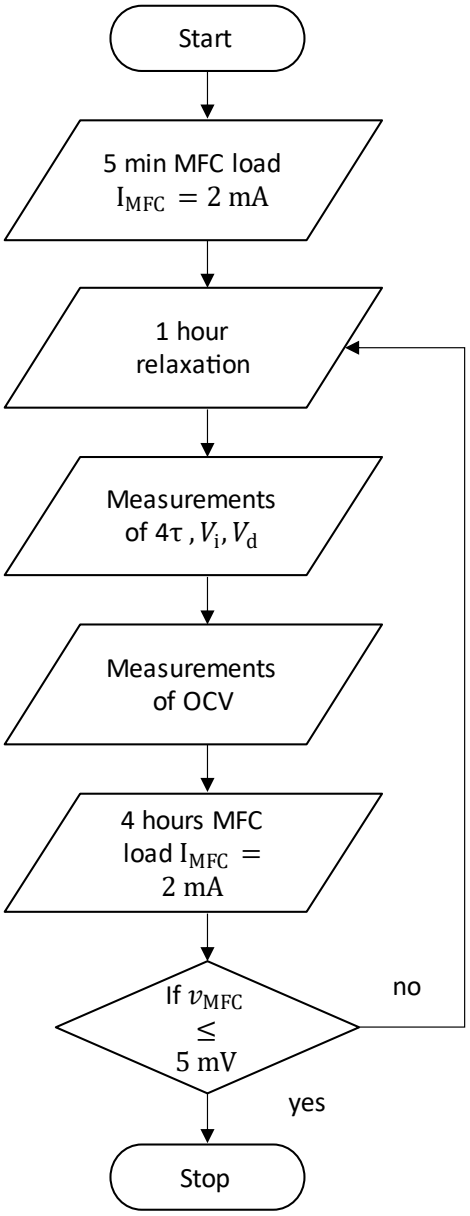

Figure 6.5 VRM test operational scenario

Because asymmetric nature of the MFC voltage curve, for load and non-load cells, the model´s parameters were divided into two groups: static parameters, based on function OCV(COD), and dynamic parameters, like ohmic and diffusion resistance ($R_i$and R_d) and diffusion capacitance (C_d). The tests were carried out under different levels of COD concentration. This testing methodology was previously described in the literature [2], [107], [110, p. 1] for batteries, but due to the convergence of the cell operation mode, the mathematical description of the battery was adapted to the expression of the MFC operation mode. The Ri, Rd, and Cd were estimated based on VRM for different COD values. Moreover, for the OCV measurements, the voltage points after 60 min of relaxation time were recorded. The dynamic coefficients Ri, Rd, and Cd were calculated as follows equations 7.10, 7.11, 7.12:

$$\mathrm{R_i} = \frac{V_\mathrm{i}}{I_\mathrm{MFC}}, \tag{6.10}$$

$$\mathrm{R_d} = \frac{V_\mathrm{d}}{I_\mathrm{MFC}}, \tag{6.11}$$

$$\mathrm{C_d} = \frac{\tau}{R_d}, \tag{6.12}$$

where V_i is the value of v_i determined immediately after applying external load current $i_\mathrm{MFC} = I_\mathrm{MFC}$ and V_d is the value of v_d determined after applying this load current over time equal to the diffusion time constant τ, V_i, V_d and I_MFC are quantities evaluated from the VRM test, as shown in Figure 6.6.

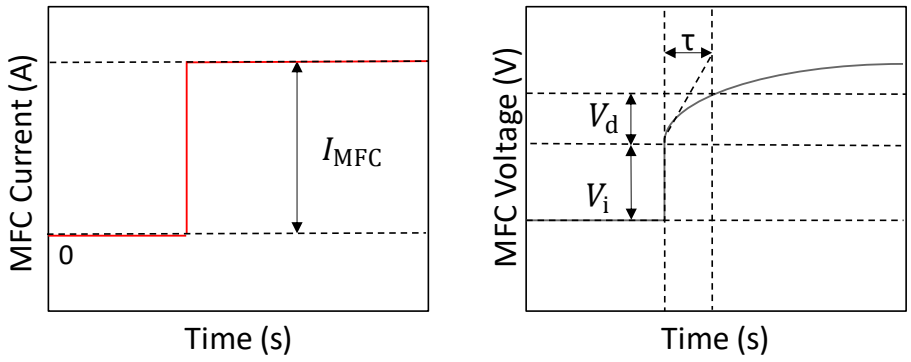

Figure 6.6 Voltage waveform during the VRM used for parameter calculation

The VRM test is used as a reference test to establish a baseline performance of MFC by measuring the time it takes for COD to be removed from the MFC chamber under the known external load. The concentration of COD during the test can be quantified using the COD evolution model.

$$S_{\mathrm{COD_{ref}}}(t_{ref}, \eta_{\mathrm{MFC_{ref}}}, i_{\mathrm{MFC_{ref}}}) = S_{\mathrm{COD_{ref}}}(t_0) \cdot e^{(-b_{ref}(\eta_{MFC_{ref}}, i_{\mathrm{MFC_{ref}}}) \cdot t_{ref})}, \tag{6.13}$$

where the COD removal rate is b_ref. The latter quantity can be determined by performing curve fitting using the nonlinear trust-region least-squares method based on the following measured values: the COD concentration of MFC for known time of experiment (t_{ref}), the MFC current during reference test $(i_{\mathrm{MFC_{ref}}})$, and the energy conversion efficiency during that test $(\eta_{\mathrm{MFC_{ref}}})$, and calculated as eq.

Assuming that b is proportional to the average MFC current (i_{MFCav}), and inversely proportional to the energy conversion efficiency, η_MFC, it can be evaluated as

$$b = b_\mathrm{ref} \cdot \frac{\eta_{\mathrm{MFC_{ref}}}}{\eta_\mathrm{MFC}} \cdot \frac{i_{MFCav}}{i_{MFCav_{ref}}}, \tag{6.14}$$

The i_{MFCav} and the average MFC current during reference test $i_{MFCav_{ref}}$ are calculated as

$$i_{\mathrm{MFCav}} = \frac{1}{t - t_0} \cdot \int_{t_0}^{t} i_{MFC}\, \mathrm{d}t, \tag{6.15}$$

6.4. Laboratory setup and test methodology

6.4.1. Experimental setup

The experiments were conducted by using two-chamber MFCs with an anodic and cathodic compartment volumes of 100 ml each. The anodic chamber of MFC hosed carbon felt (KFA10, SGL Carbon Group) electrode, which had a volume of $9\ cm^3$. The cathodic electrode was based on Toray carbon papers TGPH-120 (E-Tek, USA) and had an active area of $9\ cm^2$. On the surface of the cathodic electrode was deposited a layer of $0.5\ \frac{mgPt}{cm^2}$ and was doped with 5% Nafion® solution according to the procedure described in the literature [111], [112]. Stainless steel wires connected the electrodes of MFCs to the externally controlled electrical load. The experiments were performed under steady-state conditions at a temperature of $25℃$. For the sake of reproducibility, three replicates of the MFC were operated.

The anodic chamber was supplied with synthetic wastewater as fuel, whereas the cathodic chamber hosed a solution of Na_2SO_4. A PEM of Nafion® (PEM, Nafion 117, DuPont) was used to separate anodic and cathodic chambers. Figure 6.7a shows a schematic view of a single MFC, and Figure 6.8 shows a schematic view of series and parallel connections during the experiment.

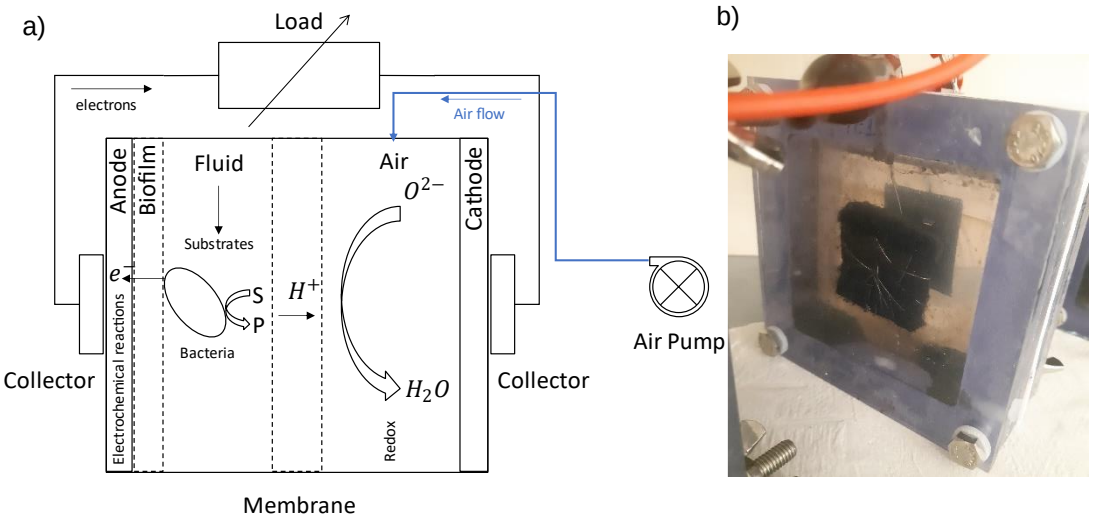

Figure 6.7 MFC experiment setup single-cell a) schematic view b) laboratory view

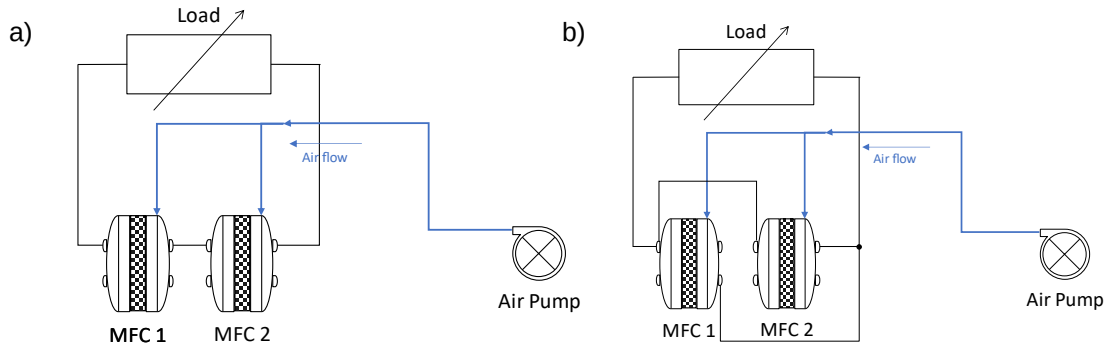

Figure 6.8 MFC experiment setup: a) series connection, b) parallel connection

6.4.2. Microorganisms and wastewater

The MFCs were operated on with a biotic anode and an abiotic cathode. The anodic compartments of the MFCs were inoculated with an anaerobic mixture. The synthetic wastewater used in this work consisted of microbial culture from domestic wastewater active sludge from the Ciudad Real WWTP. The anolyte sterile synthetic medium consisted of CH_3COONa , Na_2HPO_4 3, $(NH_4)_2SO_4$, KH_2PO_4 , $MgCl_2$, $CaCl_2$, $(NH_4)_2Fe(SO_4)_2$ prepared as previously described in [113]. The composition of the synthetic wastewater with components concentration is included in Table 6.1.

Table 6.1 Composition of the synthetic wastewater fed as fuel

Component	Concentration (mg dm^{-3})
CH_3COONa	1000
Na_2HPO_4	3000
$(NH_4)_2SO_4$	800
KH_2PO_4	700
$MgCl_2$	93.07
$CaCl_2$	30.70
$(NH_4)_2\ Fe(SO_4)_2$	28.95

Each test had an anolyte pH of 7.5 and a conductivity of about 5.7 mS/cm. The cathodic chamber hosed 100 ml solution of 4 mg/L of Na_2SO_4 with pH 6.5. Before performing the tests, the anodic chamber was filled with activated sludge with the aim to follow the inoculation procedure described in the literature [113]. In the following 2 days, 50% of the volume was replaced by fresh active sludge with synthetic wastewater. After the inoculation stage and preliminary acclimatization of electrogenic bacteria, MFCs were operated under semi-continuous mode. Because of that, 80% of the volume of anolyte and all catholyte were replaced by fresh synthetic wastewater every 2 days. As reported by previous studies, the readiness of the MFC can be assumed when OCV is at the level of 0.7 V [114]. This procedure was repeated 7 times until the steady state was reached. The characteristic power curve presented a peak power of 1.4 mW in the steady state. In order to ensure anodic conditions after feeding the anodic chamber, this chamber was purged with nitrogen gas before the beginning of each batch cycle. The anolyte and catholyte were homogenized by means of magnetic stirring.

6.4.3. Analytical measurement

Sodium acetate concentration was determined by means of high-performance liquid chromatography (HPLC) analysis using an Agilent 1260 Infinity equipment containing a column Hi-plex H (300×7.7 mm, 8 μm). The mobile phase used was $5\frac{mmol}{L}H_2\ SO_4$. The wavelength was 210 nm, and the flow rate was 0.4 mL/min . More details can be found elsewhere [34]. COD concentration in the wastewater fed as fuel to the anodic chamber was indirectly determined by taking into account the stoichiometric relationship between the acetate and the COD concentrations in mg/L, this equation is presented in equation 7.7.

$$S_{COD}(t) = \mathrm{CH_3\ COONa} \cdot 1.07, \tag{6.16}$$

where: S_{COD} is the chemical oxygen demand in mg/L, $\mathrm{CH_3\ COONa}$ is the sodium acetate concentration in mg/L.

6.5. Results and discussion

6.5.1. Microbial fuel cell performance analysis

The main reaction at the anode of the MFC was the oxidation of the sodium acetate, as it was the sole biodegradable organic substrate in the anodic chamber. This is an exo-energetic reaction that allows the oxidation of the organic substrate of the medium with the simultaneous release of protons and electrons. Then, these protons and electrons were combined with oxygen at the cathode to generate water and electrical current.

In order to characterize the MFC performance, polarization curve were performing using varying the external resistance by using an Autolab potentiostat/galvanostat (PGSTAT-302N). To ensure an accurate measurement of the OCV, the external load was disconnected from the circuit at least 1 hour before performing the polarization test.

Figure 6.9. shows the polarization and power curves of MFC when operating at different COD values of the fuel (at COD_1 = 847 mg/L, COD_2 = 365 mg/L, COD_3 = 124 mg/L). Parallel to the changes in the anodic COD concentration, anodic medium acidification was observed due to the generation of protons due to the oxidation of the sodium acetate used as fuel (pH_1 = 7.5, pH_2 = 6, pH_3 = 5). The relationship between the pH reduction and the acetate consumption was confirmed by HPLC analysis, in which it was observed that the sodium acetate concentration decreased along with the experiment. Similar results have been described in the literature [46]. The limiting currents owning to mass transfer for different COD (COD_1, COD_2 COD_3) values were reached at the pick $i_{max_1} = 6.978\ mA$, $i_{max_2} = 3.707\ mA$, $i_{max_3} = 0.027\ mA$.

Figure 6.9 reports changes in cell voltage and power at different COD values. As can be seen in this figure, the maximum OCV value reached was around 0.71 V, the maximum current reached 6.978 mA, and the maximum power was 1.46 mW. Taking into account that the objective was to favor the continuous constant current work of MFCs, an additional task was to identify a good balance between power generation and fuel consumption, in this case, sodium acetate contained in the synthetic wastewater. In order to avoid instabilities, the author decided to limit current values for the VRM test from polarization and power curves to 0.3 of maximum value (i_{max}). The equation 6.17 was used to determine the load current of MFC for the VRM test to avoid unexpected voltage drops and ensure stable system performance.

$$i = i_{max} \cdot 0.3, \tag{6.17}$$

where: i is MFC current in A, i_{max} is a maximum current peak in A.

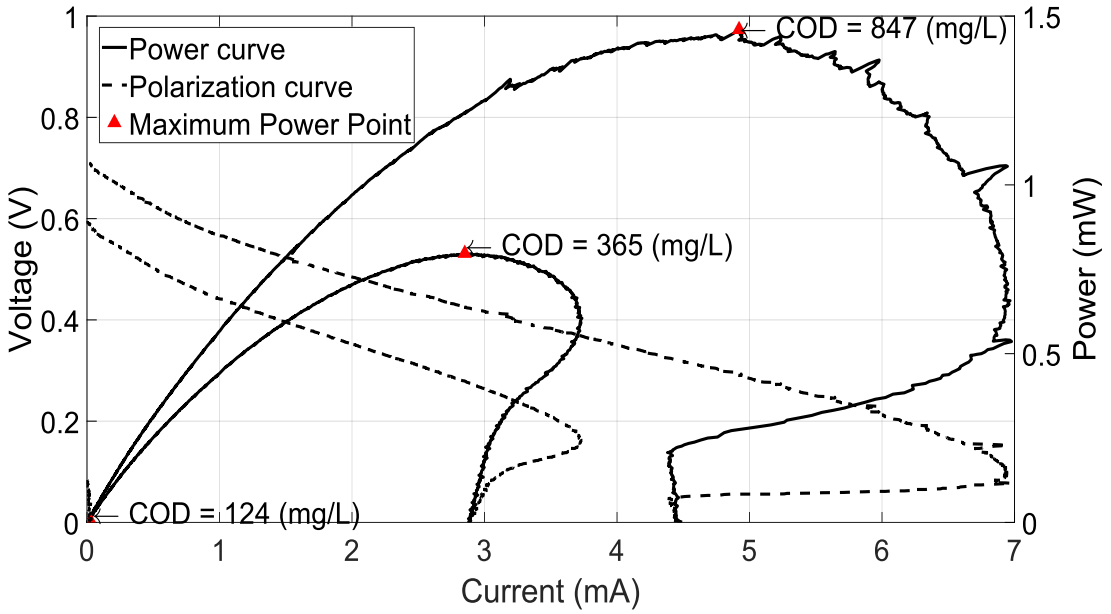

Figure 6.9 MFC single-cell power curve and maximum power point for different COD values

6.5.2. *Model parameters calibration*

Experimental data were used for calibration works, and the values of the model parameters were obtained. Figure 6.10 presents measured resistances of MFC R_i and R_d corresponding to different COD values. The experiment results show that the correlation between COD and resistances is negligible (R_i and R_d). Because of the lack of correlation, the author decided to approximate the resistances (R_i,R_d) as constant independent from COD. The estimated value of R_d was equal to 117.05 Ω and was a similar value presented in [115].

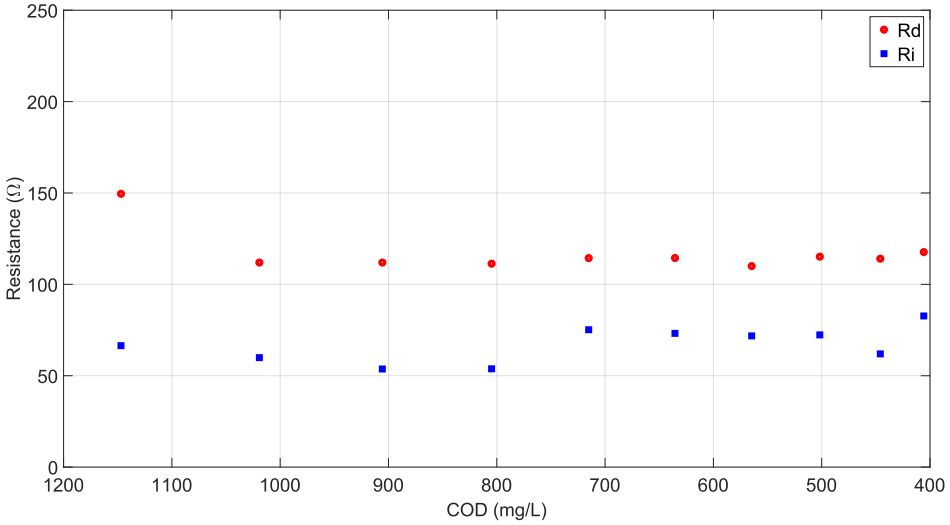

Figure 6.10 Ohmic and diffusion resistance of a single-MFC

In addition to the parameters explicitly displayed in Figure 6.4, the parameters utilized to model the OCV (cf. eq. 6.2) have to be evaluated. To evaluate the OCV model parameters (cf. eq. 6.2), curve fitting using the nonlinear trust-region least-squares method (Matlab R2020b, MathWorks, Natick, MA, USA) based on the OCV test voltage data points is necessary. The findings of the

measurements and curve fitting for v_{OCV} can be found in Figure 6.11, depicting the correlation between the COD and the OCV of the MFC during the OCV test. Estimating the changes in COD value that occurred during the batch cycle was imperative for determining the COD removal rate of the model (parameter b_{ref} in eq. 6.14). The evolution of COD was established through HPLC analysis, and the results of this analysis, along with the corresponding calculations using eq. 6.16, can be seen in Figure. 6.12. The estimated model parameters of OCV (eq. 6.2) and COD (eq. 6.6) are presented in Table 6.2.

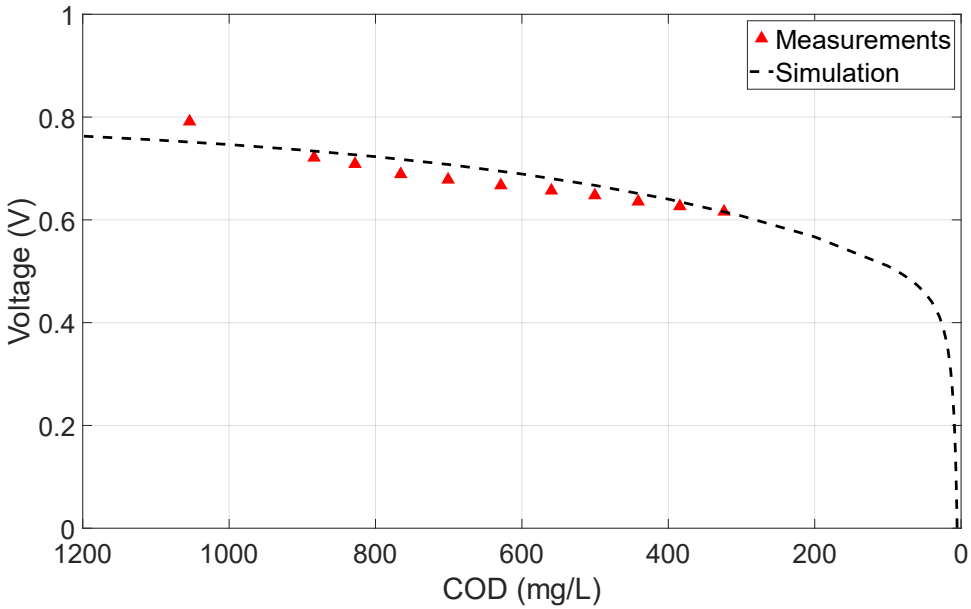

Figure 6.11 The OCV of a single MFC during the OCV test

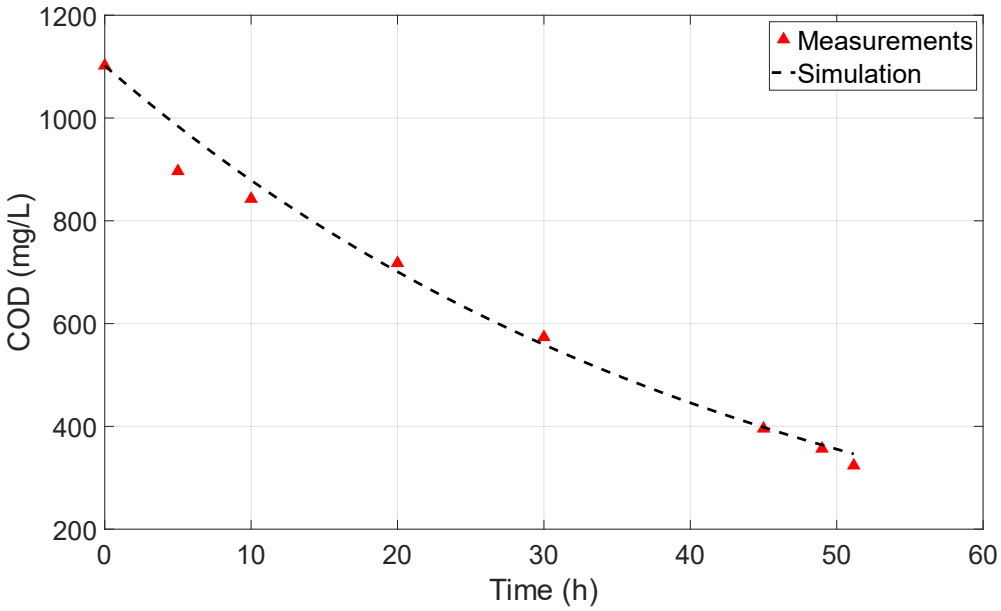

Figure 6.12 The COD evolution of the MFC during the simulation and measurements

Table 6.2 Values of the estimated parameters

Symbol	Value	Unit
$E_{0\mathrm{m}}$	0.80	V
A	0.3192	V
B	1.945	1/A
k	0.5408	1/A
J	0.004921	A
τ	1200	s
i_{ref}	0.001604	A
$\eta_{MFC_{\mathrm{ref}}}$	0.5165	-
b_{ref}	$7.95 \cdot 10^{-6}$	1/s
t_{ref}	$18 \cdot 10^{4}$	s

6.5.3. Model validation for single-cell

The model validation was performed by using data sets from three distinct configurations: The validation was conducted using three configurations a single MFC unit, a series connection of two MFC units, and a parallel connection of two MFC units.

Figures 6.14a and 6.14b present the voltage output and COD measurements corresponding to a single MFC unit (SU) that was exposed to a distinct load scenario than the one used. The solid lines correspond to the simulation results obtained with the model proposed in this Chapter. As can be seen in Figures 6.14a, accurate predictions of the voltage were obtained when operating with a single cell. The evolution of the COD concentration, the modeling results, and the experiment are presented in Figure 6.14b. In Figure 6.14b it can be seen a very good model prediction of the COD evolution. The root mean square error (RMSE) was used to assess the model quantitatively. The RMSE is calculated as:

$$RSME_V = \sqrt{\frac{\sum_{i=1}^{n}(V_{model} - V_{meas})^2}{n_m}} \cdot 100\%, \tag{6.18}$$

where: V_{model} is MFC voltage calculated by the model, V_{meas} is MFC measured voltage, n_m is the number of measurements

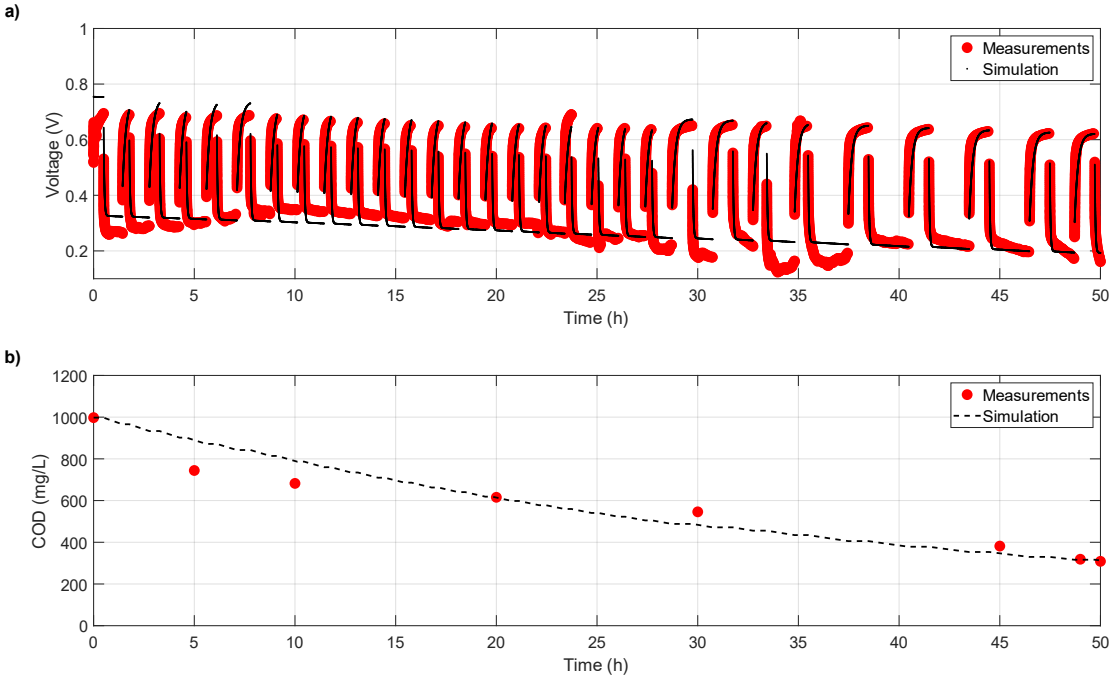

Figure 6.13 Single MFC experimental data and simulation results during VRM test: a) voltage, b) COD evolution

The parameters for the SU equivalent circuit of the proposed model were in the average as follow $R_{i_{SU}} = 54.5380\ \Omega$, $R_{d_{SU}} = 159.3841\ \Omega$ and $C_{d_{SU}} = 1.88\ \mathrm{F}$. The model presents accurate results for the transition state studied for single MFC, being the average relative model error of about RSME = 2.88%. It is important to note that the MFC does not reach a steady state during the unload periods, meaning the output voltage stays below the OCV value. In contrast, the proposed model accurately reflects this behavior. Figure 6.14b shows that the simulation results became more accurate with each subsequent COD concentration sample compared to the measurements.

6.5.4. Model validation for two cells connected in serie

The validation experiment was conducted with two identical MFC units connected electrically in series. The test bench configuration is presented in Figure 6.15a. Regarding to the electric conditions, the load current was equal $i = 2mA$. Figure 6.15b illustrates the simulated and experimental results of COD evolution. The data points labeled "Measurements 1" and "Measurements 2" correspond to the individual MFC units used in this experiment. The initial COD concentration was 1067.5 mg/L.

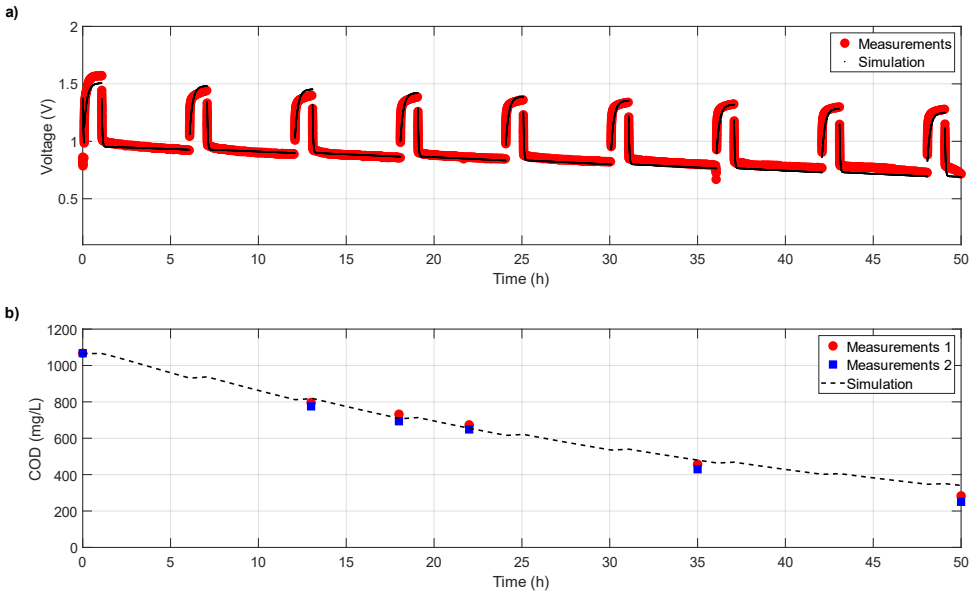

Figure 6.14 MFC stack (2 units connected in series) experimental data and simulation results during VRM test: a) total voltage, b) COD evolution

The combined resistances of the stack were $R_{i_{2S}} = 66.5380\ \Omega$ and $R_{d_{2S}} = 210.5833\ \Omega$, while the combined capacitance was $C_{d_{2S}} = 1.42\ \mathrm{F}$.

The voltage RMSE for MFCs connected in series were recorded at 3.96%. Similar to previous tests, the simulation results exhibited improved accuracy with each subsequent chemical oxygen demand (COD) concentration sample. These findings once again validate the reliability of the proposed model, demonstrating its consistent and precise performance.

6.5.5. Model validation for two cells connected in parallel

The experiment was conducted with 2 identical MFCs connected electrically in parallel with the bench configuration presented in Figure 6.8b. Regarding to the electric conditions, taking into account that two MFCs were connected parallel and each one output an electrical current ($i = 2\ \frac{mA}{cell}$) the load current was equal $i = 4\ mA$. As in the case of the cells connected in series, the cells connected parallel did not present voltage drops as a side effect of high current operational mode.

Figure 6.16a, presents the simulated and experimental voltage waveforms of two MFC units connected in parallel. In Figure 6.16b, the simulated and experimental results of Chemical Oxygen Demand (COD) evolution are presented. The initial COD concentration was 1048.2 mg/L. The data points labeled "Measurements 1" and "Measurements 2" correspond to individual Microbial Fuel Cell (MFC) units used in this experiment.

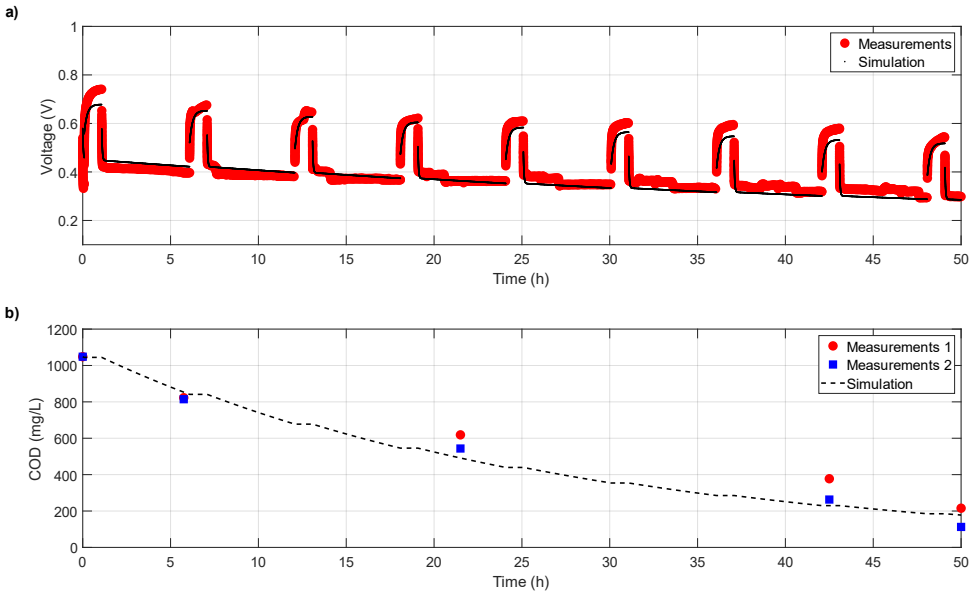

Figure 6.15 MFC stack (2 units connected parallel) experimental data and simulation results during VRM test: a) voltage, b) COD evolution

The total resistance for the parallel connection was calculated to be $R_{i_{2P}} = 99.4237\ \Omega$ and $R_{d_{2P}} = 131.6545\ \Omega$, while the combined capacitance was $C_{d_{2P}} = 2.28\ \mathrm{F}$. The RMSE of the voltage was calculated to be 2.35%, which indicates that the proposed model is well-behaved and has satisfactory accuracy. During the experiment, it was observed that the removal of COD varied among the individual MFCs, as shown in Figure 6.16b. It was also noted that when connected in parallel, the currents did not divide equally, which could potentially impact the overall performance of the MFC and the COD removal process. The model was able to predict an average fuel concentration value, which was the arithmetic mean of the COD concentration from MFCs.

6.6. Conclusions

This chapter presents an equivalent-circuit model of the MFC and outlines a methodology for evaluating its parameters. The model facilitates the analysis of MFC behavior, including transient states, under varying operating conditions. Initial tests have validated its applicability for examining multiple-unit MFC connections.

The proposed model introduces and leverages the dependency of OCV on the COD. The methodology for parameterizing the model is rooted in the VRM, originally employed for electrochemical batteries.

The studies conducted for model validation offer deeper insights into the impact of COD on the electrical characteristics of the MFC and the reciprocal effect of electrical quantities on COD removal efficiency. The efficacy of the proposed model was gauged using the RMSE to fit against experimental results. The calculated RMSE for individual MFCs was 2.88%, while for series and parallel connections, it stood at 3.96% and 2.35%, respectively. These results signify the satisfactory accuracy of the proposed modeling.

7. DIFFERENT OPERATIONAL STRATEGIES FOR CONTINUOUS ELECTRIC ENERGY GENERATION OF MICROBIAL FUEL CELL

7.1. Introduction

Many works have focused on experimental evaluation of the influence of different parameters, including structural and operating, on MFC performance. One can distinguish the following elements from the structural parameters: electrode material and their configurations. The operational parameters are temperature, fuel type, fuel concentration, HRT, pH, electric load voltage, and electric load current [87], [116].

The electrical parameter, the external electric load value, current, voltage, ohmic losses, etc. can be identified [87], [103], [116]. Special attention is required for the external electrical load, particularly its type – whether it is variable or constant. This is because the electric load affects the electrical energy generation and fuel consumption ratio. The electrical parameters affect the metabolisms of the electrogenic microbial culture, including the composition of the bacteria population, the inoculation process, and kinetic reactions. [105]. The external electrical load can be classified into two subcategories: passive (the circuit with a resistor) and active (the circuit with a DC/AC or DC/DC converter).

Previous research on MFC energy harvesting and electrochemical performance has shown that external load variations affect its performance. The previous research used a resistor to investigate the effect of external electrical load on non-electrical parameters of MFC [91], [102], [104], [105], [117], [118], [119]. When changing the resistance, the current and voltage of the MFC also changed. This simplification in conducting the research meant that it was ambiguous to determine the effect of changing the current and changing the operating voltage of a cell on its efficiency. Another critical aspect to consider during the operation of an MFC is its ability to work continuously under electrical load. The proposed research investigates the possibility of flexible operational conditions change for different scenarios (intense electric energy generation, intensive wastewater treatment). Because of that, this research proposes to carry out experiments using MFCs loaded with an external programmable power load and resistive load.

Based on the OCV(COD) (Figure 6.11) and polarization curve (Figure 6.9), it was possible to prepare further tests to determine the relationship between the electrical operating parameters and the MFC performance. Due to the non-linear nature of the MFC, the relations between the electrical and non-electrical parameters are also highly non-linear. An additional factor that had to be taken into account, in particular during the operation of the MFC with a high value of generated current, is the MFC's incidence of voltage drops and, in some cases, even polarization changes. To avoid failure during the cell operation, selecting the appropriate values of the load power, current, and voltage output was necessary.

The preliminary study results (Chapter 5) showed the effect of passive external load and organic matter removal on MFC performance. The presented in this chapter research focused on analyzing the effect passive (resistive) and active load represented by electrical operating

parameters, especially voltage, current and power ratio load, on MFC performance, including energy generation, COD removal, CE, EE and continuity of work.

7.2. Objectives

The main goal of this chapter is to analyze the effect of the external load on the output parameters of electric power generation and (synthetic) wastewater purification level corresponding to COD removal of the MFC. The partial objectives were the following:

- Analysis of the performance of MFC related to the output voltage and current levels for the selected electric operating conditions, CE, EE, and COD removal rates;
- Evaluate the quality of the treated wastewater by studying the effect of passive and active loads on the MFC performance;
- Comparative analyses of the effect of different electric operational parameters on MFC performance were represented by CE, EE, and COD removal.

7.3. Materials and methods

7.3.1. Experimental research assumptions

The experimental study aims to investigate how external load affects the MFC under different electrical operating conditions. Unlike the tests in Chapter 5, for these tests, we used a cell model operating in batch mode. This helped to eliminate the influence of fuel flow-related phenomena, such as flow fluctuations and resulting fluctuations from the MFC output values (current and voltage). Additionally, the MFC underwent testing with constant current load, constant voltage load, constant power load, and constant resistive load. Various indicators like total energy generation, CE, EE, and COD removal were assessed to evaluate the impact of different electrical loads.

The simulation experiments were standardized to standard duration for a single batch mode to ensure consistent results. This research utilizes simulation techniques, and the cell model used in the experiments is based on the model outlined in Chapter 6.

7.3.2. Experimental setup

The main objective of this chapter is to analyze the relation between the bionic and electric features of MFC. This work results can be used to select operating points and choose an operational strategy between intense electric energy generation and intensive wastewater treatment. For this purpose, the MFC working under batch mode was used.

This work aims to analyze the phenomena inside the MFC, with particular emphasis on the change of electrical parameters and their impact on the MFC performance. Because of that, simulation tests were carried out with constant electrical parameters, including constant load current and operating voltage, constant power, and external resistance. In order to maintain

consistent results, the simulation experiments were set to a standard 50-hour duration for a single batch mode. Alternatively, the experiments were limited to the time when the MFC potential dropped to zero and reached the short-circuit state. The experimental setup used in this work consisted of MFC model with model parameters values introduced in Chapter 6. The simulation environment used in this work utilized Matlab R2024a (MathWorks, Natick, MA, USA) Simulink extension Simscape.

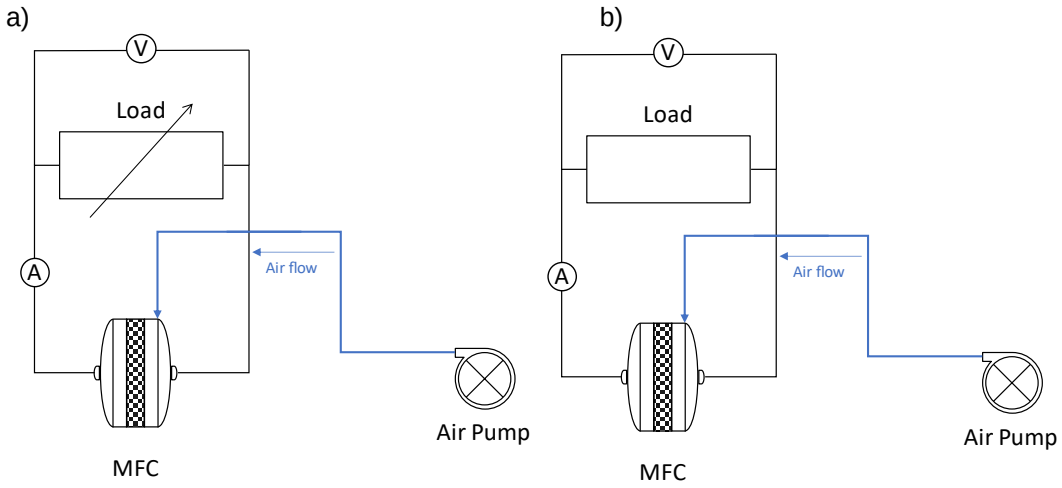

Figure 7.1 Experimental setup: a) MFC with varying active load, b) MFC with a passive electric load.

The following test scenarios presented in Figure 7.2 are used to analyze the electric scenario aims to provide comprehensive data on the electrical behavior of the MFC under specified conditions, contributing to maximizing EE or COD removal. Firstly, the type and value of the electrical load are selected for the experiment. The abbreviations CC, CV, CP, and CR presented in Figure 7.2 refer to constant current, constant voltage, constant power, and constant resistance load modes, respectively. Secondly, COD removal is calculated, and electrical measurements are taken at the terminals of the MFC. The experiment continues until one of the following conditions is met: the voltage at the MFC terminals drops to 5mV or less, or the total experiment duration reaches 50 hours. The experiment is terminated upon meeting either condition, and all logged data are saved for further analysis.

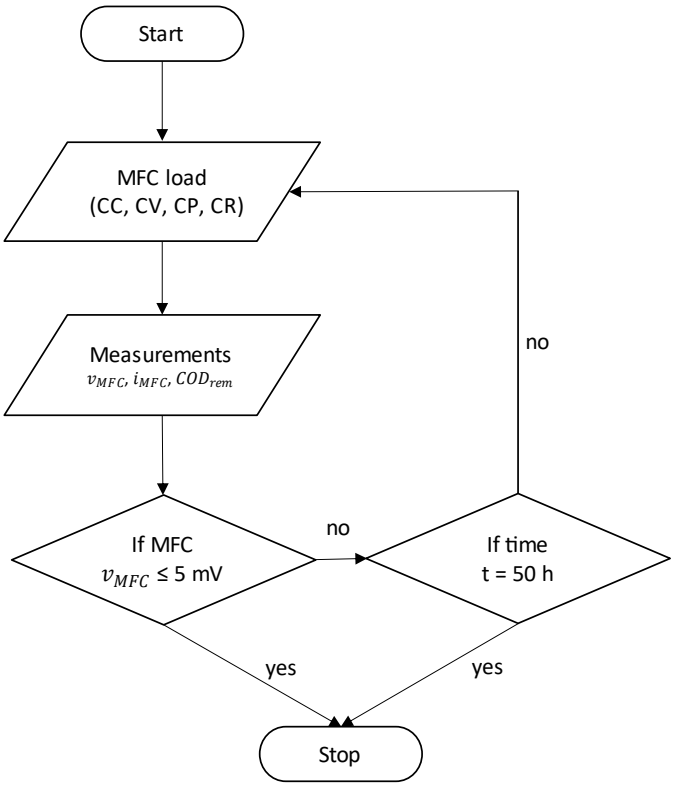

Figure 7.2 Experimental scenario

7.3.3. Coulombic and energy efficiencies

The CE (CE_a) is dependent on the anodic reaction of sodium acetate as reactant and electrons as product and can be calculated by equations 7.1, and 7.2, where: i_{MFC} is the current intensity in A, F is the Faradaic constant equal to 96,485.3 C/mol, n_i is the number of electrons participating in the electrochemical reaction per mol reactant, m_i is the molar variation of reactant in mol, V is the cell chamber volume of 0.1 L, ΔCOD is the change of COD over time.

$$\mathrm{CE_a} = \left(\frac{\int_0^t \mathrm{i_{MFC}dt}}{\mathrm{F\Sigma(n_i \Delta m_i)}}\right) = \left(\frac{\mathrm{M}\int_0^t \mathrm{i_{MFC}dt}}{\mathrm{F \cdot n_i \cdot \Delta COD \cdot V}}\right), \tag{7.1}$$

$$\mathrm{COD} = \mathrm{m_{CH_3COONa}} \cdot 1.07, \tag{7.2}$$

The EE (ε_E) describe the relation of energy conversion from potential chemical energy to the heat of combustion of the organic substrate to electric power generated by the MFC over a time interval, where ΔHac is the heat of combustion equal to 709.32 kJ/mol [120] and $\mathrm{M_{NaOAc}}$molar weight acetate equal to 82.034 g/mol,

$$\varepsilon_E = \frac{\mathrm{M_{NaOAc}} \int_0^t v_{MFC} \cdot \mathrm{i_{MFC}dt}}{\mathrm{\Delta H} m_i} = \frac{\mathrm{M_{NaOAc}} \int_0^t v_{MFC} \cdot \mathrm{i_{MFC}dt}}{\mathrm{\Delta H \cdot \Delta COD \cdot V}}, \tag{7.3}$$

7.3.4. Chemical oxygen demand removal efficiency and acetate concertation evolution

To evaluate MFC as a means to treat wastewater is important to measure COD. The percentage change of COD removal was assumed as the metric parameter to determine the qualitative degree of synthetic wastewater treatment during MFC operation. Equation 6.5 calculated the relative removal of wastewater [121], [122].

$$CODrem = \frac{S_{\mathrm{i}} - S_{\mathrm{e}}}{S_{\mathrm{i}}} \cdot 100\% \tag{7.5}$$

where: S_{i} and S_{e} stand for the influent and effluent COD concentrations, respectively.

7.4. Results and discussion

7.4.1. Performance of microbial fuel cell under constant-current regime external load

The operation of MFC can be effectively managed by selecting the appropriate electrical load. When controlling an MFC, MFC users consider three primary criteria: the percentage of wastewater purification, the amount of energy generated, and the operational work cycle of the MFC. Adjusting the electrical load allows for the maximization of these parameters, thereby enhancing the overall performance and efficiency of the MFC. By fine-tuning the load, users can achieve a desirable balance between wastewater treatment efficacy and energy generation while also controlling the work cycle (duration of batch mode) of the MFC. In this simulation test, the electrical load of the MFC varied from 0.25 mA to 3.5 mA.

The results of the load simulation in constant-current regime external load are summarized in Figure 7.3. The values presented in Figure 7.3 can be divided into those with an experiment duration 50 hours and those with an experiment duration of less than 50 hours. Due to the excessively high electric load values during the batch mode, the maximum current generated decreases as the fuel density drops. Consequently, all results for $\mathrm{I_{MFC}}$ Values greater than 2 mA are recorded for batch mode cycles that are shorter than 50 hours. For the experiment duration of 50 hours, the low energy generated values were recorded for the electric load of small values ($\mathrm{I_{MFC}} \leq 0.25$ mA) concurrently with the low CODrem rate (less than 11.7%) and the high EE value (more than 31%). For experiment durations less than 50 hours, the low energy generated values were recorded for high of electric load values ($\mathrm{I_{MFC}} \geq 2.5$ mA), concurrently with the lowest CODrem value and the highest EE value.

The highest generated energy value is observed for the electric load value of $\mathrm{I_{MFC}}$ = 1.36 mA, and for this load value, the EE value is 17.4%, and the CODrem value is 66%. More extended results, the electric load value of $\mathrm{I_{MFC}}$ = 1.36 mA presents Figure 7.4. The highest CODrem (95.2%) value was observed for $\mathrm{I_{MFC}}$ = 2 mA, and for this load value, the generated energy is 67.1 J with EE = 8.2%. The change in CE ranges from 6.7% (for a load current of 3.5 mA) to 42.6% (for a load current of 0.25 mA). Figure 7.3 was constructed based on a series of simulations similar to those in Figure 7.4.

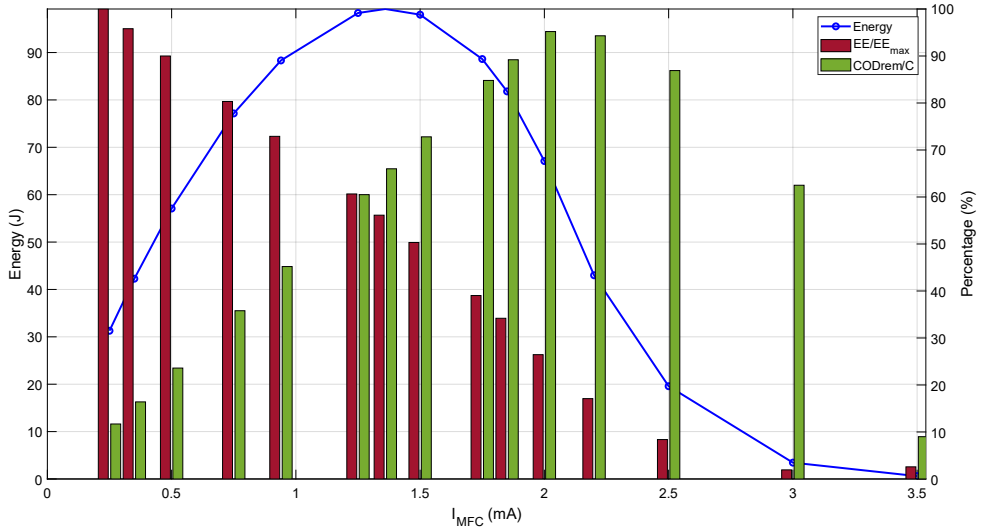

Figure 7.3 Summary of simulation results of microbial fuel cell under constant-current regime external load for different values of operational parameter

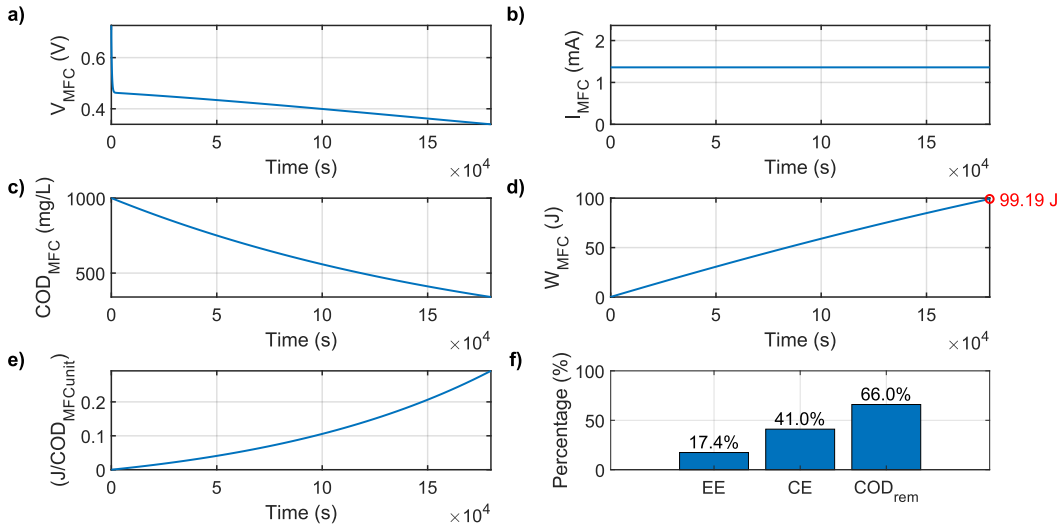

Figure 7.4 Simulation results of constant-current regime for MEP: a) voltage, b) electric current, c) COD evolution, d) energy increment, e) energy increment per COD unit f) efficiencies results

To achieve higher EE or CODrem while maintaining the criterion of maximizing generated energy, it should follow the described criterion. By reducing the assumed maximum value of generated energy by 10% from the theoretical maximum value, two operating points are obtained: one for a lower electric load value and one for a higher electric load value relative to the electric load for the maximum Energy Point (MEP). The point with the lower electric load value is characterized by higher EE efficiency and, thus, a lower CODrem value. Conversely, the point with the higher electric load value is characterized by lower EE efficiency and a higher CODrem value. Depending on the system requirements for the wastewater treatment process, an operating point can be chosen by selecting the appropriate MEP value based on maximizing either EE or CODrem.

In the case presented in Figure 7.3, MEP (99.19 J, 1.36 mA), two points are obtained after reducing the theoretical maximum energy by 10%. The first point is for the electric load current of 0.94 mA, which is characterized by higher EE (22.6%) and lower CODrem (45.2%) compared to the MFC operating at MEP. The second point is for an electric load current of 1.75 mA, which is characterized by lower EE (12.1%) and higher CODrem (84.8%) compared to the MFC operating at MEP. In the case of decreasing the electric load current, CODrem increases while simultaneously reducing the duration of the batch cycle. This is related to the electrical limitations of the MFC, reaching a short-circuit condition. This limitation forces a limitation on the current generated by the MFC.

7.4.2. Performance of microbial fuel cell under constant-voltage regime external load

Another type of active load discussed is the constant-voltage regime load of the MFC. Operating the MFC under an external load in a constant-voltage regime minimizes the risk of a short-circuit condition. Because of this, it can be said that the MFC can operate continuously throughout the entire set cycle in batch mode. It is worth noting that the tested cell had an OCV of 0.8 V for a COD concentration of 1000 mg/L. Therefore, it was assumed that the voltage of the tested MFC varied between 0.04 V and 0.7 V. Regardless of the set external load voltage, the MFC operated for the entire batch cycle, which lasted 50 hours.

The results of the experimental simulation in constant-voltage regime external load for different voltage values are summarized in Figure 7.5. The highest generated energy value (97.15 J) is observed for the load voltage value of V_{MFC} = 0.41 V, with EE = 17.5% and CODrem = 64.1%. Detailed simulation results for the load voltage of 0.41 V are presented in Figure 7.6. The highest CODrem values above 95% were noted for load voltages below $V_{MFC} \leq 0.15V$. The lowest EE values ≤ 6.1% and electrical energy generated are observed within this same load voltage range, decreasing with decreasing load voltage levels. The highest EE value of 31.2% is observed for a load voltage of 0.7 V. Similarly, the lowest CODrem value is observed for this load voltage value of 10.7%. The change in CE ranges from 26.1% (for a load voltage of 0.04 V) to 42.6% (for a load voltage of 0.7 V).

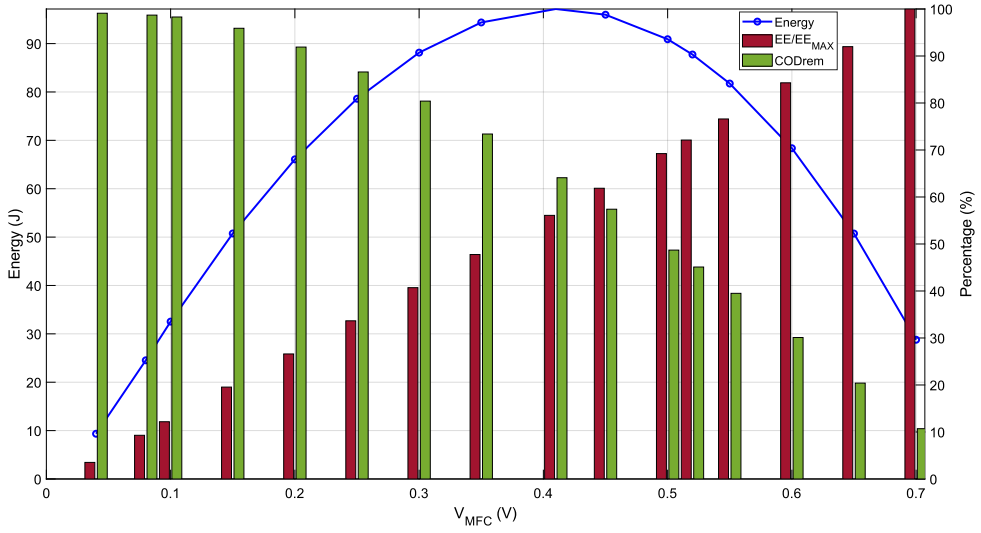

Figure 7.5 Summary of simulation results of microbial fuel cell under constant-voltage regime external load for different values of operational parameter

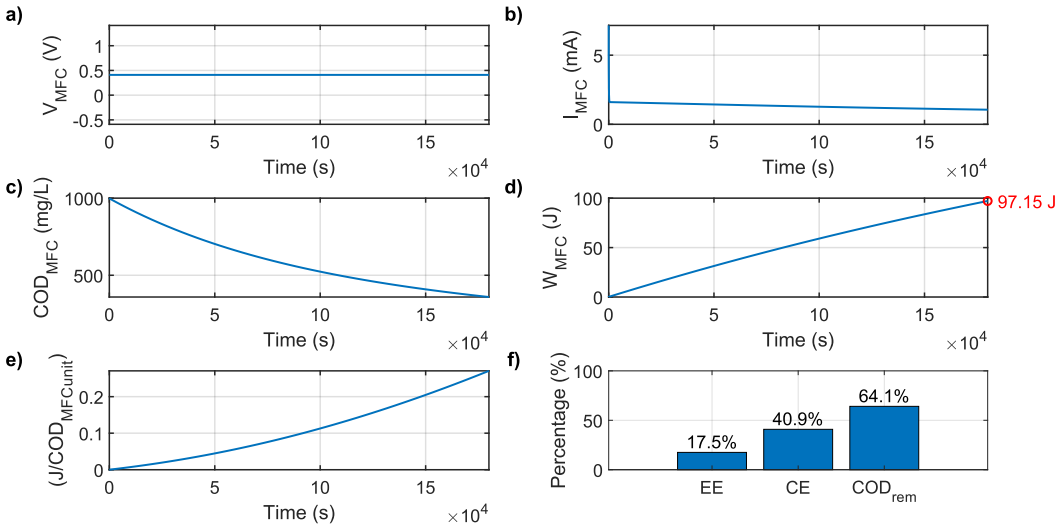

Figure 7.6 Simulation results of the constant-voltage regime for MEP: a) voltage, b) electric current, c) COD evolution, d) energy increment, e) energy increment per COD unit, f) efficiencies results

In the case presented in Figure 7.5, MEP (97.15 J, 0.41 V), two points are obtained after reducing the theoretical maximum energy by 10%. The first operating point is for a load voltage of 0.3 V, which is characterized by a lower EE value (12.7%) and a higher CODrem value (80.4%) compared to the simulation results of the MFC operating at MEP. The second point was observed for a load voltage of 0.52 V, which is characterized by a higher EE value (22.5%) and a lower CODrem value (45.1%) compared to the simulation results of the MFC operating at MEP.

Considering the simulation results for the two discussed operating points, the 0.3 V load allows for maximizing CODrem, while the 0.52 V load allows for maximizing EE and simultaneously maximizing energy generation from the MFC.

7.4.3. Performance of microbial fuel cell under constant-power regime external load

Another type of active load presented in this chapter is the constant power regime load. This load regulates the value of the power consumed while simultaneously controlling the current and voltage of MFC. This type of load is characterized by a constant rate of energy increase per unit of time. However, similar to the constant current regime load, operation at constant power is interrupted when the electrical parameters of the cell (voltage and current) are insufficient for continuous operation. In this simulation test, the electrical load of the MFC varied from 0.1 mW to 0.7 mW.

The results of the load simulation in constant power regime external load, summarized in Figure 7.7, are divided into those with an experiment duration of 50 hours and those with an experiment duration of less than 50 hours. The highest generated energy value is observed for the electric load value of P_{load} = 0.526 mW; for this load value, the EE value is 20.5%, and the CODrem value is 53.4%. The CODrem for P_{load} = 0.526 mW is the maximum value of CODrem registered in this mode. More extended results show that the electric load value of Pload = 0.526 mW, as presented in Figure 7.8. The highest value of EE (32.3%) is observed for P_{load} = 0.1 mW. The change in CE ranges from 25.4% (for a load power of 0.7 mW) to 42.8% (for a load power of 0.1 mW).

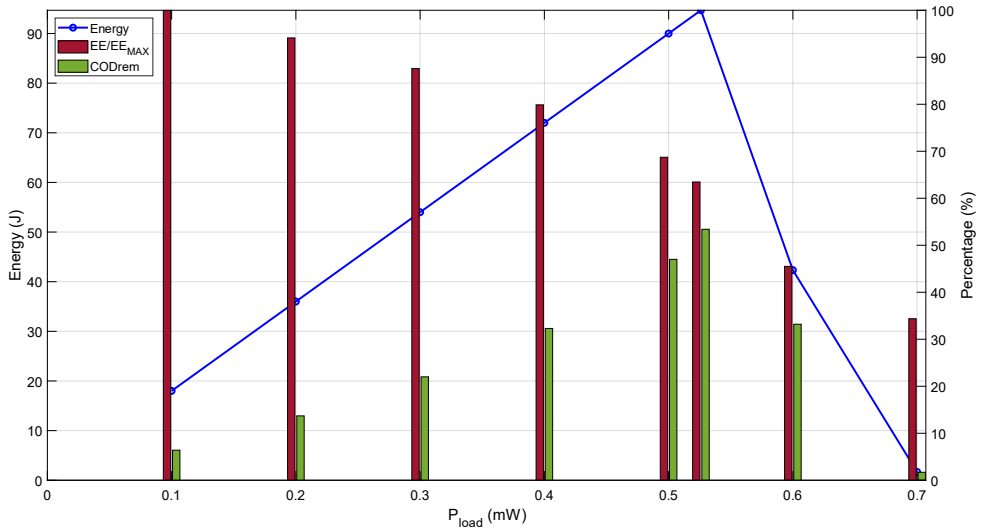

Figure 7.7 Summary of simulation results of microbial fuel cell under constant-power regime external load for different values of operational parameter

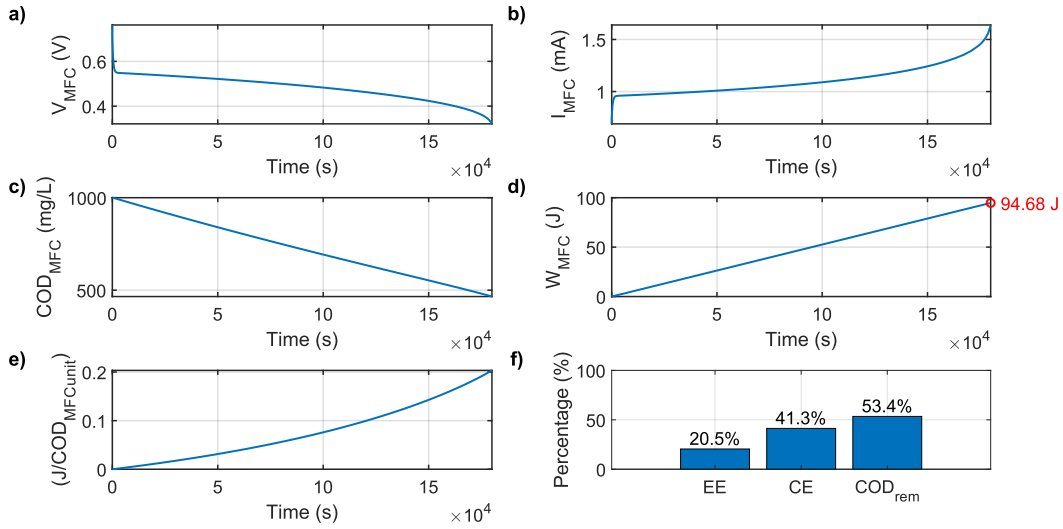

Figure 7.8 Simulation results of the constant-power regime for MEP: a) voltage, b) electric current, c) COD evolution, d) energy increment, e) energy increment per COD unit, f) efficiencies results

In the case of electrical load in a constant power regime, maximizing operation for EE or CODrem, as presented in the constant-current regime and constant-voltage regime, is limited due to the electrical constraints of the MFC for continuous power generation. Because of that, in the constant power regime, the MFC cannot be electrically overloaded to intensify CODrem. The MFC can be loaded to the MEP, achieving CODrem appropriate to this operating point. Reducing the load will consistently increase EE.

7.4.4. Performance of microbial fuel cell under constant-resistance external load

The last type of electrical load presented in this Chapter is the resistive load. It is worth noting that this type of load is a passive load. The MFC operating under a passive resistive load allows continuous operation throughout the entire batch cycle. Another benefit of this passive load type is the minimal oscillations in the momentary parameters of the generated electric energy. In this simulation test, the electrical load of the MFC varied from 24.875 Ω to 1990 Ω.

As reported in Figure 7.9, the highest value of generated energy for the resistive load is 98.64 J, recorded for R_{load} = 303.475 Ω At the same point, EE = 17.4% and CODrem = 65.6% are also recorded. Detailed simulation results for the resistive load 303.475 Ω are presented in Figure 7.10. The highest CODrem values above 93.7% were noted for resistive load below R_{load} ≤ 99.5 Ω. Within this same resistive load range are observed the lowest EE values ≤ 8.1% and electrical energy generated, decreasing with decreasing resistive load value. The highest EE value of 29.9% is observed for the resistive load of 1990 Ω. Similarly, for this load, the voltage value is observed as the lowest CODrem value of 10.7%. The change in CE ranges from 23.5% (for a resistive load of 24.875 Ω) to 42.4% (for a resistive load of 1990 Ω).

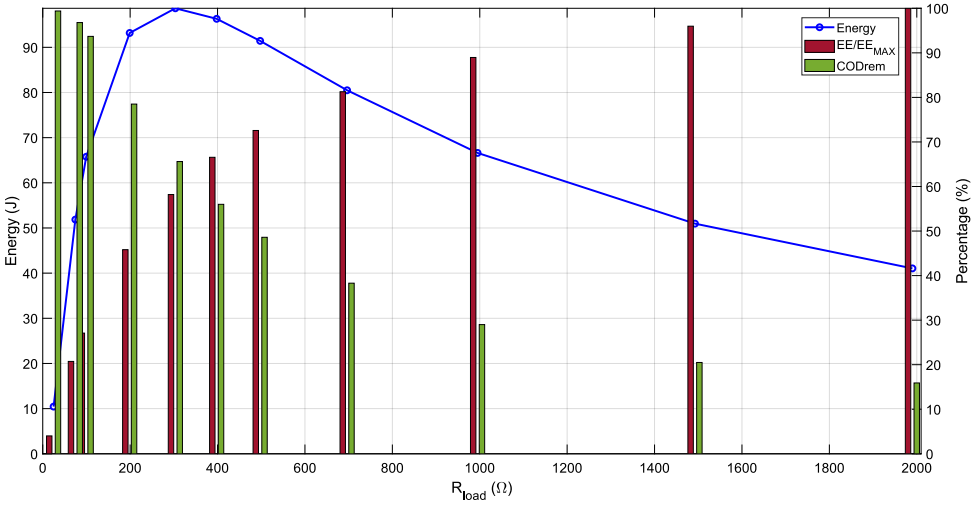

Figure 7.9 Summary of simulation results of microbial fuel cell under constant-resistance regime external load for different values of operational parameter

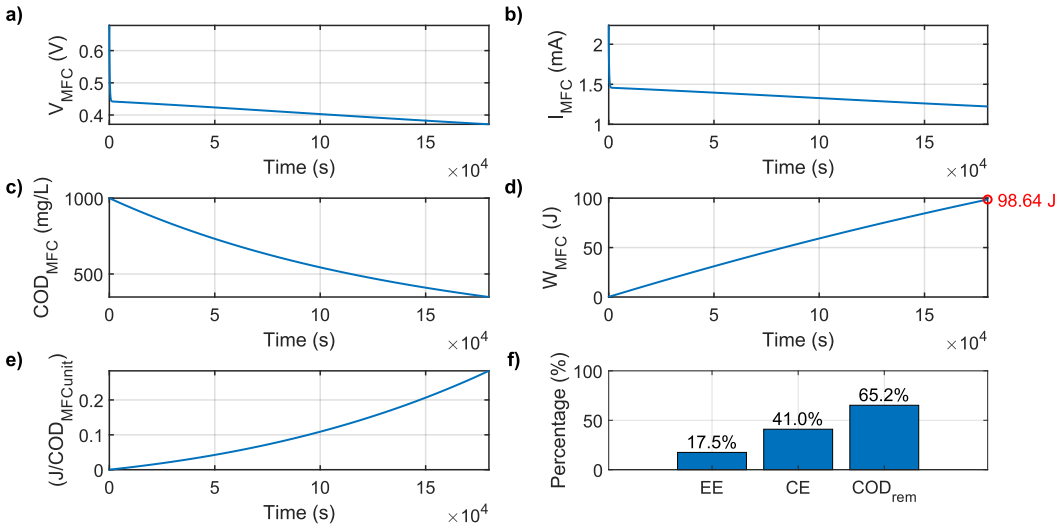

Figure 7.10 Simulation results of the constant-resistance regime for MEP: a) voltage, b) electric current, c) COD evolution, d) energy increment, e) energy increment per COD unit f) efficiencies results

In the case presented in Figure 7.5, MEP (98.64 J, 303.475 Ω), two points are obtained after reducing the theoretical maximum energy by 10%. The first operating point is for the resistive load of 169.15 Ω, which is characterized by a lower EE value (12.3%) and a higher CODrem value (83%) compared to the simulation results of the MFC operating at MEP. The second point was observed for the resistive load of 547.25 Ω, characterized by a higher EE value (22.5%) and a lower CODrem value (45.6%) compared to the simulation results of the MFC operating at MEP.

Considering the simulation results for the two discussed operating points, the load with value of 169.15 Ω allows for maximizing CODrem, while the load with value of 547.25 Ω allows for maximizing EE and simultaneously maximizing energy generation from the MFC.

7.5. Conclusions

This chapter presents simulation studies for four load modes: constant current, voltage, power, and resistance load modes. The simulation results confirm that selecting appropriate load values can control EE and COD removal. Additionally, for constant current, constant voltage, and constant resistance load modes, maximizing either EE or CODrem with a relatively low (up to 10%) limitation on maximum electrical energy generation is possible. However, in the case of constant power load mode, the maximization possibilities are limited due to the electrical constraints of the MFC for continuous power generation operated in batch mode.

8. MAXIMIZING ENERGY EFFICIENCY AND CHEMICAL OXYGEN DEMAND REMOVAL FOR CONTINUOUS ELECTRIC ENERGY GENERATION OF MICROBIAL FUEL CELL

8.1. Introduction

MFCs represent a promising technology for simultaneous wastewater treatment and sustainable energy generation. However, their performance remains a complex challenge due to the intricate interplay between various operational parameters. This chapter focuses on maximizing the EE and CODrem of MFCs to enhance their continuous electric energy generation capabilities.

Building on the foundation laid in previous chapters, particularly the model introduced in Chapter 6 and the maximization method described in Chapter 7, this chapter aims to validate and apply these methodologies to two distinct MFC configurations: one with a varying active electric load and air pump, and another with a passive electric load.

The chapter is structured to first verify the accuracy and reliability of the proposed model through detailed RMSE calculations for voltage and current. Subsequent sections will present simulation results for different electric load values, followed by a comparative analysis of the MFC performance under various operational conditions. Finally, proposals for selecting optimal operating points to achieve desired outcomes, whether prioritizing maximum energy generation, EE, or CODrem, are discussed.

8.2. Objectives

The main goal of this chapter is to analyze the effect of the external load modification, based on the maximization methods presented in Chapter 7, on the output parameters of electric power generation and (synthetic) wastewater purification level, corresponding to COD removal of the MFC. The partial objectives were the following:

- Analysis of the performance of MFC related to the output voltage and current levels for the selected electric operating conditions, CE, EE, and COD removal rates;
- Selection of electrical load values based on the maximization methods presented in Chapter 7
- Comparative analyses of the effect of different electric operational parameters on MFC performance were represented by CE, EE, and COD removal.
- Design guidelines for the design of a DC/DC converter to control MFC operation

8.3. Materials and methods

8.3.1. Experimental research assumptions

The experimental study aims to investigate how the modification of external load affects the MFC under different electrical operating conditions. Two different MFCs were tested using different setups and operating parameters. Various indicators like total energy generation, CE, EE, and COD removal were assessed to evaluate the impact of different electrical loads. As mentioned earlier, the methods for calculating the indicators are presented in Chapter 7.

The simulation experiments were standardized to the standard duration for a single batch mode to ensure consistent results. This research applies simulation techniques based on the model outlined in Chapter 6. The results of the research were then compared with the laboratory test results.

8.3.2. Experimental setup

The main objective presented in this chapter is to analyze the effect of external load modification, based on the maximization methods presented in Chapter 7, on the output parameters of electric power generation and the level of (synthetic) wastewater purification corresponding to COD removal in the MFC. This analysis aims to provide valuable information for selecting operating points and choosing an operational strategy between intense electric energy generation and intensive wastewater treatment. The MFCs were operated in batch mode.

The MFCs operated with different configurations but the same culture and medium. Details of the culture and medium composition are presented in Chapter 6 (6.4.2). In both cases, the MFC anodes were fed with a medium with COD = 1000 mg/L. The first MFC, shown in Figure 8.1a, was a replica of the MFC presented in Chapter 6. It is worth noting that the cathode of the MFC was air-fed, and the electrical load was imposed by Autolab (PGSTAT-302N) with a scan rate of 1 s. The load current was set to 3.5 mA. The second MFC, shown in Figure 8.1b, was a modified replica of the MFC shown in Chapter 6. The modification involved the size of the electrodes (2.5 x 2.5 x 1) cm. In this case, the active surface area of the electrodes was approximately 31% smaller than that of the MFC shown in Figure 8.1a. Additionally, the cathode of the second MFC was not air-fed by a pump.

In order to maintain consistent results, the simulation experiments were set to duration laboratory tests. Alternatively, the simulation experiments were limited to the time when the MFC may drop to zero and reach the short-circuit state. Additionally, the experimental setup used in this Chapter consisted of the MFC model introduced in Chapter 6 with simulation environment of Matlab R2024a (MathWorks, Natick, MA, USA) Simulink extension Simscape.

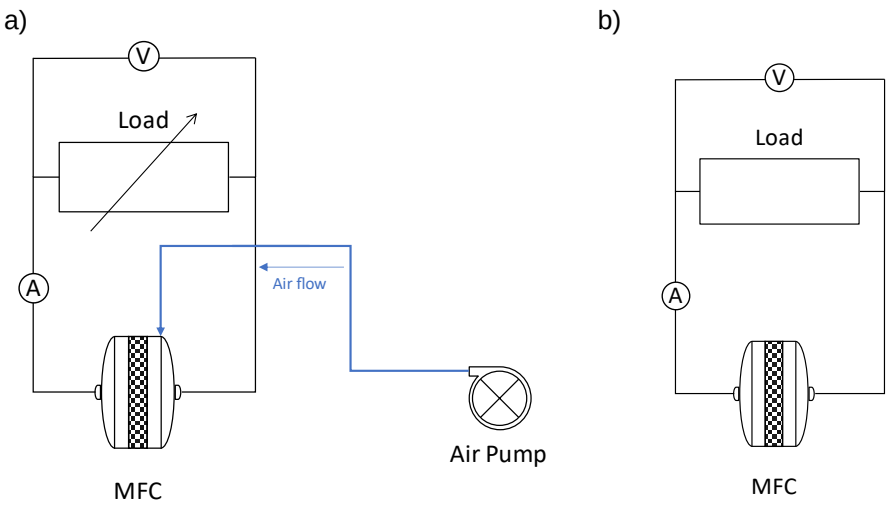

Figure 8.1 Experimental setup: a) MFC with varying active electric load and air pump, b) MFC with a passive electric load.

It is worth noting that the common feature of the tests was the selection of the external electrical load values to force the MFC to operate with maximized COD removal while maintaining a satisfactory level of generated electrical energy. Due to the differing operational parameters during the laboratory tests, two scenarios were used.

The first test scenario (Figure 8.2a) is as follows: The starting point is the replacement of the medium in the anode and cathode. Then, the MFC operates for 1 hour under an external electrical load of I_{MFC} = 3.5 mA. After this period, the electrical circuit of the cell is opened for 10 minutes (during this time, Ri, Rd, and Cd measurements are taken to calibrate the model parameters). This cycle repeats until a 7-hour operation cycle is achieved. During the scenario, measurements of MFC voltage, MFC current, and COD are performed.

The second test scenario (Figure 8.2b) is as follows: The starting point is replacing the medium in the anode and cathode. Then, the MFC operates for 40 hours under an external electrical load of R_{load} = 120 Ω. After 40 hours of operation, the test concludes. To avoid disrupting the MFC's operation in the resistive load mode, the parameters of the MFC circuit model were estimated using the results of polarization curve and power curve measurements.

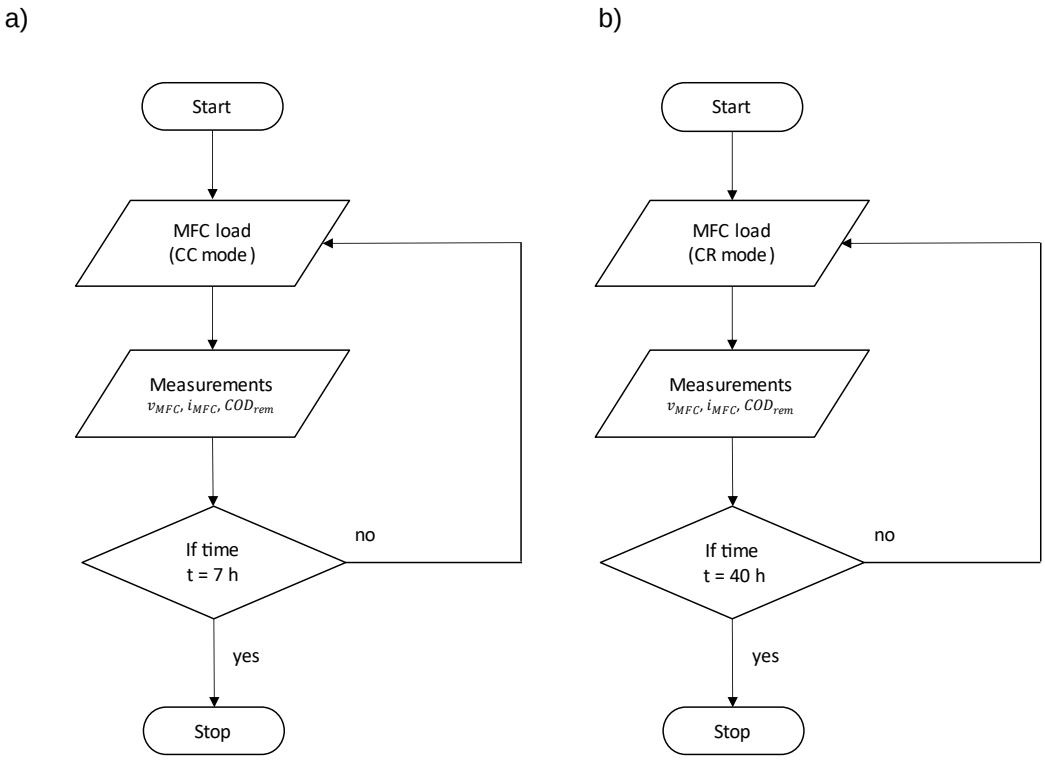

Figure 8.2 Test scenario: a) MFC with varying active electric load b) MFC with a passive electric load

8.4. Results and discussion

8.4.1. Introduction

The studies refer to two types of electrical loads: active and passive. The results for each case can be divided into three parts. The first part is dedicated to the calibration of model parameters, simulation results, and evaluation of its accuracy based on laboratory findings. The quality of the simulation was assessed by calculating RMSE for voltage and current. In the second part, the simulation results for different values of the electrical load parameters are presented. In the third part, the performance of the MFC is evaluated, and load values are proposed to maximize energy generation, COD removal, and EE.

8.4.2. Performance of microbial fuel cell under active electric load

Figure 8.3 reports the voltage and current output and COD measurements corresponding to a single MFC unit under active electric load (AEL test) that was exposed to the load scenario presented in Figure 8.2a. The efficiency indicators (i.e., EE CE and CODrem) were calculated using the formulas from Chapter 7. To determine the RMSE value for voltage, formula 6.18 from Chapter 6 was used. RMSE for current was used to assess the model quantitatively. The $RMSE_I$ is calculated as:

$$RSME_I = \sqrt{\frac{\sum_{i=1}^{n}(I_{model} - I_{meas})^2}{n}} \cdot 100\%, \tag{8.1}$$

The solid lines represent the results obtained with the model proposed in Chapter 6. Figure 8.3a and 8.3c clearly show that accurate voltage and COD predictions were achieved during the AEL test operation.

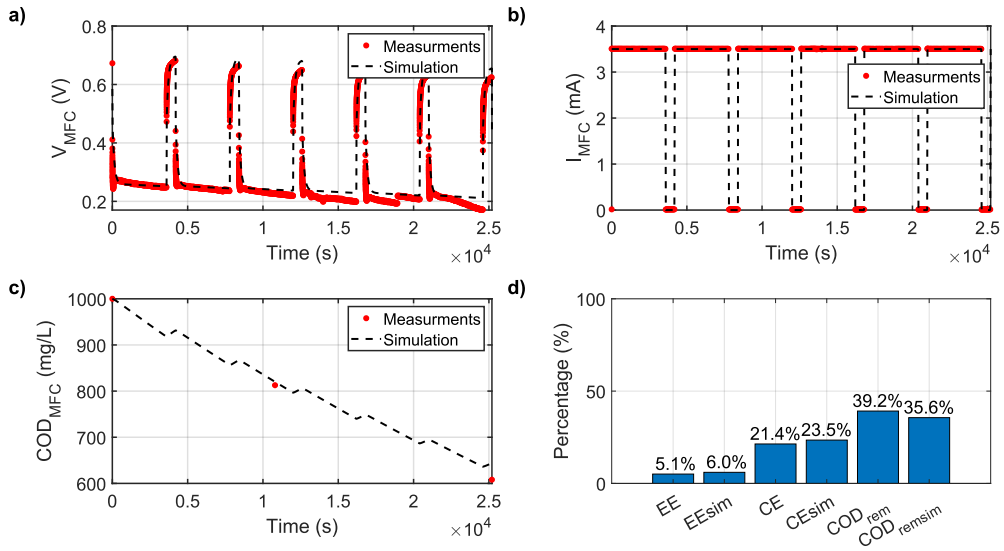

Figure 8.3 MFC experimental data and simulation results during AEL test for MEP: a) voltage, b) current, c) COD evolution, d) performance indicators

The parameters for the MFC AEL test equivalent circuit of the proposed model were in average as follow $R_{i_{\mathrm{AEL}}} = 61.5380\ \Omega$, $R_{d_{\mathrm{AEL}}} = 65.3840\ \Omega$ and $C_{d_{\mathrm{AEL}}} = 18.8\ \mathrm{F}$. The model presents accurate results for the transition state studied for a MFC AEL test, being the average relative model error for voltage of about RSME = 3.21%. RSME for the current was not taken to the consideration because the laboratory measurements AEL test and simulation were using the same data set. The MFC during AEL test does not achieve a stable state during unloading periods, which results in the output voltage remaining lower than the OCV value. In contrast, the proposed model accurately reflects this behavior. Figure 6.8.3c shows that the simulation results became more accurate with each subsequent COD concentration sample compared to the measurements. Figure 6.8.3d reports the performance indicators for the AEL test. The EE calculated was 5.1% and the model estimation was EEsim 6% (difference 17.6 %). The CE was 21.4% and 9.3% lower than the value of CEsim. CODrem was calculated at 39.2% and was 9.2% higher than the value of CODremsim. The nature of this behavior can be explained by the fact that we have different species of bacteria (non-electroactive and electroactive) inside the MFC. Although any external load does not influence the MFC, the sodium acetate biodegradation reaction takes place and reduces EE [124]. Another crucial factor affecting efficiency is the operation of the MFC, which is close to its maximum power point (MPP). When the MFC operates away from the MPP, most of the time, efficiency is also affected [94].

The next step is to identify, using the calibrated model, the load that may achieve a desirable Chapter 7 balance between wastewater treatment efficacy and energy generation while also controlling the work cycle (duration of batch mode) of the MFC. In this simulation test, the

electrical load of the MFC varied from 1 mA to 4.5 mA to maintain experimental duration of 7 hours.

The results of the load simulation in the current controlled external load are summarized in Figure 8.4. The low energy generated values are recorded for the electric load of small values ($I_{MFC} \leq 1$ mA) concurrently with the low CODrem rate (less than 6.3%) and the high EE value (more than 22.7%). Additionally, the second low of energy generated values is recorded for high electric load values ($I_{MFC} = 4.5$ mA), concurrently with the highest CODrem value (64%) and the lowest EE value (1.5%).

The highest generated energy value (20.67 J) is observed for the electric load value of I_{MFC} = 2.7 mA, and for this load value, the EE value is 10.4%, and the CODrem value is 22.9%. More extended results, the electric load value of I_{MFC} = 2.7 mA presents Figure 8.5. The highest CODrem (64%) value was observed for I_{MFC} = 4.5 mA, and for this load value, the generated energy is 8.56 J with EE = 1.5%. The change in CE ranges from 16.8% (for a load current of 4.5 mA) to 37.6% (for a load current of 1 mA).

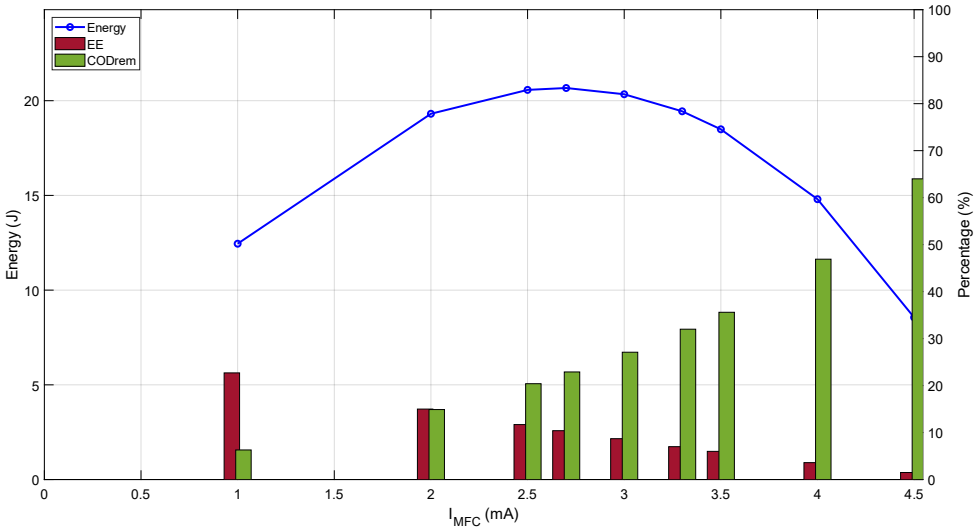

Figure 8.4 Summary of simulation results of MFC for AEL test for different values of electric load

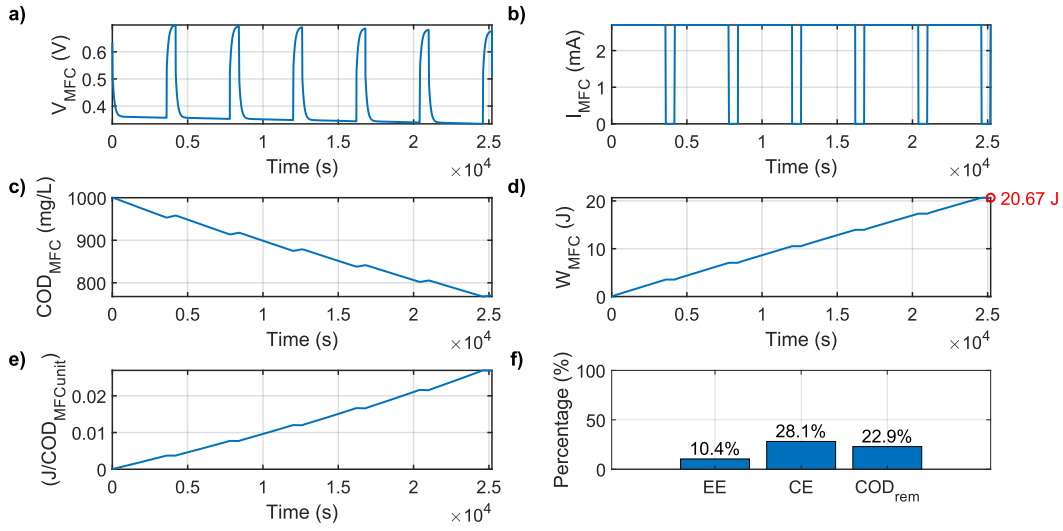

Figure 8.5 Simulation results of AEL test for MEP: a) voltage, b) electric current, c) COD evolution, d) energy increment, e) energy increment per COD unit, f) efficiencies results

To achieve higher EE or CODrem while maintaining the criterion of maximizing generated energy, it should follow the criteria described in Chapter 7. Once again, by reducing the assumed maximum value of generated energy by 10% from the theoretical maximum value, two operating points are obtained: one for a lower electric load value and one for a higher electric load value relative to the electric load for MEP.

In the case presented in Figure 8.4, MEP (20.67 J, 2.7 mA), two points are obtained after reducing the theoretical maximum energy by 10%. The first point is for the electric load current of 1.8 mA, which is characterized by higher EE (16.4%) and lower CODrem (12.9%) compared to the MFC operating at MEP. The second point is for an electric load current of 3.5 mA. This point was the subject of laboratory tests, and the test results are presented in Figure 8.3. This point is characterized by a lower EE value and higher CODrem value compared to the MFC operating at MEP.

8.4.3. Performance of microbial fuel cell under passive electric load

In order to avoid disruption to the MFC's operation in the resistive load mode, the parameters of the MFC circuit model were estimated using the results of polarization curve and power curve measurements. The results of the electric test performance presented in Figure 8.6a report that the OCV value for the MFC unit used in the test under passive electric load (PEL test) was almost 30% lower than the MFC used for the AEL test. This was caused by the lack of air supply to the cathode chamber. The MPP 0.4267 mW for current value of 1.7609 mA was reported in Figure 8.6b

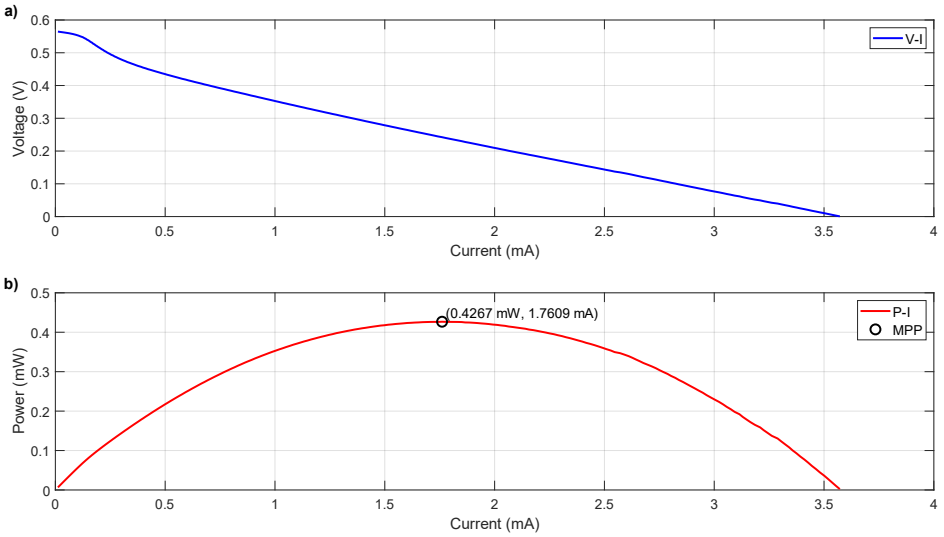

Figure 8.6 MFC used for PEL test: a) polarisation curve b) power cure with MPP

Figure 8.3 presents the voltage and current output, and COD measurements correspond to a single MFC unit used in the PEL test that was exposed to the load scenario presented in Figure 8.2a. The results obtained with the proposed model are represented by the solid. In the case of the MFC performance indicator results presented in Figure 8.7d, all results based on simulation results are appended with “sim”.

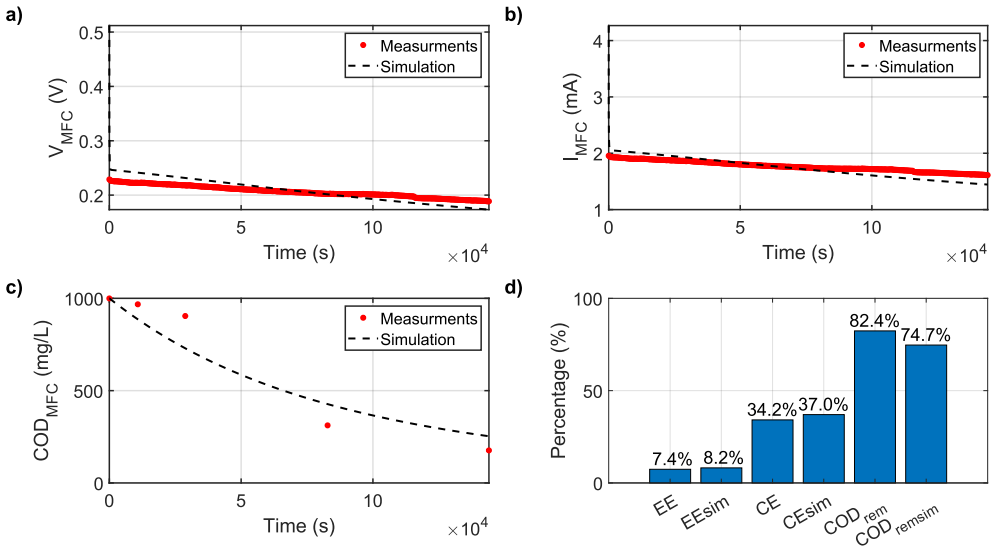

Figure 8.7 MFC experimental data and simulation results during PEL test: a) voltage, b) current, c) COD evolution, d) performance indicators

The parameters for the MFC PEL test equivalent circuit of the proposed model were in the average as follow $R_{i_{\mathrm{PEL}}} = 67.5380\ \Omega$, $R_{d_{\mathrm{AEL}}} = 69.6841\ \Omega$ and $C_{d_{\mathrm{PEL}}} = 1.88\ \mathrm{F}$. The model presents accurate results for the transition state studied for the MFC PEL test, being the average relative model error for voltage of about RSME = 1.73%. RSME$_{\mathrm{I}}$ for the current period was 14.38 %, and the result was almost 42% better than that presented in [123]. Figure 8.7c shows that the simulation results became more accurate with each subsequent COD concentration sample compared to the measurements. Figure 8.7d reports the performance indicators for the PEL test.

The EE calculated was 7.4%, and the model estimation was EEsim 8.2% (difference 10.8 %). The CE was 34.2% and was 6.6% lower than the value of CEsim. CODrem was calculated at 82.4% and was 10.7% higher than the value of CODremsim. Once again, the model showed satisfactory results.

The next step is to identify, using the calibrated model, the load that may achieve a desirable Chapter 7 balance between wastewater treatment efficacy and energy generation of the MFC. In this simulation test, the electrical load of the MFC varied from 35 Ω to 1380 Ω.

As reported in Figure 8.8, the highest value of generated energy for the resistive load is 58.31 J, recorded for R_{load} = 207 Ω. At the same work point of MFC, EE = 11.7% and CODrem = 57.6% are also recorded. Detailed simulation results for the resistive load 207 Ω are presented in Figure 7.10. The highest CODrem values above 96.7% were noted for resistive load below R_{load} ≤ 35 Ω. Within this same resistive load range are observed the lowest EE values ≤ 2.3% and electrical energy generated, decreasing with decreasing resistive load value. The highest EE value of 20.9% is observed for the resistive load of 1380 Ω. Similarly, for this load, the voltage value is observed to be the lowest CODrem value of 13%. The change in CE ranges from 31% (for a resistive load of 35 Ω) to 42% (for a resistive load of 1380 Ω).

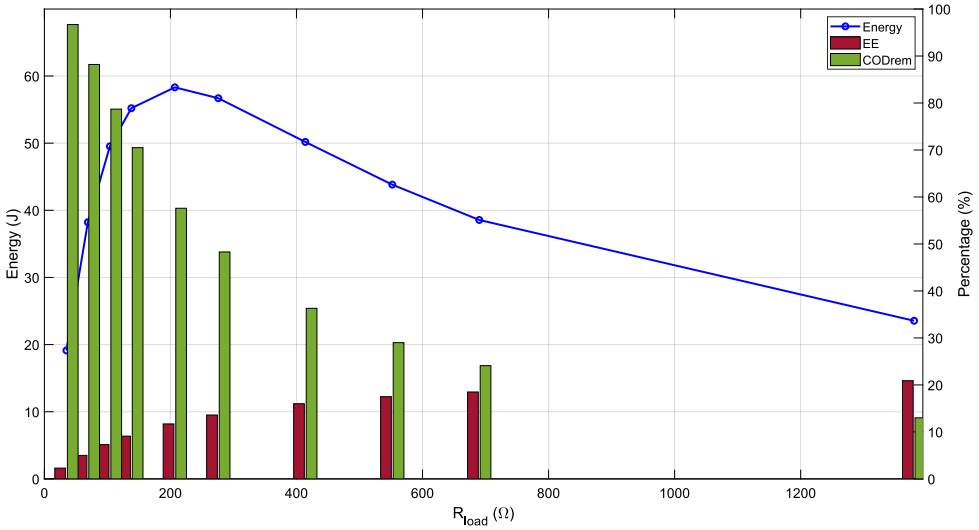

Figure 8.8 Summary of simulation results of MFC for PEL test for different values of electric load

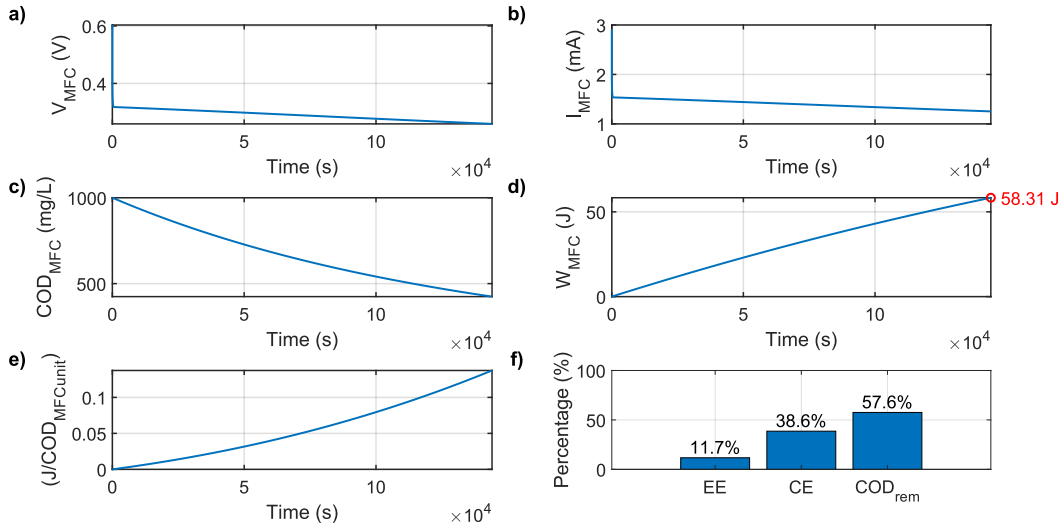

Figure 8.9 MFC experimental data and simulation results during PEL test for MEP: a) voltage, b) current, c) COD evolution, d) performance indicators

In the case presented in Figure 7.5, MEP (58.31 J, 207 Ω), two points are obtained after reducing the theoretical maximum energy by 10%. The first operating point is for the resistive load of 120 Ω. This point was the subject of laboratory tests, and the test results are presented in Figure 8.7, which is characterized by a lower EE value and a higher CODrem value compared to the simulation results of the MFC operating at MEP. The second point was observed for the resistive load of 372 Ω, which is characterized by a higher EE value (14.4%) and a lower CODrem value (36.3%) compared to the simulation results of the MFC operating at MEP.

Considering the simulation results for the two discussed operating points, the load with value of 120 Ω allows for maximizing CODrem, while the load with a value of 372 Ω allows for maximizing EE and simultaneously maximizing energy generation from the MFC.

8.4.4. Proposal guidelines for designing a DC-DC converter for MFC

MFCs are bioelectrochemical systems that convert organic matter directly into electrical energy through microbial activity. MFCs require an efficient DC-DC converter, which transforms the low and variable output of MFCs into a stable and usable form of electrical energy.

Here are outlines of requirement guidelines for designing a DC-DC converter tailored for MFC applications. These guidelines focus on ensuring high efficiency (EE and CODrem), and reliability of the power conversion process, thus enhancing the overall functionality and applicability of MFC systems. By addressing key design aspects such as input voltage range, efficiency, and current handling, these guidelines aim to assist engineers and researchers in developing robust and effective DC-DC converters that can meet the unique demands of MFC technology.

Input Voltage Range: Ensure the converter can operate within the voltage range generated by the MFC, which is typically low voltage for a single MFC unit lower than 1 V.

Efficiency: MFC is characterized by low energy density. The converter for high efficiency to minimize energy losses, which is important for the overall system performance.

Current Handling: The generated electric current of the MFC is very low (typically 0.5 - 2 mA). Design the converter to handle the minimum (0.01 mA) and maximum current produced by the MFC, considering potential peaks up to 20 mA.

Regulation: Depending on the case, implement precise voltage, current or power regulation to maintain stable output despite fluctuations in MFC output.

Load Matching: Ensure the converter can adjust to varying loads to maximize power transfer from the MFC, CODrem, or EE.

Compact Design: Aim for a compact and lightweight design to facilitate integration with the MFC system.

Scalability: Design the converter to be scalable, accommodating potential future increases in power output or system expansion.

Protection Mechanisms: Include protection features such as overcurrent, overvoltage, and short-circuit protection to safeguard both the MFC and the converter.

Startup Characteristics: Ensure the converter has a low startup voltage to allow operation even when the MFC output is minimal.

8.5. Conclusions

This chapter presents the application of the maximization method for different MFCs operating under various parameters. The research results presented in this chapter confirm that the model proposed in Chapter 6 and the maximization method from Chapter 7 can effectively maximize MFC performance for different desired outcomes (maximalizing energy generation, EE or CODrem).

The RMSE values for voltage and current were calculated. For voltages, the RMSE ranged from 1.73% to 3.21%. In the current case, the RMSE was only calculated for the MFC under PEL conditions. This value was $RMSE_I$ = 14.38% and was better than the results of models presented in the literature.

In the final subsection, proposal guidelines for designing a DC-DC converter for MFC were described, including the most important requirements that this converter must meet to effectively control the operation of the MFC.

9. CONCLUSION

The following conclusions can be drawn from the results that have been presented and discussed in previous chapters:

- **Influence of the flow rate on the parameters of microbial fuel cell**

  This research, presented in this Chapter, addresses one of the most important challenges for achieving industrial-scale MFC. To investigate this, we evaluated the short-term effects of influent flow rate variations by operating an MFC. The results indicate that increasing the flow rate from 0.72 to 7.2 L/d increased electric power generation and COD removal rate while reducing COD removal efficiency and CE. High flow rates result in high OLR, increased mixing intensity, and reduced mass transfer limitations. Upon returning to initial conditions, a hysteresis loop was observed, attributed to microbial culture growth under high OLR. The CE figures reflect a decline in electrogenic activity at high flow rates. From a practical standpoint, the overall evaluation suggests that variations in influent flow rate have minimal impact on the MFC's performance in terms of both electrogenic activity and pollutant removal.

- **The effect of external load on the performance of microbial fuel cells**

  The research results presented in this Chapter can be concluded as follows: The external load significantly affects the microbial consortia distribution in the MFC. Firstly, the external load significantly influences the distribution of microbial consortia within the MFC. High external resistance prompts a transition in microbial populations from more electrogenic to more fermentative cultures. This shift impacts all operational variables, particularly noticeable in the current density output, which decreased from 0.06 to 0.02 mA. Regarding power output, the system generally conforms to predictions outlined by the Jacobi Theorem. However, peak power production was observed across a broad range of load resistances (1000 to 3000 Ω) rather than precisely at the point where external and internal resistances are equal. In terms of fuel consumption, its dependency on external resistance is minimal, with this classification referring to the internal resistance of the MFC, with only a slight decrease noted after operation at high external resistance. Lastly, fuel consumption only marginally decreases despite the decrease in electric energy generation with increasing external resistance. This results in lower CE after operating under conditions of high external resistance, with this classification referring to the internal resistance of the MFC.

- **Terminal voltage modeling of microbial fuel cells**

  In this chapter, the performance of the reduced-order combined model was studied and compared with the recorded terminal voltage of MFCs. The modeling methodology based on VRM was applied, and the model parameters were accurately estimated. With these parameter values, the model was able to

accurately predict the voltage and COD evolution of single cells and two cells connected in series and in parallel, presenting errors lower than 8%. The tested cells operated under high current generation showed that the voltage oscillations were smaller. Voltage drops and polarity changes were not observed, which means the cells had higher operational stability for stacks (series or parallel) configuration of MFCs than for single-cells. The proposed models can be the subject of further research as a tool for designing and developing concepts using MFC technologies for wastewater treatment.

- **Different operational strategies for continuous electric energy generation of microbial fuel cell**

  In this chapter, MFC performances were compared with two different operational parameters. A smaller amplitude of power surges characterized the work of the cell at a constant voltage. In the case of operation at a constant current, the cyclic relaxation of the cell was forced, thus switching on and off the load. During the experiment, the cells were loaded with a constant current. Despite loading the cells with the same load but with different intervals between the load state and the idle state, the cell operating in the scenario with regular cell loading generated more electric energy. The MFC work at constant current was characterized by greater electric power output by the cell, while they work at constant voltage, which guaranteed a constant and uninterrupted load on the cell and thus increased the CE and COD removal.

- **Maximizing energy efficiency and chemical oxygen demand removal for continuous electric energy generation of microbial fuel cell**

  The model and maximization method from Chapter 7 were validated in this chapter for two scenarios: an MFC with varying active electric load and air pump and an MFC with a passive electric load. In both cases, the accuracy of the model presented in Chapter 6 was initially confirmed. The RMSE values for voltage and current were computed. The RMSE for voltage ranged from 1.73% to 3.21%. The RMSE for the current was calculated only for the MFC under PEL conditions, resulting in an RMSEI of 14.38%, which surpassed the findings of models presented in the literature. The research findings in this chapter validate that the model proposed in Chapter 6 and the maximization method from Chapter 7 can effectively optimize MFC performance for various objectives, whether it is maximizing energy generation, energy efficiency (EE), or chemical oxygen demand removal (CODrem). Based on the results contained in this chapter, it can be concluded that the research hypothesis presented in this work is correct.

REFERENCES

1.1 Publications constituting the thesis.

[D1]. S. Potrykus, S. Mateo, J. Nieznański, and F. J. Fernández-Morales, “The Influent Effects of Flow Rate Profile on the Performance of Microbial Fuel Cells Model,” Energies, vol. 13, no. 18, p. 4735, Sep. 2020, doi: 10.3390/en13184735.

[D2]. S. Potrykus, L. F. León-Fernández, J. Nieznański, D. Karkosiński, and F. J. Fernandez-Morales, “The Influence of External Load on the Performance of Microbial Fuel Cells,” Energies, vol. 14, no. 3, p. 612, Jan. 2021, doi: 10.3390/en14030612.

1.2 Other publications

[1] European Commission. Directorate General for Energy., Guidehouse., and Tractebel Impact., *Hydrogen generation in Europe: overview of costs and key benefits.* LU: Publications Office, 2020. Accessed: Jul. 28, 2021. [Online]. Available: https://data.europa.eu/doi/10.2833/122757

[2] S. Potrykus, F. Kutt, J. Nieznański, and F. J. Fernández Morales, “Advanced Lithium-Ion Battery Model for Power System Performance Analysis,” *Energies*, vol. 13, no. 10, p. 2411, May 2020, doi: 10.3390/en13102411.

[3] Wolfgang Klebsch, Patrick Heininger, Jan Geder, and Andreas Hauser, “Battery systems for Multiple Units,” *VDE*, 2018.

[4] D. Karkosiński, W. A. Rosiński, P. Deinrych, and S. Potrykus, “Onboard Energy Storage and Power Management Systems for All-Electric Cargo Vessel Concept,” *Energies*, vol. 14, no. 4, p. 1048, Feb. 2021, doi: 10.3390/en14041048.

[5] M. de los Ángeles Fernandez *et al.*, “A grey box model of glucose fermentation and syntrophic oxidation in microbial fuel cells,” *Bioresource Technology*, vol. 200, pp. 396–404, Jan. 2016, doi: 10.1016/j.biortech.2015.10.010.

[6] S. Mateo, P. Cañizares, F. J. Fernandez-Morales, and M. A. Rodrigo, “A Critical View of Microbial Fuel Cells: What Is the Next Stage?,” *ChemSusChem*, vol. 11, no. 24, pp. 4183–4192, 2018, doi: 10.1002/cssc.201802187.

[7] A. J. Appleby, “From Sir William Grove to today: fuel cells and the future,” *Journal of Power Sources*, vol. 29, no. 1–2, pp. 3–11, Jan. 1990, doi: 10.1016/0378-7753(90)80002-U.

[8] W. R. Grove, “XXIV. *On voltaic series and the combination of gases by platinum*,” *The London, Edinburgh, and Dublin Philosophical Magazine and Journal of Science*, vol. 14, no. 86–87, pp. 127–130, Feb. 1839, doi: 10.1080/14786443908649684.

[9] F. Bidault and P. H. Middleton, “Alkaline Fuel Cells,” in *Comprehensive Renewable Energy*, Elsevier, 2012, pp. 179–202. doi: 10.1016/B978-0-08-087872-0.00405-4.

[10] Y. Luo, Y. Shi, and N. Cai, “Bridging a bi-directional connection between electricity and fuels in hybrid multienergy systems,” in *Hybrid Systems and Multi-energy Networks for the Future Energy Internet*, Elsevier, 2021, pp. 41–84. doi: 10.1016/B978-0-12-819184-2.00003-1.

[11] H. S. Das, Md. F. F. Chowdhury, S. Li, and C. W. Tan, “Fuel cell and hydrogen power plants,” in *Hybrid Renewable Energy Systems and Microgrids*, Elsevier, 2021, pp. 313–349. doi: 10.1016/B978-0-12-821724-5.00009-X.

[12] K. Scott and L. Xing, “Direct Methanol Fuel Cells,” in *Advances in Chemical Engineering*, vol. 41, Elsevier, 2012, pp. 145–196. doi: 10.1016/B978-0-12-386874-9.00005-1.

[13] H. Nagamoto, “Fuel Cells: Electrochemical Reactions,” in *Encyclopedia of Materials: Science and Technology*, Elsevier, 2001, pp. 3359–3367. doi: 10.1016/B0-08-043152-6/00600-8.
[14] K. Scott and E. H. Yu, Eds., *Microbial electrochemical and fuel cells: fundamentals and applications*. in Woodhead publishing series in energy, no. number 88. Amsterdam Boston Cambridge Heidelberg London: Woodhead Publishing is an imprint of Elsevier, 2016.
[15] B. E. Logan, *Microbial fuel cells*. Hoboken, N.J: Wiley-Interscience, 2008.
[16] H. Abdi, R. Rasouli Nezhad, and M. Salehimaleh, “Fuel Cells,” in *Distributed Generation Systems*, Elsevier, 2017, pp. 221–300. doi: 10.1016/B978-0-12-804208-3.00005-4.
[17] S. A. Kalogirou, “Industrial Process Heat, Chemistry Applications, and Solar Dryers,” in *Solar Energy Engineering*, Elsevier, 2014, pp. 397–429. doi: 10.1016/B978-0-12-397270-5.00007-8.
[18] S. Dharmalingam, V. Kugarajah, and M. Sugumar, “Membranes for Microbial Fuel Cells,” in *Microbial Electrochemical Technology*, Elsevier, 2019, pp. 143–194. doi: 10.1016/B978-0-444-64052-9.00007-8.
[19] I. Dincer and Y. Bicer, “4.22 Electrochemical Energy Conversion,” in *Comprehensive Energy Systems*, Elsevier, 2018, pp. 856–894. doi: 10.1016/B978-0-12-809597-3.00439-9.
[20] I. Dincer and M. A. Rosen, “Exergy analyses of fuel cell systems,” in *Exergy*, Elsevier, 2021, pp. 479–514. doi: 10.1016/B978-0-12-824372-5.00018-X.
[21] T. Leo, “Molten Carbonate Fuel Cells,” in *Comprehensive Renewable Energy*, Elsevier, 2012, pp. 247–259. doi: 10.1016/B978-0-08-087872-0.00408-X.
[22] A. Husain, M. U. Shariq, I. Khan, S. P. Ansari, M. M. A. Khan, and A. Khan, “Solid oxide fuel cell technology for sustainable development,” in *Advanced Technology for the Conversion of Waste Into Fuels and Chemicals*, Elsevier, 2021, pp. 93–109. doi: 10.1016/B978-0-323-90150-5.00015-7.
[23] R. Mishra and R. S. Ningthoujam, “High-Temperature Ceramics,” in *Materials Under Extreme Conditions*, Elsevier, 2017, pp. 377–409. doi: 10.1016/B978-0-12-801300-7.00011-5.
[24] K. Li, “Ceramic Hollow Fiber Membranes and Their Applications,” in *Comprehensive Membrane Science and Engineering*, Elsevier, 2010, pp. 253–273. doi: 10.1016/B978-0-08-093250-7.00027-X.
[25] Potter, “Electrical effects accompanying the decomposition of organic compounds,” *Proc. R. Soc. Lond. B.*, vol. 84, no. 571, pp. 260–276, Sep. 1911, doi: 10.1098/rspb.1911.0073.
[26] B. Cohen, “The bacterial culture as an electrical half-cell,” *J. Bacteriol*, vol. 21, no. 1, pp. 18–19, 1931.
[27] J. B. Davis and H. F. Yarbrough, “Preliminary Experiments on a Microbial Fuel Cell,” *Science*, vol. 137, no. 3530, pp. 615–616, Aug. 1962, doi: 10.1126/science.137.3530.615.
[28] K. Noll, “Microbial Fuel Cells,” in *Fuel Cell Technology*, N. Sammes, Ed., in Engineering Materials and Processes. , London: Springer London, 2006, pp. 277–296. doi: 10.1007/1-84628-207-1_9.
[29] H. Luo, G. Liu, R. Zhang, Y. Bai, S. Fu, and Y. Hou, “Heavy metal recovery combined with H2 production from artificial acid mine drainage using the microbial electrolysis cell,” *Journal of Hazardous Materials*, vol. 270, pp. 153–159, Apr. 2014, doi: 10.1016/j.jhazmat.2014.01.050.
[30] B. E. Logan *et al.*, “Microbial Fuel Cells: Methodology and Technology,” *Environ. Sci. Technol.*, vol. 40, no. 17, pp. 5181–5192, Sep. 2006, doi: 10.1021/es0605016.
[31] M. Maktabifard, E. Zaborowska, and J. Makinia, “Evaluating the effect of different operational strategies on the carbon footprint of wastewater treatment plants – case studies from northern Poland,” *Water Science and Technology*, vol. 79, no. 11, pp. 2211–2220, Jun. 2019, doi: 10.2166/wst.2019.224.

[32] M. Maktabifard *et al.*, “Comprehensive evaluation of the carbon footprint components of wastewater treatment plants located in the Baltic Sea region,” *Science of The Total Environment*, vol. 806, p. 150436, Feb. 2022, doi: 10.1016/j.scitotenv.2021.150436.
[33] X. Dominguez-Benetton *et al.*, “Metal recovery by microbial electro-metallurgy,” *Progress in Materials Science*, vol. 94, pp. 435–461, May 2018, doi: 10.1016/j.pmatsci.2018.01.007.
[34] R. P. O’Hayre, S.-W. Cha, W. G. Colella, and F. B. Prinz, *Fuel cell fundamentals*, Third edition. Hoboken, New Jersey: John Wiley & Sons Inc, 2016.
[35] Y. Feng, W. He, J. Liu, X. Wang, Y. Qu, and N. Ren, “A horizontal plug flow and stackable pilot microbial fuel cell for municipal wastewater treatment,” *Bioresource Technology*, vol. 156, pp. 132–138, Mar. 2014, doi: 10.1016/j.biortech.2013.12.104.
[36] D. R. Bond and D. R. Lovley, “Electricity production by Geobacter sulfurreducens attached to electrodes,” *Applied and Environmental Microbiology*, vol. 69, no. 3, pp. 1548–1555, 2003, doi: 10.1128/AEM.69.3.1548-1555.2003.
[37] U. Schröder, “Anodic electron transfer mechanisms in microbial fuel cells and their energy efficiency,” *Phys. Chem. Chem. Phys.*, vol. 9, no. 21, pp. 2619–2629, 2007, doi: 10.1039/B703627M.
[38] B. Min, J. Kim, S. Oh, J. M. Regan, and B. E. Logan, “Electricity generation from swine wastewater using microbial fuel cells,” *Water Research*, vol. 39, no. 20, pp. 4961–4968, 2005, doi: http://dx.doi.org/10.1016/j.watres.2005.09.039.
[39] S. Jung, “Impedance analysis of Geobacter sulfurreducens PCA, Shewanella oneidensis MR-1, and their coculture in bioeletrochemical systems,” *International Journal of Electrochemical Science*, vol. 7, no. 11, pp. 11091–11100, 2012.
[40] B. R. Ringeisen *et al.*, “High power density from a miniature microbial fuel cell using Shewanella oneidensis DSP10,” *Environmental Science and Technology*, vol. 40, no. 8, pp. 2629–2634, 2006, doi: 10.1021/es052254w.
[41] N. Samsudeen, T. K. Radhakrishnan, and M. Matheswaran, “Bioelectricity production from microbial fuel cell using mixed bacterial culture isolated from distillery wastewater,” *Bioresource Technology*, vol. 195, pp. 242–247, 2015, doi: 10.1016/j.biortech.2015.07.023.
[42] R. Kumar, L. Singh, Z. A. Wahid, and M. F. M. Din, “Exoelectrogens in microbial fuel cells toward bioelectricity generation: a review,” *International Journal of Energy Research*, vol. 39, no. 8, pp. 1048–1067, Jun. 2015, doi: 10.1002/er.3305.
[43] K. Rabaey, G. Lissens, S. D. Siciliano, and W. Verstraete, “A microbial fuel cell capable of converting glucose to electricity at high rate and efficiency,” *Biotechnology Letters*, vol. 25, no. 18, pp. 1531–1535, 2003, doi: 10.1023/A:1025484009367.
[44] R. Alipanahi and M. Rahimnejad, “Effect of different ecosystems on generated power in sediment microbial fuel cell,” *International Journal of Energy Research*, vol. 42, no. 15, pp. 4891–4897, Dec. 2018, doi: 10.1002/er.4199.
[45] F. J. Fernandez, V. Sanchez-Arias, J. Villasenor, and L. Rodriguez, “Evaluation of carbon degradation during co-composting of exhausted grape marc with different biowastes,” *Chemosphere*, vol. 73, no. 5, pp. 670–677, Oct. 2008, doi: 10.1016/j.chemosphere.2008.07.007.
[46] F. J. Fernandez-Morales, J. Villasenor, and D. Infantes, “Modeling and monitoring of the acclimatization of conventional activated sludge to a biohydrogen producing culture by biokinetic control,” *International Journal of Hydrogen Energy*, vol. 35, no. 20, pp. 10927–10933, Oct. 2010, doi: 10.1016/j.ijhydene.2010.07.054.
[47] L. Zhang, J. Li, X. Zhu, D. Ye, Q. Fu, and Q. Liao, “Startup performance and anodic biofilm distribution in continuous-flow microbial fuel cells with serpentine flow fields: effects of external resistance,” *Industrial & Engineering Chemistry Research*, vol. 56, no. 14, pp. 3767–3774, 2017.
[48] S. Mateo, A. D’Angelo, O. Scialdone, P. Cañizares, M. A. Rodrigo, and F. J. Fernandez-Morales, “The influence of sludge retention time on mixed culture microbial fuel cell start-

ups," *Biochemical Engineering Journal*, vol. 123, pp. 38–44, Jul. 2017, doi: http://dx.doi.org/10.1016/j.bej.2017.03.018.
[49] S.-H. Liu, H.-H. Lin, S. Wen, and C.-W. Lin, "Performance of trickling bed microbial fuel cell treating isopropyl alcohol vapor: Effects of shock-load and shut-down episodes," *Chemosphere*, vol. 224, pp. 168–175, Feb. 2019, doi: 10.1016/j.chemosphere.2019.02.149.
[50] P. Aelterman, M. Versichele, M. Marzorati, N. Boon, and W. Verstraete, "Loading rate and external resistance control the electricity generation of microbial fuel cells with different three-dimensional anodes," *Bioresource Technology*, vol. 99, no. 18, pp. 8895–8902, 2008, doi: 10.1016/j.biortech.2008.04.061.
[51] M. Behera and M. M. Ghangrekar, "Performance of microbial fuel cell in response to change in sludge loading rate at different anodic feed pH," *Bioresource Technology*, vol. 100, no. 21, pp. 5114–5121, 2009.
[52] P. Sobieszuk, A. Zamojska-Jaroszewicz, and Ł. Makowski, "Influence of the operational parameters on bioelectricity generation in continuous microbial fuel cell, experimental and computational fluid dynamics modelling," *Journal of Power Sources*, vol. 371, pp. 178–187, 2017.
[53] A. Larrosa-Guerrero, K. Scott, I. M. Head, F. Mateo, A. Ginesta, and C. Godinez, "Effect of temperature on the performance of microbial fuel cells," *Fuel*, vol. 89, no. 12, pp. 3985–3994, 2010.
[54] A. Gonzalez del Campo, J. Lobato, P. Cañizares, M. A. Rodrigo, and F. J. Fernandez Morales, "Short-term effects of temperature and COD in a microbial fuel cell," *Applied Energy*, vol. 101, pp. 213–217, Jan. 2013, doi: 10.1016/j.apenergy.2012.02.064.
[55] A. D'Angelo, S. Mateo, O. Scialdone, P. Cañizares, F. J. Fernandez-Morales, and M. A. Rodrigo, "Optimization of the performance of an air-cathode MFC by changing solid retention time," *Journal of Chemical Technology and Biotechnology*, 2017, doi: 10.1002/jctb.5175.
[56] P. Ledezma, J. Greenman, and I. Ieropoulos, "MFC-cascade stacks maximise COD reduction and avoid voltage reversal under adverse conditions," *Bioresource Technology*, vol. 134, pp. 158–165, 2013, doi: 10.1016/j.biortech.2013.01.119.
[57] X. A. Walter, S. Forbes, J. Greenman, and I. A. Ieropoulos, "From single MFC to cascade configuration: The relationship between size, hydraulic retention time and power density," *Sustainable Energy Technologies and Assessments*, vol. 14, pp. 74–79, 2016, doi: 10.1016/j.seta.2016.01.006.
[58] L. Wei, Z. Yuan, M. Cui, H. Han, and J. Shen, "Study on electricity-generation characteristic of two-chambered microbial fuel cell in continuous flow mode," *International Journal of Hydrogen Energy*, vol. 37, no. 1, pp. 1067–1073, Jan. 2012, doi: https://doi.org/10.1016/j.ijhydene.2011.02.120.
[59] X. Li, N. Zhu, Y. Wang, P. Li, P. Wu, and J. Wu, "Animal carcass wastewater treatment and bioelectricity generation in up-flow tubular microbial fuel cells: Effects of HRT and non-precious metallic catalyst," *Bioresource Technology*, vol. 128, pp. 454–460, 2013, doi: 10.1016/j.biortech.2012.10.053.
[60] W.-W. Li, H.-Q. Yu, and Z. He, "Towards sustainable wastewater treatment by using microbial fuel cells-centered technologies," *Energy & Environmental Science*, vol. 7, no. 3, pp. 911–924, 2014, doi: 10.1039/C3EE43106A.
[61] M. Ragab, A. Elawwad, and H. Abdel-Halim, "Simultaneous power generation and pollutant removals using microbial desalination cell at variable operation modes," *Renewable Energy*, vol. 143, pp. 939–949, Dec. 2019, doi: 10.1016/j.renene.2019.05.068.
[62] S. Mateo, F. J. Fernandez-Morales, P. Cañizares, and M. A. Rodrigo, "Influence of the Cathode Platinum Loading and of the Implementation of Membranes on the Performance of Air-Breathing Microbial Fuel Cells," *Electrocatalysis*, pp. 1–8, 2017.

[63] H. Liu and B. E. Logan, “Electricity generation using an air-cathode single chamber microbial fuel cell in the presence and absence of a proton exchange membrane,” *Environmental science & technology*, vol. 38, no. 14, pp. 4040–4046, 2004.
[64] M. Christwardana, D. Frattini, G. Accardo, S. P. Yoon, and Y. Kwon, “Early-stage performance evaluation of flowing microbial fuel cells using chemically treated carbon felt and yeast biocatalyst,” *Applied Energy*, vol. 222, pp. 369–382, 2018, doi: 10.1016/j.apenergy.2018.03.193.
[65] S. Mateo, P. Cañizares, M. A. Rodrigo, and F. J. Fernandez-Morales, “Driving force behind electrochemical performance of microbial fuel cells fed with different substrates,” *Chemosphere*, vol. 207, pp. 313–319, 2018.
[66] A. González del Campo, P. Cañizares, M. A. Rodrigo, F. J. Fernández, and J. Lobato, “Microbial fuel cell with an algae-assisted cathode: A preliminary assessment,” *Journal of Power Sources*, vol. 242, pp. 638–645, Nov. 2013, doi: 10.1016/j.jpowsour.2013.05.110.
[67] T. Jafary, A. A. Ghoreyshi, G. D. Najafpour, S. Fatemi, and M. Rahimnejad, “Investigation on performance of microbial fuel cells based on carbon sources and kinetic models,” *International Journal of Energy Research*, vol. 37, no. 12, pp. 1539–1549, Oct. 2013, doi: 10.1002/er.2994.
[68] L. Rodríguez Mayor, J. Villaseñor Camacho, and F. J. Fernández Morales, “Operational optimisation of pilot scale biological nutrient removal at the Ciudad Real (Spain) domestic wastewater treatment plant,” *Water, Air, and Soil Pollution*, vol. 152, no. 1–4, pp. 279–296, 2004, doi: 10.1023/B:WATE.0000015366.39480.b1.
[69] A. De Lucas, L. Rodriguez, J. Villasenor, and F. J. Fernandez, “Fermentation of agro-food wastewaters by activated sludge,” *Water Research*, vol. 41, no. 8, pp. 1635–1644, Apr. 2007, doi: 10.1016/j.watres.2007.01.041.
[70] F. W. Gilcreas, “Future of standard methods for the examination of water and wastewater,” *Health Lab Sci*, vol. 4, no. 3, pp. 137–141, Jul. 1967.
[71] S. Mateo, M. Rodrigo, L. P. Fonseca, P. Cañizares, and F. J. Fernandez-Morales, “Oxygen availability effect on the performance of air-breathing cathode microbial fuel cell,” *Biotechnology Progress*, vol. 31, no. 4, pp. 900–907, 2015, doi: 10.1002/btpr.2106.
[72] V. G. Gude, “Microbial fuel cells for wastewater treatment and energy generation,” in *Microbial Electrochemical and Fuel Cells*, Elsevier, 2016, pp. 247–285.
[73] D. Vigolo *et al.*, “Flow dependent performance of microfluidic microbial fuel cells,” *Physical Chemistry Chemical Physics*, vol. 16, no. 24, pp. 12535–12543, 2014.
[74] D. Ma, Z.-H. Jiang, C.-H. Lay, and D. Zhou, “Electricity generation from swine wastewater in microbial fuel cell: Hydraulic reaction time effect,” *International Journal of Hydrogen Energy*, vol. 41, no. 46, pp. 21820–21826, 2016.
[75] D. F. Juang, P. C. Yang, and T. H. Kuo, “Effects of flow rate and chemical oxygen demand removal characteristics on power generation performance of microbial fuel cells,” *International Journal of Environmental Science and Technology*, vol. 9, no. 2, pp. 267–280, 2012.
[76] Y. Park, V. K. Nguyen, S. Park, J. Yu, and T. Lee, “Effects of anode spacing and flow rate on energy recovery of flat-panel air-cathode microbial fuel cells using domestic wastewater,” *Bioresource Technology*, vol. 258, pp. 57–63, 2018.
[77] Z. He, S. D. Minteer, and L. T. Angenent, “Electricity generation from artificial wastewater using an upflow microbial fuel cell,” *Environmental Science and Technology*, vol. 39, no. 14, pp. 5262–5267, 2005, doi: 10.1021/es0502876.
[78] Y. Ahn and B. E. Logan, “A multi-electrode continuous flow microbial fuel cell with separator electrode assembly design,” *Applied microbiology and biotechnology*, vol. 93, no. 5, pp. 2241–2248, 2012.
[79] H. Shukor *et al.*, “Production of butanol by Clostridium saccharoperbutylacetonicum N1-4 from palm kernel cake in acetone–butanol–ethanol fermentation using an empirical model,” *Bioresource Technology*, vol. 170, pp. 565–573, Oct. 2014, doi: 10.1016/j.biortech.2014.07.055.

[80] X. Zhang, X. Li, X. Zhao, and Y. Li, “Factors affecting the efficiency of a bioelectrochemical system: a review,” *RSC Adv.*, vol. 9, no. 34, pp. 19748–19761, 2019, doi: 10.1039/C9RA03605A.
[81] S. Mateo, P. Cañizares, M. A. Rodrigo, and F. J. Fernández-Morales, “Reproducibility and robustness of microbial fuel cells technology,” *Journal of Power Sources*, vol. 412, pp. 640–647, 2019.
[82] S. Babanova *et al.*, “Continuous flow, large-scale, microbial fuel cell system for the sustained treatment of swine waste,” *Water Environ Res*, vol. 92, no. 1, pp. 60–72, Jan. 2020, doi: 10.1002/wer.1183.
[83] S. Wu *et al.*, “A novel pilot-scale stacked microbial fuel cell for efficient electricity generation and wastewater treatment,” *Water Research*, vol. 98, pp. 396–403, Jul. 2016, doi: 10.1016/j.watres.2016.04.043.
[84] M. Lu *et al.*, “Long-term performance of a 20-L continuous flow microbial fuel cell for treatment of brewery wastewater,” *Journal of Power Sources*, vol. 356, pp. 274–287, Jul. 2017, doi: 10.1016/j.jpowsour.2017.03.132.
[85] C. Xia, D. Zhang, W. Pedrycz, Y. Zhu, and Y. Guo, “Models for Microbial Fuel Cells: A critical review,” *Journal of Power Sources*, vol. 373, pp. 119–131, Jan. 2018, doi: 10.1016/j.jpowsour.2017.11.001.
[86] O. B. Rizvandi and S. Yesilyurt, “Modeling and performance analysis of branched microfluidic fuel cells with high utilization,” *Electrochimica Acta*, vol. 318, pp. 169–180, Sep. 2019, doi: 10.1016/j.electacta.2019.06.032.
[87] M. Kadivarian and M. Karamzadeh, “Electrochemical modeling of microbial fuel cells performance at different operating and structural conditions,” *Bioprocess Biosyst Eng*, vol. 43, no. 3, pp. 393–401, Mar. 2020, doi: 10.1007/s00449-019-02235-1.
[88] M. Esfandyari, M. A. Fanaei, R. Gheshlaghi, and M. Akhavan Mahdavi, “Mathematical modeling of two-chamber batch microbial fuel cell with pure culture of Shewanella,” *Chemical Engineering Research and Design*, vol. 117, pp. 34–42, Jan. 2017, doi: 10.1016/j.cherd.2016.09.016.
[89] M. Karamzadeh, M. Kadivarian, P. Mahmoodi, S. S. Asefi, and A. Taghipour, “Modeling and experimental investigation of the effect of carbon source on the performance of tubular microbial fuel cell,” *Sci Rep*, vol. 13, no. 1, p. 11070, Jul. 2023, doi: 10.1038/s41598-023-38215-5.
[90] J.-D. Park and Z. Ren, “Hysteresis-Controller-Based Energy Harvesting Scheme for Microbial Fuel Cells With Parallel Operation Capability,” *IEEE Trans. Energy Convers.*, vol. 27, no. 3, pp. 715–724, Sep. 2012, doi: 10.1109/TEC.2012.2196044.
[91] P. M. D. Serra, A. Espírito-Santo, and M. Magrinho, “A steady-state electrical model of a microbial fuel cell through multiple-cycle polarization curves,” *Renewable and Sustainable Energy Reviews*, vol. 117, p. 109439, Jan. 2020, doi: 10.1016/j.rser.2019.109439.
[92] D. Kashyap *et al.*, “Application of electrochemical impedance spectroscopy in bio-fuel cell characterization: A review,” *International Journal of Hydrogen Energy*, vol. 39, no. 35, pp. 20159–20170, Dec. 2014, doi: 10.1016/j.ijhydene.2014.10.003.
[93] Y. Yin, G. Huang, Y. Tong, Y. Liu, and L. Zhang, “Electricity production and electrochemical impedance modeling of microbial fuel cells under static magnetic field,” *Journal of Power Sources*, vol. 237, pp. 58–63, Sep. 2013, doi: 10.1016/j.jpowsour.2013.02.080.
[94] J. Coronado, B. Tartakovsky, and M. Perrier, “On-line monitoring of microbial fuel cells operated with pulse-width modulated electrical load,” *Journal of Process Control*, vol. 35, pp. 59–64, Nov. 2015, doi: 10.1016/j.jprocont.2015.08.004.
[95] M. Alaraj and J.-D. Park, “Net power positive maximum power point tracking energy harvesting system for microbial fuel cell,” *Journal of Power Sources*, vol. 418, pp. 225–232, Apr. 2019, doi: 10.1016/j.jpowsour.2019.02.042.

[96] I. Baccouche, S. Jemmali, B. Manai, N. Omar, and N. Amara, “Improved OCV Model of a Li-Ion NMC Battery for Online SOC Estimation Using the Extended Kalman Filter,” *Energies*, vol. 10, no. 6, p. 764, May 2017, doi: 10.3390/en10060764.
[97] Ö. Atlam and G. Dündar, “A practical Equivalent Electrical Circuit model for Proton Exchange Membrane Fuel Cell (PEMFC) systems,” *International Journal of Hydrogen Energy*, vol. 46, no. 24, pp. 13230–13239, Apr. 2021, doi: 10.1016/j.ijhydene.2021.01.108.
[98] P. T. Ha, H. Moon, B. H. Kim, H. Y. Ng, and I. S. Chang, “Determination of charge transfer resistance and capacitance of microbial fuel cell through a transient response analysis of cell voltage,” *Biosensors and Bioelectronics*, vol. 25, no. 7, pp. 1629–1634, Mar. 2010, doi: 10.1016/j.bios.2009.11.023.
[99] K. S. Aiyer, “How does electron transfer occur in microbial fuel cells?,” *World J Microbiol Biotechnol*, vol. 36, no. 2, p. 19, Feb. 2020, doi: 10.1007/s11274-020-2801-z.
[100] S.-I. Pyun, “Thermodynamic and electro-kinetic analyses of direct electron transfer (DET) and mediator-involved electron transfer (MET) with the help of a redox electron mediator,” *J Solid State Electrochem*, vol. 24, no. 11–12, pp. 2685–2693, Nov. 2020, doi: 10.1007/s10008-020-04780-2.
[101] A. J. Slate, K. A. Whitehead, D. A. C. Brownson, and C. E. Banks, “Microbial fuel cells: An overview of current technology,” *Renewable and Sustainable Energy Reviews*, vol. 101, pp. 60–81, Mar. 2019, doi: 10.1016/j.rser.2018.09.044.
[102] D. Recio-Garrido, M. Perrier, and B. Tartakovsky, “Combined bioelectrochemical–electrical model of a microbial fuel cell,” *Bioprocess Biosyst Eng*, vol. 39, no. 2, pp. 267–276, Feb. 2016, doi: 10.1007/s00449-015-1510-8.
[103] S. Potrykus, S. Mateo, J. Nieznański, and F. J. Fernández-Morales, “The Influent Effects of Flow Rate Profile on the Performance of Microbial Fuel Cells Model,” *Energies*, vol. 13, no. 18, p. 4735, Sep. 2020, doi: 10.3390/en13184735.
[104] L. Koók, N. Nemestóthy, K. Bélafi-Bakó, and P. Bakonyi, “Investigating the specific role of external load on the performance versus stability trade-off in microbial fuel cells,” *Bioresource Technology*, vol. 309, p. 123313, Aug. 2020, doi: 10.1016/j.biortech.2020.123313.
[105] S. Potrykus, L. F. León-Fernández, J. Nieznański, D. Karkosiński, and F. J. Fernandez-Morales, “The Influence of External Load on the Performance of Microbial Fuel Cells,” *Energies*, vol. 14, no. 3, p. 612, Jan. 2021, doi: 10.3390/en14030612.
[106] M. Muloiwa, S. Nyende-Byakika, and M. Dinka, “Comparison of unstructured kinetic bacterial growth models.,” *South African Journal of Chemical Engineering*, vol. 33, pp. 141–150, Jul. 2020, doi: 10.1016/j.sajce.2020.07.006.
[107] V. Pop, Ed., *Battery management systems: accurate state-of-charge indication for battery powered applications*. in Philips research book series, no. v. 9. Dordrecht: Springer, 2008.
[108] Z. Lv, D. Xie, F. Li, Y. Hu, C. Wei, and C. Feng, “Microbial fuel cell as a biocapacitor by using pseudo-capacitive anode materials,” *Journal of Power Sources*, vol. 246, pp. 642–649, Jan. 2014, doi: 10.1016/j.jpowsour.2013.08.014.
[109] K. R. Fradler, J. R. Kim, H. C. Boghani, R. M. Dinsdale, A. J. Guwy, and G. C. Premier, “The effect of internal capacitance on power quality and energy efficiency in a tubular microbial fuel cell,” *Process Biochemistry*, vol. 49, no. 6, pp. 973–980, Jun. 2014, doi: 10.1016/j.procbio.2014.02.021.
[110] G. L. Plett, *Battery management systems: battery modeling. Volume 1*. Boston : London: Artech House, 2015.
[111] A. Gonzalez del Campo, J. F. Perez, P. Cañizares, M. A. Rodrigo, F. J. Fernandez, and J. Lobato, “Study of a photosynthetic MFC for energy recovery from synthetic industrial fruit juice wastewater,” *International Journal of Hydrogen Energy*, vol. 39, no. 36, pp. 21828–21836, Dec. 2014, doi: 10.1016/j.ijhydene.2014.07.055.
[112] A. Gonzalez del Campo, J. F. Perez, P. Cañizares, M. A. Rodrigo, F. J. Fernandez, and J. Lobato, “Characterization of light/dark cycle and long-term performance test in a

photosynthetic microbial fuel cell," *Fuel*, vol. 140, pp. 209–216, Jan. 2015, doi: 10.1016/j.fuel.2014.09.087.
[113] L. F. Leon-Fernandez, J. Villaseñor, L. Rodriguez, P. Cañizares, M. A. Rodrigo, and F. J. Fernández-Morales, "Dehalogenation of 2,4-Dichlorophenoxyacetic acid by means of bioelectrochemical systems," *Journal of Electroanalytical Chemistry*, vol. 854, p. 113564, Dec. 2019, doi: 10.1016/j.jelechem.2019.113564.
[114] G. S. Jadhav and M. M. Ghangrekar, "Performance of microbial fuel cell subjected to variation in pH, temperature, external load and substrate concentration," *Bioresource Technology*, vol. 100, no. 2, pp. 717–723, Jan. 2009, doi: 10.1016/j.biortech.2008.07.041.
[115] S. Cheng, D. Xing, and B. E. Logan, "Electricity generation of single-chamber microbial fuel cells at low temperatures," *Biosensors and Bioelectronics*, vol. 26, no. 5, pp. 1913–1917, Jan. 2011, doi: 10.1016/j.bios.2010.05.016.
[116] S. Carreon-Bautista, C. Erbay, A. Han, and E. Sanchez-Sinencio, "An Inductorless DC–DC Converter for an Energy Aware Power Management Unit Aimed at Microbial Fuel Cell Arrays," *IEEE J. Emerg. Sel. Topics Power Electron.*, vol. 3, no. 4, pp. 1109–1121, Dec. 2015, doi: 10.1109/JESTPE.2015.2398851.
[117] Y. Hong, D. F. Call, C. M. Werner, and B. E. Logan, "Adaptation to high current using low external resistances eliminates power overshoot in microbial fuel cells," *Biosensors and Bioelectronics*, vol. 28, no. 1, pp. 71–76, Oct. 2011, doi: 10.1016/j.bios.2011.06.045.
[118] H. Rismani-Yazdi, A. D. Christy, S. M. Carver, Z. Yu, B. A. Dehority, and O. H. Tuovinen, "Effect of external resistance on bacterial diversity and metabolism in cellulose-fed microbial fuel cells," *Bioresource Technology*, vol. 102, no. 1, pp. 278–283, Jan. 2011, doi: 10.1016/j.biortech.2010.05.012.
[119] W.-F. Cai *et al.*, "Investigation of a two-dimensional model on microbial fuel cell with different biofilm porosities and external resistances," *Chemical Engineering Journal*, vol. 333, pp. 572–582, Feb. 2018, doi: 10.1016/j.cej.2017.09.189.
[120] W. M. Haynes, D. R. Lide, and T. J. Bruno, Eds., *CRC Handbook of Chemistry and Physics*, 97th ed. CRC Press, 2016. doi: 10.1201/9781315380476.
[121] E. W. Rice and American Public Health Association, Eds., *Standard methods for the examination of water and wastewater*, 22. ed. Washington, DC: American Public Health Association, 2012.
[122] S. Heydari Orojlou, S. Rastegarzadeh, and B. Zargar, "Experimental and modeling analyses of COD removal from industrial wastewater using the TiO2–chitosan nanocomposites," *Sci Rep*, vol. 12, no. 1, p. 11088, Jun. 2022, doi: 10.1038/s41598-022-15387-0.
[123] J. Li and Z. He, "Development of a dynamic mathematical model for membrane bioelectrochemical reactors with different configurations," *Environ Sci Pollut Res*, vol. 23, no. 4, pp. 3897–3906, Feb. 2016, doi: 10.1007/s11356-015-5611-3.

Appendix A: Simulation results of microbial fuel cell different types and values of loads

Table A.1 Data of simulation results of microbial fuel cell under constant-current regime external load for different values of operational parameter

I_{MFC} (mA)	Energy (J)	EE (%)	CE (%)	CODrem (%)	Time (s)
0.25	31.28	31	42.6	11.7	180000
0.35	42.27	29.7	42.4	16.4	180000
0.5	57.08	27.9	42.1	23.6	180000
0.75	77.15	24.9	41.7	35.8	180000
0.94	88.33	22.6	41.4	45.2	180000
1	91.09	21.9	41.3	48.1	180000
1.25	98.34	18.8	41.1	60.5	180000
1.36	99.19	17.4	41	66	180000
1.5	98	15.6	41	72.8	180000
1.75	88.63	12.1	41.1	84.8	180000
1.85	81.8	10.6	41.3	89.2	180000
2	67.1	8.2	41.8	95.2	180000
2.2	42.99	5.3	32.5	94.3	125910
2.5	19.58	2.6	19.5	86.9	61338.3
3	3.45	0.6	7.6	62.5	14329.4
3.5	0.6	0.8	6.7	9	1543.69

Table A.2 Data of simulation results of microbial fuel cell under constant-current regime external load for different values of operational parameter

V_{MFC} (V)	Energy (J)	EE (%)	CE (%)	CODrem (%)	Time (s)
0.04	9.35	1.1	26.1	99.1	180000
0.08	24.53	2.9	34.3	98.7	180000
0.1	32.53	3.8	36.6	98.3	180000
0.15	50.75	6.1	39	95.9	180000
0.2	66.07	8.3	39.8	91.9	180000
0.25	78.6	10.5	40.1	86.6	180000
0.3	88.13	12.7	40.4	80.4	180000
0.35	94.37	14.9	40.6	73.4	180000
0.4	97.06	17.1	40.8	65.7	180000
0.41	97.15	17.5	40.9	64.1	180000
0.45	95.97	19.3	41	57.4	180000
0.5	90.9	21.6	41.3	48.7	180000
0.52	87.74	22.5	41.4	45.1	180000
0.55	81.74	23.9	41.5	39.5	180000
0.6	68.37	26.3	41.9	30.1	180000
0.65	50.73	28.7	42.2	20.4	180000
0.7	28.78	31.2	42.6	10.7	180000

Table A.3 Data of simulation results of microbial fuel cell under constant-current regime external load for different values of operational parameter

P_{load} (V)	Energy (J)	EE (%)	CE (%)	CODrem (%)	Time (s)
0.1	18	32.3	42.8	6.4	180000
0.2	36	30.4	42.5	13.7	180000
0.3	54	28.3	42.2	22	1800
0.4	72	25.8	41.8	32.3	180000
0.5	90	22.2	41.4	47	180000
0.526	94.68	20.5	41.3	53.4	180000
0.6	42.33	14.7	31.8	33.2	70548.4
0.7	1.67	11.1	25.4	1.7	2391.44

Table A.4 Data of simulation results of microbial fuel cell under constant-resistance regime external load for different values of operational parameter

R_{load} (Ω)	Energy (J)	EE (%)	CE (%)	CODrem (%)	Time (s)
24.875	10.45	1.2	23.5	99.4	180000
49.75	32.72	3.8	37.1	98.9	180000
74.625	51.86	6.2	39.8	96.8	180000
99.5	65.77	8.1	40.3	93.7	180000
169.15	88.32	12.3	40.7	83	180000
199	93.18	13.7	40.7	78.5	180000
298.5	98.63	17.3	40.9	65.7	180000
303.475	98.64	17.4	41	65.6	180000
398	96.31	19.9	41.1	56	180000
497.5	91.43	21.7	41.3	48.6	180000
547.25	88.69	22.5	41.4	45.6	180000
696.5	80.49	24.3	41.6	38.3	180000
995	66.62	26.6	41.9	29	180000
1492.5	50.96	28.7	42.2	20.5	180000
1990	41.05	29.9	42.4	15.9	180000

Appendix B: Simulation results of microbial fuel cell under active electric load and cathode air supply

Table B.1 Data of simulation results of microbial fuel cell under active electric load and cathode air supply

I_{MFC} (mA)	Energy (J)	EE (%)	CE (%)	CODrem (%)	Time (s)
1	12.45	22.7	37.6	6.3	25200
1.8	18.39	16.4	33.2	12.9	25200
2	19.31	15	32.1	14.9	25200
2.5	20.57	11.7	29.3	20.4	25200
2.7	20.67	10.4	28.1	22.9	25200
3	20.34	8.7	26.4	27.1	25200
3.3	19.44	7	24.7	32	25200
3.5	18.49	6	23.5	35.6	25200
4	14.8	3.6	20.3	46.9	25200
4.5	8.56	1.5	16.8	64	25200

Table B.2 Data of simulation results of microbial fuel cell under passive resistive electric load and cathode without air supply

R_{load} (Ω)	Energy (J)	EE (%)	CE (%)	CODrem (%)	Time (s)
35	19.13	2.3	31	96.7	144000
69	38.22	5	34.9	88.2	144000
104	49.53	7.3	36.5	78.7	144000
120	52.71	8.2	37	74.7	144000
138	55.2	9.1	37.5	70.5	144000
207	58.31	11.7	38.6	57.6	144000
276	56.69	13.6	39.3	48.3	144000
372	52.26	14.4	40	39.3	144000
414	50.18	16	40.2	36.3	144000
552	43.82	17.5	40.8	29	144000
690	38.56	18.5	41.2	24.1	144000
1380	23.55	20.9	42	13	144000

TABLE OF FIGURES